

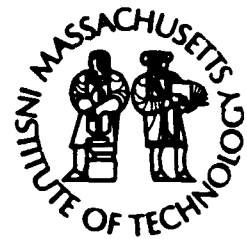
AD-A247 635



# Woods Hole Oceanographic Institution Massachusetts Institute of Technology



Joint Program  
in Oceanography  
and  
Oceanographic Engineering



---

**DOCTORAL DISSERTATION**

## The Structure and Transport of the Brazil Current between 27° and 36° South

by

Jan Campbell Zemba

June 1991

This document has been approved  
for public release and sale; its  
distribution is unlimited.

DTIC  
ELECTE  
MAR 19 1992  
S D D

92 2 12 007

92-06973

WHOI-91-37

**The Structure and Transport of the Brazil Current  
between 27° and 36° South**

by

**Jan Campbell Zemba**

**Woods Hole Oceanographic Institution  
Woods Hole, Massachusetts 02543**

and

**The Massachusetts Institute of Technology  
Cambridge, Massachusetts 02139**

June 1991


**Doctoral Dissertation**


Funding was provided by the Office of Naval Research under Contract No. N00014-82-C-0019 and the National Science Foundation through Grant No. OCE86-14486.

Reproduction in whole or in part is permitted for any purpose of the United States Government. This thesis should be cited as:  
Jan Campbell Zemba, 1991. The Structure and Transport of the Brazil Current between 27° and 36° South. Ph.D. Thesis. MIT/WHOI, WHOI-91-37.

Approved for publication; distribution unlimited.

**Approved for Distribution:**

  
**James Luyten**  
Department of Physical Oceanography

  
**John W. Farrington**  
Dean of Graduate Studies

Accession For	
NTIS	CRA&I
DTIC	TAB
Unannounced	
Justification	
By	
Distribution /	
Availability Codes	
Dist	Avail and/or Special
A-1	

**The Structure and Transport of the Brazil Current  
between 27° and 36° South**

by

**Jan Campbell Zemba**

B.S. Mechanical Engineering, University of California, Irvine  
(1982)

and

M.S. Mechanical Engineering, University of California, Irvine  
(1984)

Submitted in partial fulfillment of the  
requirements for the degrees of

Doctor of Philosophy

at the

MASSACHUSETTS INSTITUTE OF TECHNOLOGY

and the

WOODS HOLE OCEANOGRAPHIC INSTITUTION

June 1991

© Jan C. Zemba 1991

The author hereby grants to MIT and to WHOI permission to reproduce  
and to distribute copies of this thesis document in whole or in part.

Signature of Author ..... *Jan C. Zemba* .....

Joint Program in Physical Oceanography  
Massachusetts Institute of Technology  
Woods Hole Oceanographic Institution

May 21, 1991

Certified by ..... *Michael S. McCartney* .....

Michael S. McCartney

Associate Scientist

Thesis Supervisor

Accepted by ..... *Carl Wunsch* .....

Carl Wunsch

Chairman, Joint Committee for Physical Oceanography  
Massachusetts Institute of Technology  
Woods Hole Oceanographic Institution



## Contents

<b>Abstract</b>	<b>5</b>
<b>Acknowledgments</b>	<b>7</b>
<b>1 Introduction</b>	<b>10</b>
<b>2 Water Masses in the Brazil Current Region</b>	<b>19</b>
2.1 Water Mass Characteristics . . . . .	20
2.2 The Density Structure of the Sections . . . . .	26
2.3 The Water Masses . . . . .	32
2.3.1 Central Water . . . . .	32
2.3.2 Antarctic Intermediate Water . . . . .	41
2.3.3 Upper Circumpolar Water . . . . .	42
2.3.4 North Atlantic Deep Water . . . . .	43
2.3.5 Lower Circumpolar Water . . . . .	45
2.3.6 Antarctic Bottom Water . . . . .	45
<b>3 Transport of the Brazil Current</b>	<b>48</b>
3.1 Transport Calculations . . . . .	51
3.2 Reference Choices for Each Section . . . . .	52
3.2.1 Section I. 27°S . . . . .	53
3.2.2 Section II. 31°S . . . . .	54
3.2.3 Section III. 34°S . . . . .	58
3.2.4 Section IV. 36°S . . . . .	59
3.3 Resulting Flow Patterns . . . . .	63

3.4	How Good are the Results? . . . . .	69
3.5	Summary . . . . .	71
<b>4</b>	<b>A Simple Layer Model of the South Atlantic at 31° South</b>	<b>73</b>
4.1	Construction of the Layer Systems . . . . .	75
4.2	Two Layer Systems . . . . .	79
4.3	Three Layer Systems . . . . .	86
4.4	Four Layer System . . . . .	95
4.5	Summary . . . . .	102
<b>5</b>	<b>Potential Vorticity in the Brazil Current</b>	<b>104</b>
5.1	Calculating Potential Vorticity from Hydrographic Data . . . . .	108
5.2	Potential Vorticity as a Tracer . . . . .	114
5.3	Potential Vorticity as a Dynamical Tool . . . . .	120
5.4	Conclusions . . . . .	130
<b>6</b>	<b>Conclusions</b>	<b>132</b>
	<b>References</b>	<b>137</b>
	<b>Appendix A</b>	<b>142</b>
	<b>Appendix B</b>	<b>157</b>
	<b>Appendix C</b>	<b>154</b>
	<b>Appendix D</b>	<b>158</b>

## Abstract

A set of four hydrographic sections through the Brazil Current are analyzed to identify downstream changes in the Brazil Current. The data, from the Thomas Washington Marathon Cruise, Leg 9, are at 27, 31, 34 and 36° S. The region they span details the change of the current from a relatively small near surface feature to a large, deep current. While the Brazil Current does not appear to develop transports as large as those found in the Gulf Stream, the calculated transports greatly exceed previous estimates. At 27° S the current extends down to approximately 700 m and transports 12 Sv southward; this value is consistent with previous estimates farther north. Downstream, surface layer transport increases, the current deepens, and the transport reaches a maximum of 80 Sv at 36°S. Part of the growth comes from the tight recirculation found just offshore of the Brazil Current. The recirculation strengthens and deepens to the south, with a minimum transport of 4 Sv north at 27° S and a maximum of 33 Sv at 36° S.

The change in the current is also reflected in its shear profiles. At 27° S Brazil Current shear is found only in the upper portion of the water column, over the continental slope. Downstream, the current moves off the slope into deeper water and develops top-to-bottom, monotonic shear. To obtain velocity from the shear profiles, zero velocity surfaces are chosen based on conservative use of tracer information.

A simple basin-wide model is used at 31° S to tie limits on the size of the Brazil Current and recirculation to various limits on layer-to-layer exchanges south of the section. The multi-layer model — based on changes in depth of several isotherms — is used to extend the interpretation of the current beyond that of an isolated ocean feature. The model is required to conserve mass in each layer, either by applying barotropic transports or by allowing layer-to-layer exchanges south of the section. Solutions are deemed acceptable if the sense, or direction, of the various layer-to-layer conversions are consistent with accepted ideas of water mass formation. Initially, a two layer model is employed. Governed by the conservation of mass in each layer, the two layer model has only one constraint on the resulting solutions: a conversion of cold-to-warm water in the south (or the surface layer flowing north and the deep layer flowing south). Such a meridional flow pattern is consistent with the equatorward heat flux in the South Atlantic. The single constraint, however, is not strong enough to limit the solution region in any significant way. The final model presented has four layers, and acceptable solutions have the net transports of the surface layer and the bottom water northward and form intermediate water from North Atlantic Deep Water in the south. The resulting solution set has a fairly small range of transports for the Brazil Current, with surface layer transports between 20 and 35 Sv; this range is consistent with the value calculated from hydrographic data at 31° S. Given the complex interleavings of the South Atlantic water masses, the four layer model performs remarkably well.

Finally, total potential vorticity is calculated from the hydrographic sections. Contrary to what one might expect, the reference level choice is not a significant problem: where currents are large, most of the signal in relative potential vorticity comes from

the measured shear, and where currents are small, the relative potential vorticity is not significant compared to the planetary vorticity. Unfortunately, the process of taking two horizontal derivatives of the density field results in a jittery relative potential vorticity signal. As a result, a clear potential vorticity profile could not be constructed for the current. This variability may be real —the ocean is frequently much noisier than one imagines. It may also be possible, though, to smooth the data sufficiently so that a cleaner picture emerges.

Despite the problems involved in obtaining a quantitative profile of the potential vorticity, qualitative changes are useful in detecting different flow regimes. By comparing the downstream changes in total and planetary potential vorticity, one can deduce frictional and inertial regimes in the different layers. The presence of a frictional regime at the inshore edge suggests that care should be taken in assuming that potential vorticity is conserved in western boundary currents. In addition the potential vorticity sections trace a pattern of the recirculation feeding into the Brazil Current in the upper layers; other tracers did not provide a clear image.

The final picture which emerges is not of a small, surface-trapped Brazil Current; rather, it is that of a classic western boundary current, increasing in strength and depth before turning east into the interior ocean.



## Acknowledgements

How far back does one go in their acknowledgements? I decided to go back to that fateful day when the thought of being an oceanographer first occurred to me. I was sixteen, and my father asked me what I wanted to be when I grew up. Apparently Dad didn't know that the answer to that question changed weekly, but I gave it my best shot. "An oceanographer" was my reply. Soon, of course, the answer was a musician; nevertheless, Mom and Dad encouraged me to work hard, make my own choices and look forward to challenges. All that plus their love has brought me farther than I ever imagined.

Since then I have been encouraged by many people. Faculty at the University of California, Irvine, urged me to continue my graduate studies. Many students at MIT and WHOI have cheered me on, offering friendship, advice, softball games and great scientific discussions. Special note has to go to LuAnne Thompson and Greg Johnson who combined all the above with superb food on a *very* regular basis in the last few months of my pregnancy. In addition, many staff members at WHOI have made my work there easier; I think you all know who you are. Two rose continually above the call of duty: Theresa Turner and Ruth Gorski. Thank you!!!

My committee members, both past and present, have all contributed to the evolution of my thesis and my evolution as a scientist. Glenn Flierl, who sits on more committees than any three people should, offered a number of incisive comments along the way. John Toole took me on my first cruise; in addition to midnight watch he shared his enthusiasm for boat racing, science and New Zealand. He has been a wonderful advocate and has offered many useful ideas on my work. Mindy Hall and Nick Fofonoff took me on my next cruise; I learned that oceanography could be a *high* seas adventure. The cruise was also a lesson in dealing with less than optimal data collection (a sad but necessary lesson for any experimentalist). Mindy and Nick contributed at many stages to this work, both through scientific conversations and written commentary.

After I'd been broken in I went to sea with my advisor, Mike McCartney (Always, always, always think three times before agreeing to do any cruise with Gerard bottles). Throughout my work with him Mike has always tried to be a mentor; usually he succeeded. He built my confidence in my ability to do good scientific work and showed his confidence by turning a large data set over to me for analysis. In addition to being a hydrography guru, Mike has constantly reminded me that this work is truly fun – being able to earn a living studying anything is a wonderful opportunity (studying the ocean is a bonus). I'm looking forward to spending more of my time learning about the ocean.

Natalie has been a source of joy and grace since she first got here. She certainly keeps the rest of my life in perspective. While I can't say she made the thesis process easier she did make it more interesting. I might never have finished if I didn't think Natalie was getting wonderful, loving care in my absence, and for that I thank Suzie Szava-Kovats.

Acknowledging the extent of support I have gotten from my husband, Steve, is virtually impossible. He has cheerfully filled the roles we usually share and has been chief cheerleader, editor, cook, launderer and best friend. Now what will we do for fun?

Financial support for the data collection and initial analysis was provided through the Office of Naval Research South Atlantic Accelerated Research proposal under contract N00014-82-C-0019. Continued analysis was supported by the National Science Foundation under grant OCE86-14486.

Val Worthington once offered a copy of his book to any student who wrote a haiku about their thesis. The idea of summarizing one's thesis in seventeen syllables is a bit daunting, but I know not many people will read my whole thesis, so I thought I'd give it a try. For those of you who fall into the above category (or who just appreciate bad poetry) here it is.

Warm surface current  
Fed by recirculation  
Becomes deep and strong.

## Chapter 1

### Introduction

Western boundary currents entrance oceanographers. These strong currents close the circulation of the subtropical gyres in each ocean: the Gulf Stream in the North Atlantic, the Kuroshio in the North Pacific, the Agulhas in the Indian Ocean and the Brazil Current in the South Atlantic. The relatively narrow, high velocity currents are critical to general circulation schemes for the large basins; they are important in the balances of mass, heat, salt, and other nutrients. What really intrigues us, is that after literally hundreds of years of study, we continue to learn more about western boundary currents.

Theoretical investigations of western boundary currents (the majority of which are specifically about the Gulf Stream) generally take one of two approaches: examining the current as an integral element of the entire basin circulation, or treating it as an entity unto itself. In the first group are early theoretical investigations which showed that western boundary currents could result from gyre-scale wind forcing (Stommel, 1948) or inertial effects (Fofonoff, 1954). These initial idealized models have been extended in numerous ways to include more layers, topographic forcing or other effects. In a different vein are the large scale computer models of general circulation (e.g. Holland and Lin, 1975) which resolve many scales of motion and are able to reproduce some of the characteristics of western boundary currents.

Models in the second group are usually designed to look at a specific feature of the

current such as growth, separation or instability. For example, Rossby (1936), in an effort to explain the downstream growth of the current, modeled the Gulf Stream as a turbulent jet which entrained water downstream. Warren (1963) developed a model of the Gulf Stream which treated it as a narrow jet whose path was determined by changes in latitude and topography, i.e., vorticity. Stommel (1954) modeled a constant potential vorticity current which gave a velocity profile similar to the Gulf Stream.

An even simpler way to look at western boundary currents is to treat them just as the closure for a wind driven circulation. Using wind stress estimates for a basin to drive a Sverdrup interior, one can calculate the western boundary current transport needed to balance the system. One of the problems that this raises is that wind stress estimates for the North and South Atlantic suggest that the Brazil Current and Gulf Stream should be of the same size, in fact, Godfrey (1989) computed a larger Brazil Current than Gulf Stream. Most experimental studies have not shown this to be true. The Gulf Stream is almost always reported to be much larger than the Brazil Current. Stommel (1965) suggested the difference in the thermohaline circulation was the cause of the difference in strength of the currents, with the Gulf Stream being augmented by the surface thermal circulation, and the Brazil Current being degraded by the northward surface thermal circulation (fig 1.1). Indeed, the South Atlantic is unique in the sense that it is the only ocean with meridional heat flux towards the equator (Bryan, 1962). The complicated structure of the thermohaline circulation in the South Atlantic creates one of the perennial problems for those who study the Brazil Current: how to define the Brazil Current.

The general path of the Brazil Current was mapped by Rennell (1832) on the basis of surface currents (fig 1.2). He described the Brazil Current branching off the Equatorial Current at about  $8^{\circ}$  S, and continuing as a weak current to about  $17^{\circ}$  S, where it was strengthened by drift currents of the South East trade winds. Rennell's Brazil Current continued down the coast to Cabo Frio, where the coastline breaks, throwing the current farther offshore for a stretch until it rejoined the coastline at

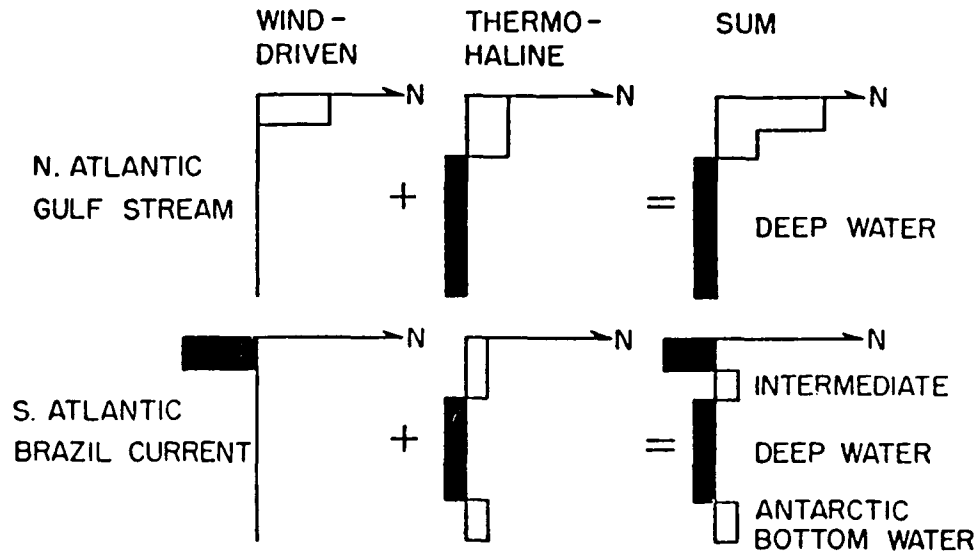


Figure 1.1: Schematic diagram of a possible explanation of the different transports of the Gulf Stream and the Brazil Current. from Stommel (1965).

about 30° S. His description breaks down at La Plata river, which he has emerging as a strong oceanic stream. His Brazil Current branches in two, one part forming part of the Southern Connecting Current (the Brazil-Falklands confluence), and the other continuing south of La Plata, eventually rounding Cape Horn. Findlay (1853) corrects the direction of flow to the south of La Plata; he shows the Cape Horn Current (Falklands Current), coming north along the coast and joining the Southern Connecting Current.

More modern descriptions of the Brazil Current differ only in detail from the above description; they also illustrate some of the problems involved in estimating transport of the Brazil Current. The warm, saline surface current flows south, drawing only 4 Sv from the South Equatorial Current (Peterson and Stramma, 1991). At about 15° S the shelf widens, causing the current to move farther away from the coast, although it sometimes meanders onto the shelf. At 20.5° S the current encounters the Vitoria-Trindade Ridge, where it splits to follow several paths through the ridge (Evans, Signorini and Miranda, 1983). Off the coast of Cabo Frio, at 23° S, the current usually meanders offshore, but direct current

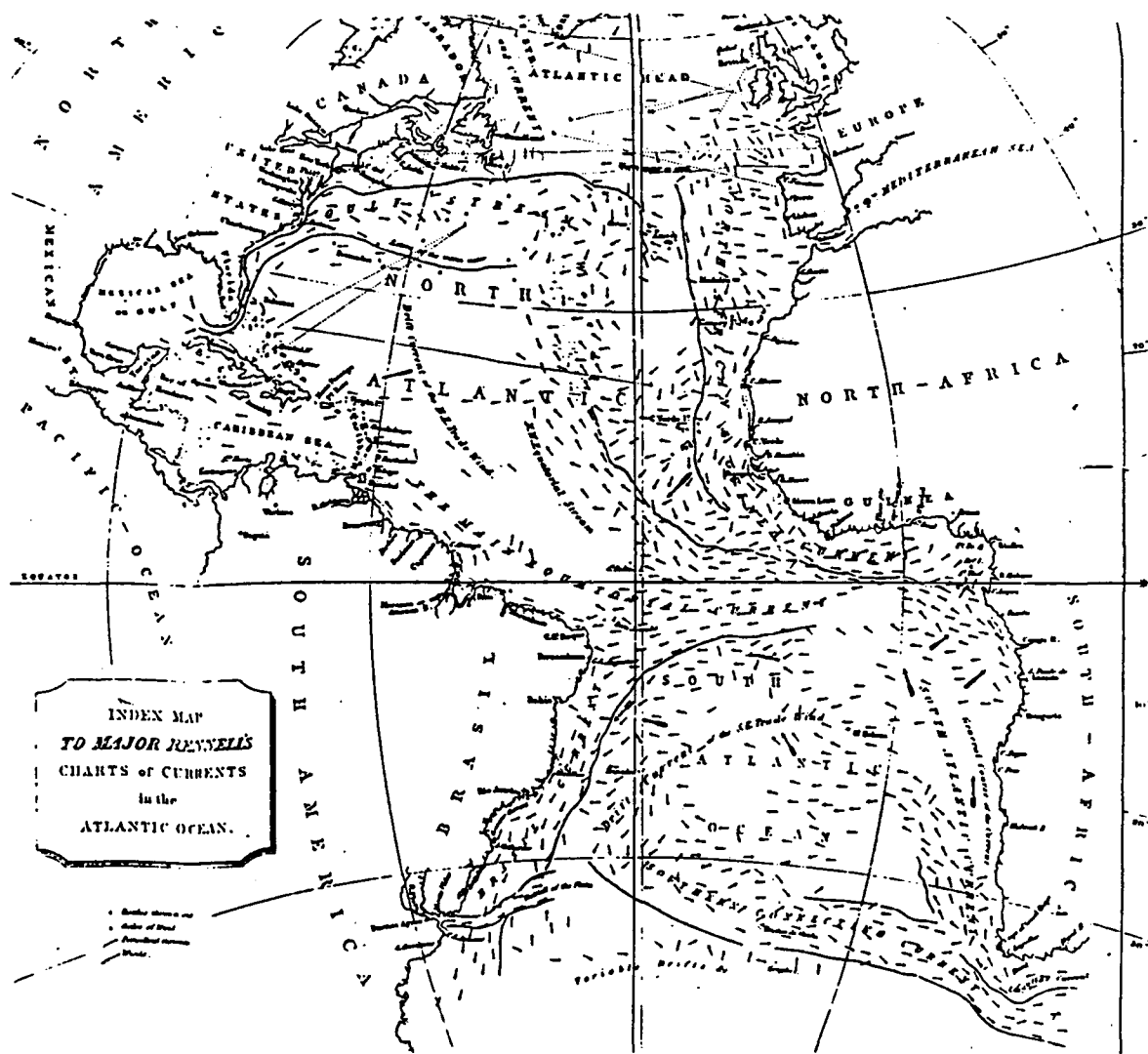


Figure 1.2: Surface currents of the South Atlantic as charted by Major Rennell (1832).

measurements in the area suggest that half the current is still confined to the shelf, inshore of the 200 m isobath (Evans and Signorini, 1985). Indeed, satellite images of the region suggest that the inshore edge of the current may be on the shelf from 21° to 35° S (Garfield, 1988). South of Cabo Frio the transport of the Brazil Current grows at a rate of five percent per 100 km (Gordon and Greengrove, 1986). The growth has led some to suggest the presence of a recirculation cell offshore (Gordon and Greengrove, 1986; Stramma, 1989). Stramma estimates the strength of the recirculation at 30° S to be 7.5 Sv. At about 36° S the Brazil Current joins with the northward flowing Falklands Current in an eastward confluence.

Not mentioned at all in the above description is the presence of a southward deep western boundary current of North Atlantic Deep Water. The fact that it flows in the same direction as the surface western boundary current, brings about part of the problem of how to define the Brazil Current. Historically, the Brazil Current is defined to be a warm, saline surface current. The obvious problem with this definition is that, by definition, the Brazil Current cannot deepen. A second definition, similar to that for the Gulf Stream, is that the Brazil Current comprises all the contiguous southward flowing water aligned with the surface expression. The problem with this definition is that as the current deepens, it eventually joins with the southward flowing North Atlantic Deep Water; this results in a large jump in transport. This ambiguity does not pertain to either the Gulf Stream or the Kuroshio because they have no deep western boundary currents flowing in the same direction as the surface current.

A simple solution would be to omit the term Brazil Current from the discussion and just present total transports. Although this accomplishes the goal of not mixing interpretation with observation, it seems a bit extreme. The second definition seems to be the only way to consistently compare the Brazil Current with other western boundary currents, and it is the definition used here. However, the transport results from this data set will be presented with both surface layer and total transports, so that comparisons can be made with either definition.



Despite an inability to agree on what constitutes the Brazil Current, the last decade has seen a resurgence of interest in the Brazil Current, with several studies recently completed. These experiments have focused on two regions: 19 to 24° S, the nutrient rich fishing grounds off the coast of Brazil, and 38 to 42°S, the Brazil-Falklands confluence region. Between the two regions are the Meteor (1925) section at 28° S, the IGY (1959) section across 32° S and the CATO (1972) section at 33° S. A table summarizing the results is given in chapter 3 (Table 3.1). It shows a fair amount of variation in transport estimates which are taken at the same latitude. These differences have four main sources: incomplete sampling of the current, the reference choice used for the velocity shear profiles, temporal variations in the data, and the definition of the Brazil Current. We have already discussed the problems involved in defining the Brazil Current. Little can be done about time dependent variations in the transport; obviously changes will occur, and those changes are part of the rich nature of the study of oceanography. The choice of a reference surface has been an ongoing debate ever since this method of transport calculation was developed. There may be good reason to question some of the choices made (and this is done in chapter 3), but there is a legitimate range of choices, and this will continue to be true until more direct velocity measurements are made. Incomplete sampling of the current is largely a result of its geographic lie. The current frequently runs over the shelf, and it is difficult to get measurements in shallow water where the current is very strong. For this reason, it is difficult to sample the inshore edge of the Brazil Current. In addition, much of the remainder of the current lies over a region with a strongly sloping bottom, making calculation of transport near the bottom difficult if the hydrographic stations are not close.

The collection of the data used in this thesis is one attempt to alleviate many of these problems. Sampling of four cross sections of the Brazil Current was done inshore to a depth of 150 m (fig 1.3). In the slope region, station spacing averaged 17 km, which enables better estimates of bottom transport. Farther offshore, station spacing averages 40 km. In addition to being a high resolution data set (measuring

pressure, temperature, salinity, oxygen, silicate, phosphate and nitrate), the region surveyed lies between the fishing grounds and the retroflection. The four Brazil Current crossings were nominally at 27, 31, 34, and 36° S. They were sequential in time, taken as one cruise, in the time period from November to December 1984. The cruise was part of the Thomas Washington Marathon Cruise, leg 9. The two northern sections extend offshore to the far side of the Vema Channel; the two southern sections extend about 1000 km offshore. The resulting data set is therefore appropriate for addressing some of the problems surrounding the mid-regions of the Brazil Current.

The main focus of this thesis is the transport of the Brazil Current between 27 and 36° S. To that end, the characteristics of the main water masses in the Brazil Current region are described in chapter 2. The water masses are traced through the four sections of data in an effort to deduce flow direction. The water mass analysis is used to choose zero velocity surfaces for the velocity sections (chapter 3). From these, transport estimates for the Brazil Current are calculated for each section. Various alternate choices for the zero velocity surface (ZVS) are also explored.

Because there is some arbitrariness to the choice of the ZVS, some further investigation is warranted. Several different approaches to this could be taken. One approach would be to do an inverse calculation using the data. This method involves setting limits on certain definable quantities, such as heat flux, salt, and mass balances, making a best first guess of what the ZVS should be, and then adjusting this first estimate so that the limits which have been set are satisfied. One could imagine doing an inverse calculation on the boxes formed by this data; however, this was not done for two reasons. First, Rintoul (1988), in his inverse of the South Atlantic found the conservation of salt constraint added little information to that contained in the mass conservation constraints, and second, the transports over the shelf (which are not measured) can be significant. Both of these would reduce the constraints on an already underconstrained system. Instead, a different approach has been taken. A simple, multilayer model has been constructed across the basin

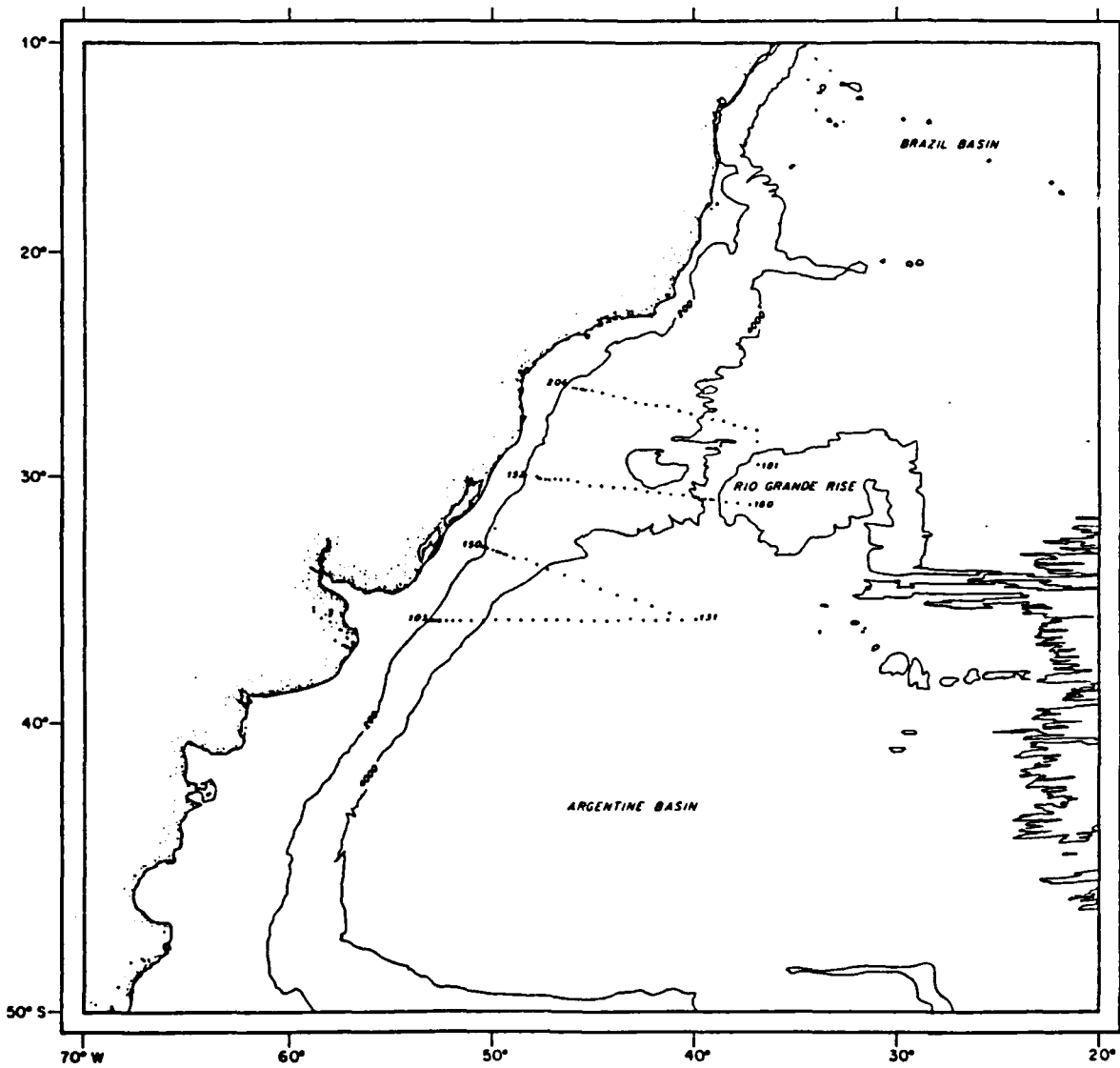


Figure 1.3; Location of the four transects of the Brazil Current taken on the Thomas Washington Marathon Cruise, Leg 9.

at one latitude to look at gross mass balances (chapter 4). Initial baroclinic transports are determined by the slope of various isotherms across the South Atlantic basin, which reflect the equatorward heat flux found in this ocean; these are balanced with computed barotropic transports and layer-to-layer exchange. It is essentially a constrained inverse, and allows one to explore a range of barotropic transports and the effect they have on the solution in the rest of the basin. The goal is not to find "the right" solution, but rather, to observe how different choices for the barotropic portion of the Brazil Current affect the solution across the basin.

Finally, the data will be used to construct potential vorticity sections for the four transects (chapter 5). The use of potential vorticity to construct theoretical models of western boundary currents leads one to try to calculate the actual potential vorticity profile. Away from regions of strong mixing or forcing, potential vorticity should be conserved following streamlines; this is assumed to be true in many models. Thus, it would be useful to try to calculate the potential vorticity, and to determine whether it is conserved downstream. Although calculating planetary potential vorticity from hydrographic data is simple, trying to obtain meaningful relative vorticity estimates is more difficult. The ability to do so, however, would greatly enhance the usefulness of hydrographic measurements in areas of high velocity.

## **Chapter 2**

### **Water Masses in the Brazil Current Region**

To compute velocity from hydrographic data, a reference velocity at some depth has to be determined. In the absence of other data, a choice can be made by tracing patterns in the water masses. Water mass characteristics often can be mapped from source regions throughout ocean basins, providing an indication of the "spread" of the water mass. In a very well sampled survey such maps would provide a three dimensional picture of the flow path of a water mass. In the four Brazil Current transects, the water masses are traced by following the changes in isolated extrema, i.e. they are extrema both vertically and horizontally; these are referred to as water mass "cores." The assumption made in this method is that the direction of flow of the water mass should be consistent with the information found tracing the cores through the sections. This does not mean that mixing and diffusion of the water mass characteristics are not taking place — the erosion of the cores clearly indicates that they are. Rather, the underlying assumption is that the spread of a water mass is driven primarily by advection.

The Brazil Current region has six major water masses in its system: Central Water (CW), Antarctic Intermediate Water (AAIW), Upper Circumpolar Water (UCPW), North Atlantic Deep Water (NADW), Lower Circumpolar Water (LCPW), and Antarctic Bottom Water (AABW). Extensive descriptions of the water masses can be found in Reid, Nowlin and Patzert (1977) and Reid(1989). Some of that

information is summarized here in order to develop a more basin-wide perspective. Each water mass is first described in terms of its source region and characteristics. A meridional transect is shown which shows some of the spread of the water masses. Then the four density sections from each Brazil Current transect are described to provide a structure for tracing the water masses. As the water masses are followed through the four sections, an indication of the flow is given which will be used in chapter 3 to calculate velocity.

The water masses are described here primarily in terms of their signatures in fields of potential temperature ( $\theta$ ), salinity, dissolved silica (silica), and dissolved oxygen (oxygen) concentrations. Other tracers (phosphate, nitrate, and in situ temperature) are available, but the information they contain is consistent with that in the tracers discussed here. Thus, to avoid too much repetition, I limit the discussion to four tracers and present the others in Appendix A.

## 2.1 Water Mass Characteristics

The water masses are characterized in this section by  $\theta$ , salinity, oxygen and silica. Meridional sections of each, from Reid (1989) are shown (fig 2.1- 2.4) as well as some station plots of  $\sigma_2$ -salinity and  $\sigma_2$ -oxygen (fig 2.5 and 2.6). The description proceeds from top (CW) to bottom (AABW).

From the surface down through the thermocline the slope of the  $\sigma_2$ -salinity curve is basically constant; this is the Central Water (CW). It is generally warm, salty water, although some low salinity shelf water is occasionally found. Nutrient concentrations are low because of biological activity. In the sections (fig 2.1 - 2.4) CW is most extreme at the surface in the north; its signal has generally disappeared by 40° S, as the water has gone east in the Brazil-Falklands Confluence. Antarctic Intermediate Water (AAIW), below CW, is low in salinity and high in oxygen and silica. It can be seen in the sections at about 1000 m at 32° S, and traced back to

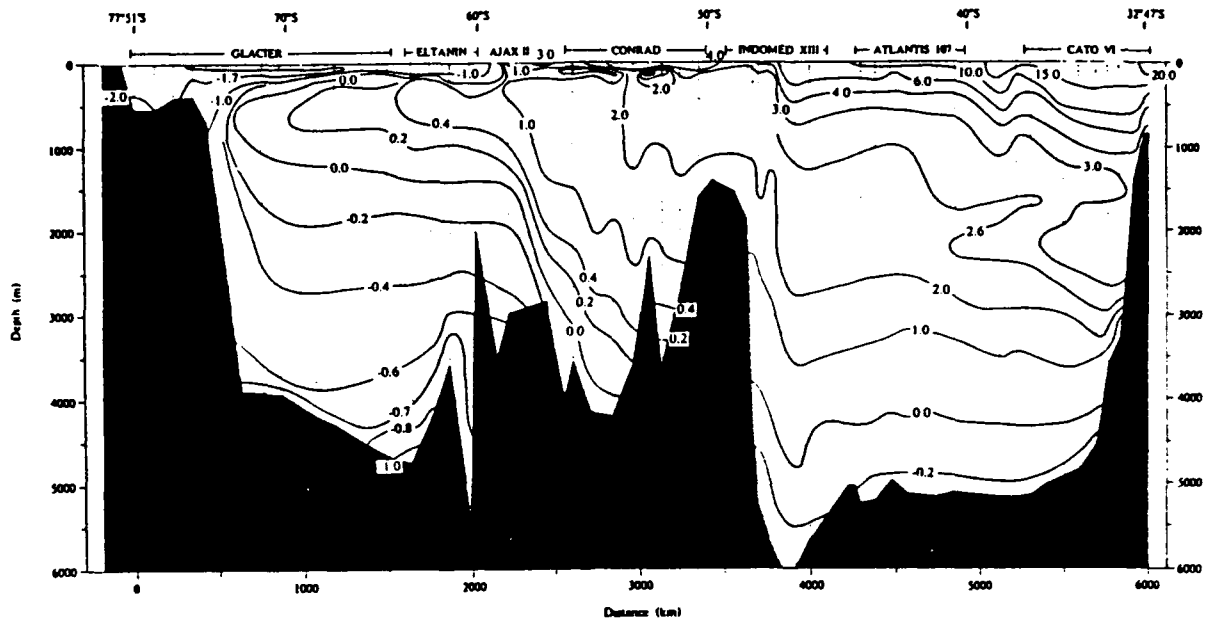


Figure 2.1: Potential temperature ( $^{\circ}\text{C}$ ) section from Antarctica to Brazil, along  $40^{\circ}\text{W}$  in the Weddell Sea and northwestward to the coast at  $32^{\circ}\text{S}$ . From Reid (1989).

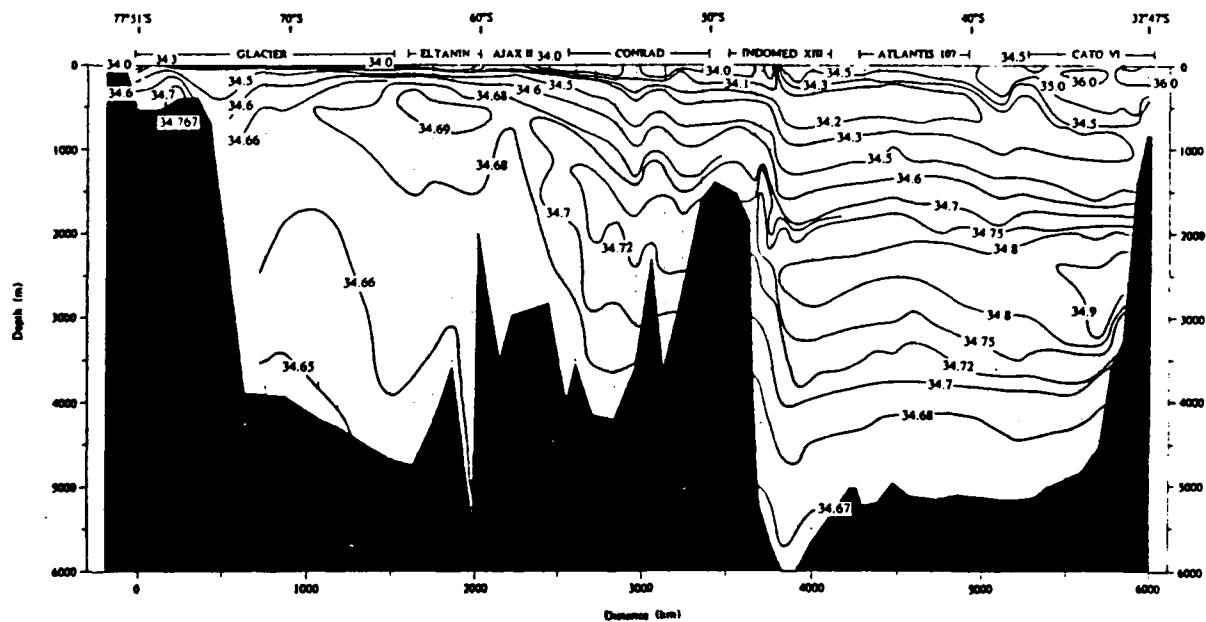


Figure 2.2: Salinity (psu) section from Antarctica to Brazil, along  $40^{\circ}\text{W}$  in the Weddell Sea and northwestward to the coast at  $32^{\circ}\text{S}$ . From Reid (1989).

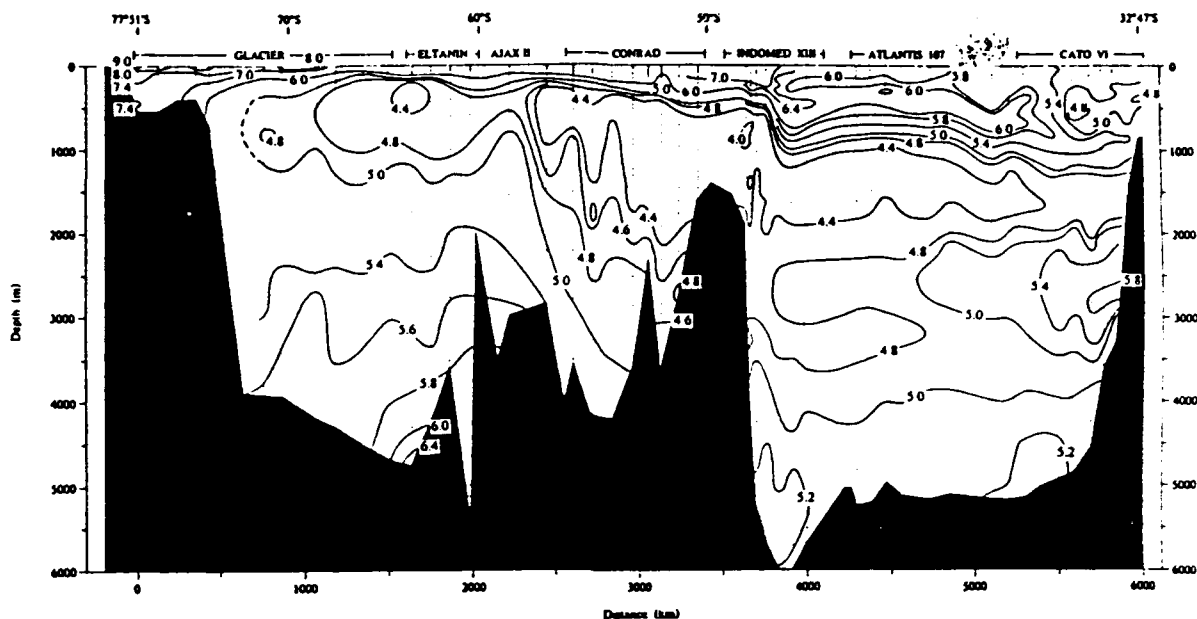


Figure 2.3: Oxygen section from Antarctica to Brazil, along 40° W in the Weddell Sea and northwestward to the coast at 32° S. From Reid (1989).

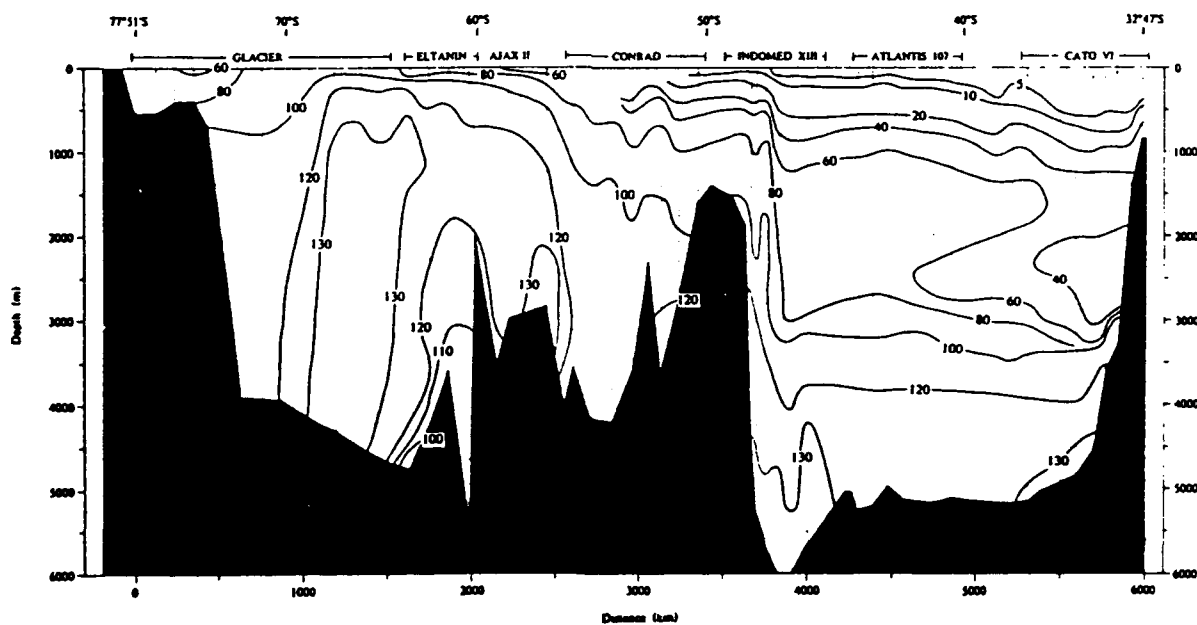


Figure 2.4: Silica section from Antarctica to Brazil, along 40° W in the Weddell Sea and northwestward to the coast at 32° S. From Reid (1989).



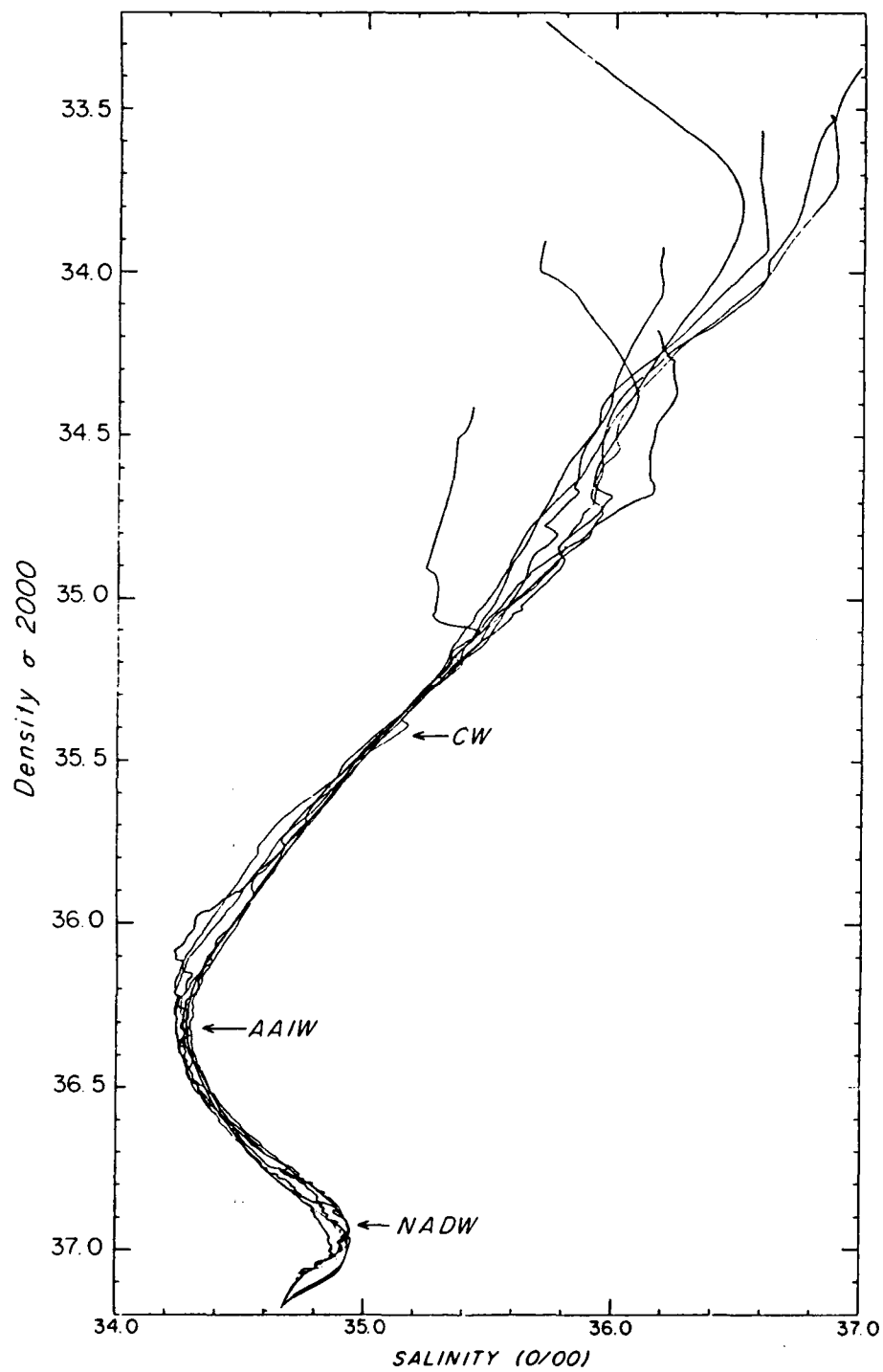


Figure 2.5: Salinity plotted as a function of sigma two for various stations from the Thomas Washington data set.

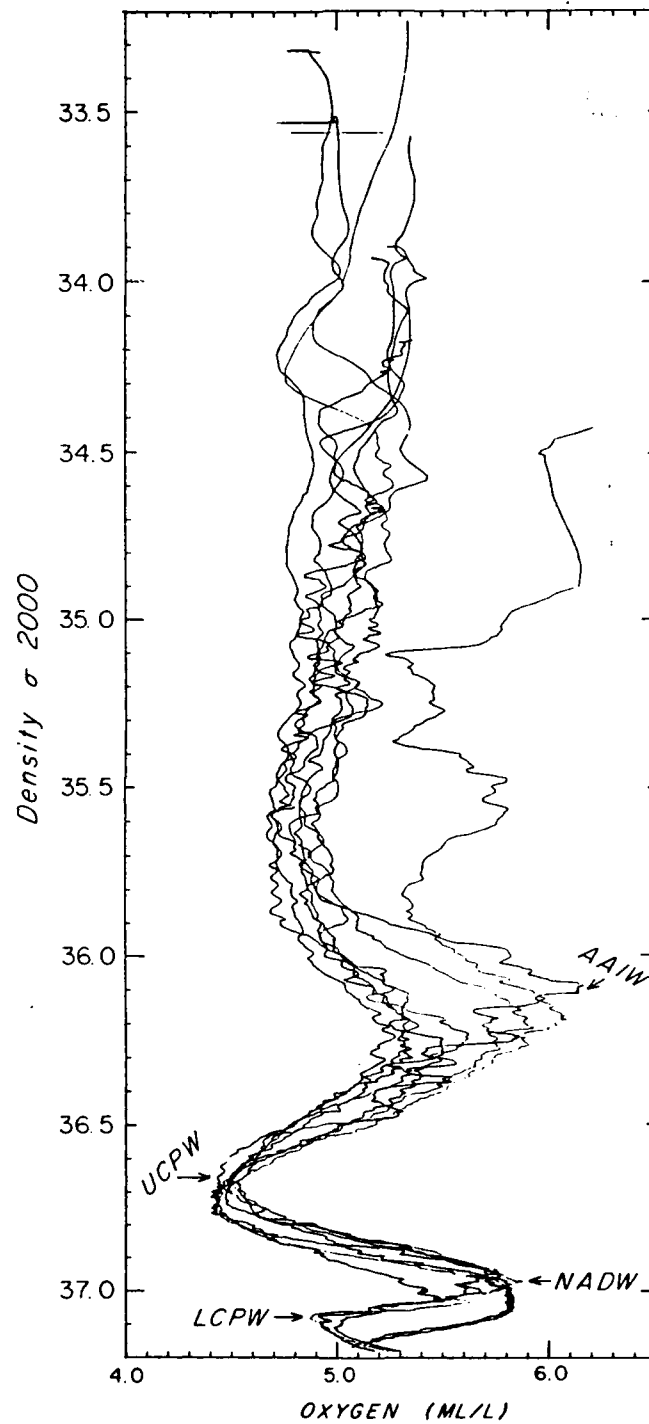


Figure 2.6: Oxygen plotted as a function of sigma two for various stations from the Thomas Washington data set.

the south to about 50° S. The extrema can be seen in each property-property plot at  $\sigma_2$  near 36.2. Next in the water column comes Upper Circumpolar Water (UCPW), whose primary characteristic is low oxygen. In the oxygen section, fig 2.3, it can be seen at 1500 m at about 36° S as a 4.4  $ml\ l^{-1}$  contour. This extends southward to the circumpolar region. It can also be seen as a high in the silica section. The  $\sigma_2$ -salinity plot shows stations with UCPW as slightly less salty than those with no UCPW; the  $\sigma_2$ -oxygen plot shows a clear low at 36.7  $\sigma_2$ .

North Atlantic Deep Water (NADW), below UCPW, is high in salinity and oxygen, low in nutrients. NADW forms the “knee” seen in the  $\sigma_2$ -salinity plot. It “splits” the circumpolar water into two parts, as is seen in the  $\sigma_2$ -oxygen plot. This image of the circumpolar water being split is strengthened in the sections, where NADW intrudes from the north at about 2500 m; the signal weakens to the south. Lower Circumpolar Water (LCPW) below is low in oxygen, similar to UCPW. The sections show UCPW extending farther north than LCPW, and circulation maps (Reid, 1989) show LCPW turning east. In the four Brazil Current transects, LCPW is not found in the northern two sections. Thus an offset can be seen in both property-property plots between the stations in the north and those in the south. The deepest water mass, Antarctic Bottom Water (AABW), is of southern origin. Its high oxygen and silica, and low salinity, can be seen in cores near the bottom of the sections. Clearly the topography prevents following the “spread” of the water mass through the section; it is moving perpendicular to this section where the cores are seen (see fig. 30 in Reid (1989)).

To summarize, CW and NADW have their sources in the north; AAIW, UCPW, LCPW and AABW all have southern sources.

## 2.2 The Density Structure of the Sections

Before looking at the tracer sections, the general structure of each section should be established. Using sections of density, stations groups are associated with the Brazil Current, the recirculation or counterflow, the Vema Channel, etc. When tracers are discussed, if a core is said to be in or under the Brazil Current, it should be understood that it lies in those stations which have been identified as having Brazil Current shear in their surface layers. Brazil Current shear at the surface occurs when isopycnals are shallower in the west (on the left) than in the east; this may also be described as isopycnals sloping down. The stations considered to be part of the Brazil Current are marked in each section, as are those of the counterflow, or recirculation. The counterflow (flow going counter, or opposite the Brazil Current) is that region with surface shear of the opposite sense of that in the Brazil Current (i.e. isopycnals deeper in the west than in the east) just offshore from the Brazil Current. In later chapters the counterflow will be shown to be a recirculation cell for the Brazil Current.

The locations of the four transects (nominally at 27, 31, 34, and 36° S) are shown in fig 1.3. The density sections (fig 2.7 - 2.10) are of stacked potential density anomaly ( $\sigma$ ):  $\sigma$  referenced to zero decibars ( $\sigma_0$ ) down to about 1000 m,  $\sigma$  referenced to two thousand db ( $\sigma_2$ ) down to 3000 m, and  $\sigma$  referenced to four thousand db ( $\sigma_4$ ) below. Stacked  $\sigma$  allows the entire density field to be contoured without introducing the artificial density inversions that would result from a single  $\sigma$ . In addition, the slope of the isopycnals reflects the local geostrophic shear.

The Brazil Current at 27° S is shallow (fig 2.7). Brazil Current shear is found down to 1000 m (sta. 199-206), with an offshore counterflow (sta. 196-199) extending to 750 m. Below the counterflow the sign of the shear reverses, as can be seen in the 36.8 and 36.9  $\sigma_2$  surfaces. Offshore, very little structure is found in the upper water column density. Between stations 190 to 196 the 36.9 to 37.0  $\sigma_2$  contours spread apart, with strong shear below. The deep stations, 184 to 190, are at the northern

edge of the Vema Channel and have deep shear.

At 31° S the Brazil Current shear is deeper (fig 2.8). Stations 153 to 160 show Brazil Current shear down to the bottom, with an offshore counterflow (sta. 160-164) to 2500 m. Below 2500 m the sign of the shear reverses. Again, the upper waters offshore show very little structure, but strong horizontal density gradients are found deeper in the Vema Channel (sta. 172-178). Above the deep shear in the Channel the isopycnals change slope, at about the 37.0  $\sigma_2$  surface.

The structure of the Brazil Current at 34° S (fig 2.9) differs markedly from the previous sections. In the upper thousand meters, Brazil Current shear and a counterflow are found (sta. 142-150 and sta. 139-142 respectively). However, the baroclinic signature in the counterflow is stronger than that in the Brazil Current, i.e. if an 800 or 900 m zero velocity reference were used for both the current and counter flow, the transport in the counterflow would be greater. Below 1000 m, the shear under both regions has the same sign as that in the Brazil Current. Offshore of the current and counter flow, the isopleths slope down, top to bottom (sta. 131-139). The net baroclinic shear across this section is large.

The final section at 36° S has Brazil Current shear extending from the surface to the bottom (fig 2.10). Inshore of the Brazil Current the slope of the isopycnals indicates northward flow (sta. 103-109); this is the Falkland Current intruding from the south. Off the shelf, the Brazil Current is in deep water, with coherent top to bottom shear (sta. 109-114). In the counterflow, above the 37.0  $\sigma_2$  contour, the isopycnals slope up quickly, flatten out, and then rise again (sta. 114-123), recovering the full shear of the Brazil Current. Below the 37.0 contour the isopycnals continue to slope down a few more stations before rising; they do not recover fully. Beyond station 123 the shear reverses again, coherent from top to bottom, with the net baroclinic shear across the section large. Apparently the section crosses the Brazil Current as it begins its meandering to the east.

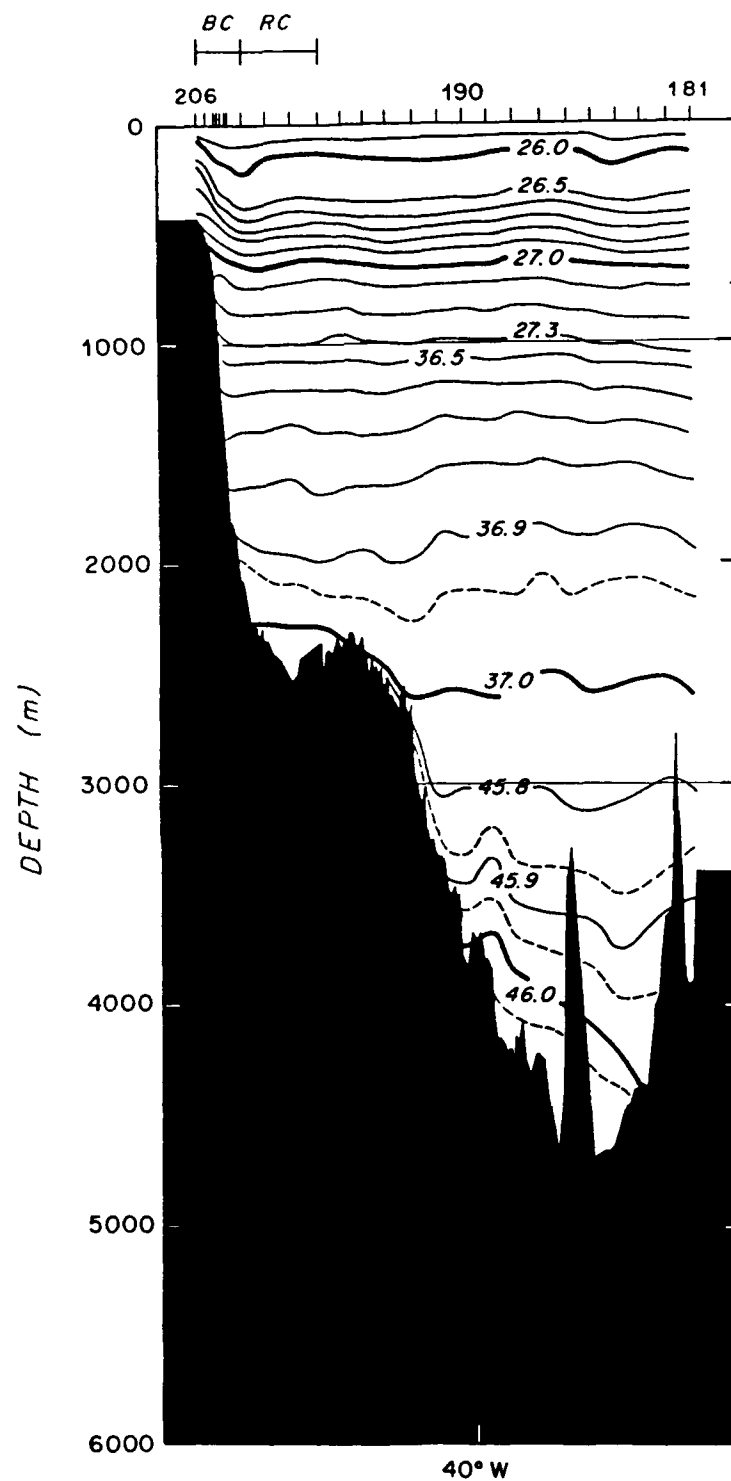


Figure 2.7: Section of potential density anomaly ( $\text{kg m}^{-3}$ ) with several reference pressures at 27° S. From the Thomas Washington Marathon Cruise, Leg 9.

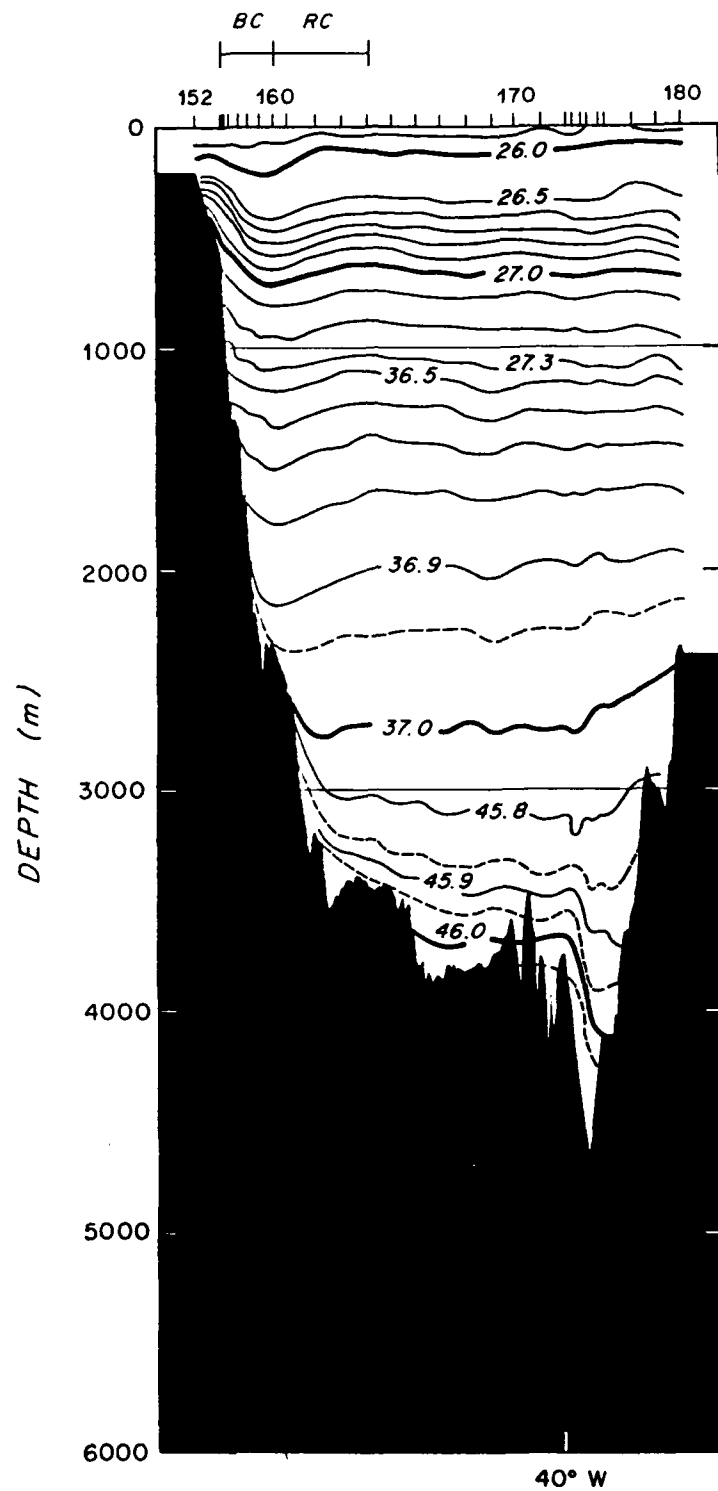


Figure 2.8: Section of potential density anomaly ( $kg\ m^{-3}$ ) with several reference pressures at  $31^{\circ}$  S. From the Thomas Washington Marathon Cruise, Leg 9.

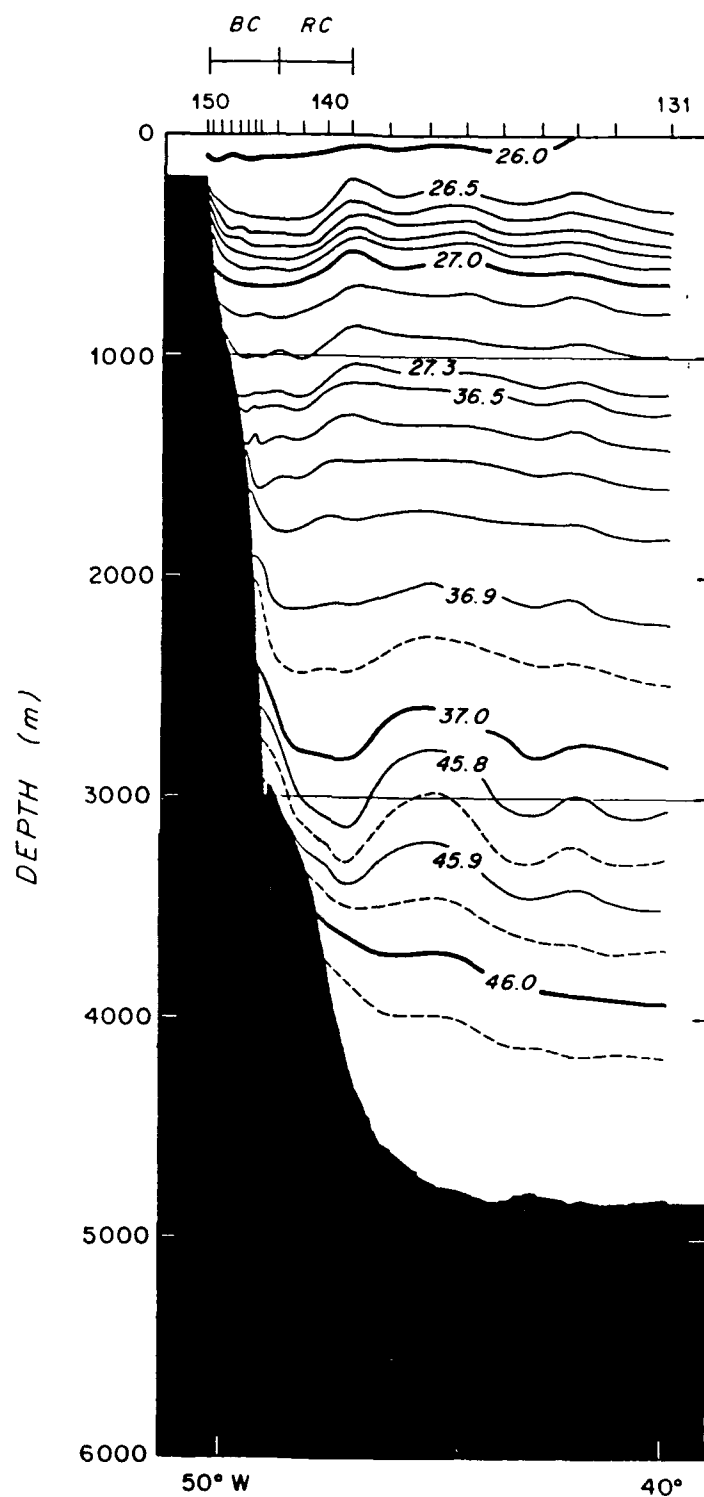


Figure 2.9: Section of potential density anomaly ( $\text{kg m}^{-3}$ ) with several reference pressures at 34° S. From the Thomas Washington Marathon Cruise, Leg 9.



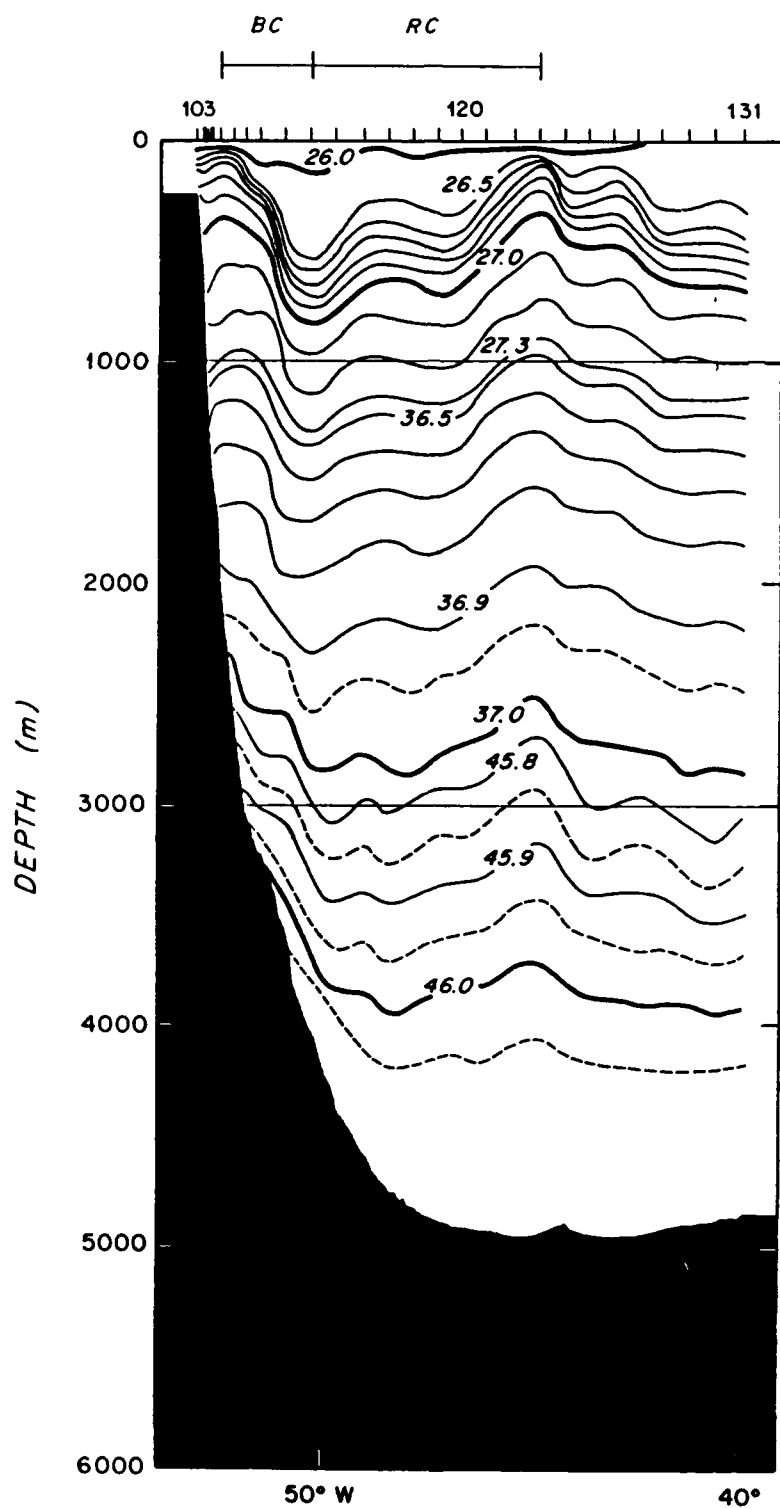


Figure 2.10: Section of potential density anomaly ( $kg\ m^{-3}$ ) with several reference pressures at 36° S. From the Thomas Washington Marathon Cruise, Leg 9.

## 2.3 The Water Masses

This section traces the six water masses through each of the four transects, moving from north to south. Each water mass is identified with a particular density range; this is for convenience – it is not meant to imply that all the water within a given density range is all from a single source. The characteristics being followed are described in section 2.1. Contoured sections of the tracers are used to follow the water masses through the transects. Figures 2.3 to 2.14 (a.  $\theta$ , b. salinity, c. oxygen, and d. silica) are the sections from the transects at 27, 31, 34, and 36° S, respectively. Contoured sections of temperature, phosphate, and nitrate are in Appendix A; the density sections are presented in figures 2.7 to 2.10. The water masses are traced through the transects in order to establish the flow direction of each water mass and to ascertain where, in each transect, that direction is well or ill defined. The direction of flow is determined by following the erosion of the water mass characteristics through the sections. The results will be used in chapter 3 to determine zero velocity surfaces for each transect.

### 2.3.1 Central Water

The changes in CW (the surface down to 27.1  $\sigma_0$ ) clearly show the characteristics of the northern origin water eroding away as we move downstream. The warm salty surface water found at 27° S (fig 2.3) remains about the same temperature at 31° S (fig 2.12), 20 C, but the 36.5 psu salinity contour shrinks to a surface core in the Brazil Current. At 34° S (fig 2.13) the 36.5 psu salinity contour disappears, and the 36.0 psu contour is a core in the Brazil Current and recirculation. The 20°C temperature contour is similarly reduced. Finally at 36° S (fig 2.14) the 36.0 psu core shrinks further, and the 20 C temperature core is a small blip in the section.

This pattern, both of the most extreme northern origin water being found in the current and of the slow erosion of northern characteristics in the tracers, indicates

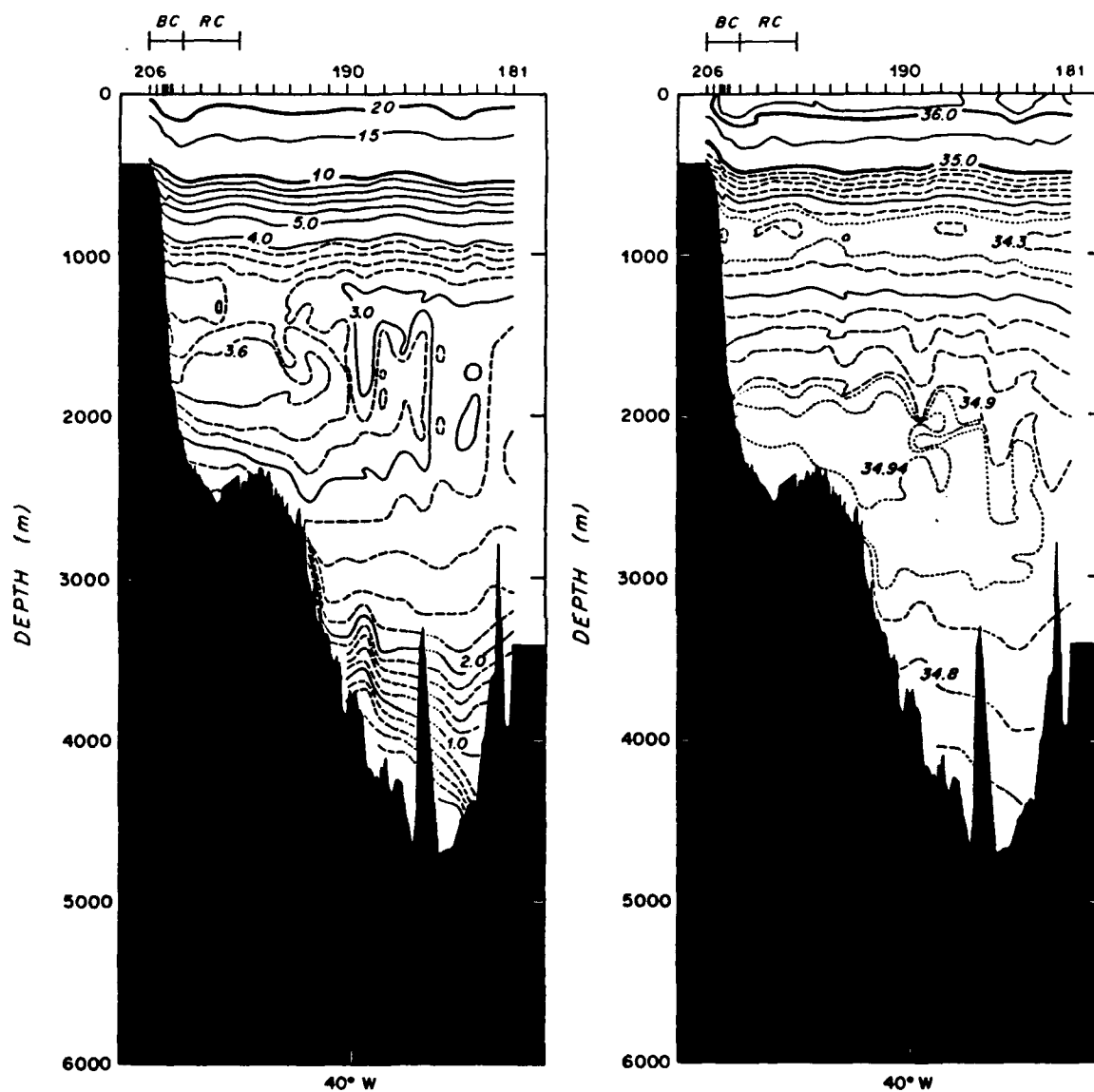


Figure 2.11: Sections of (a)  $\theta(^{\circ}\text{C})$  and (b) salinity (psu) for 27° S. From the Thomas Washington Marathon Cruise, Leg 9.

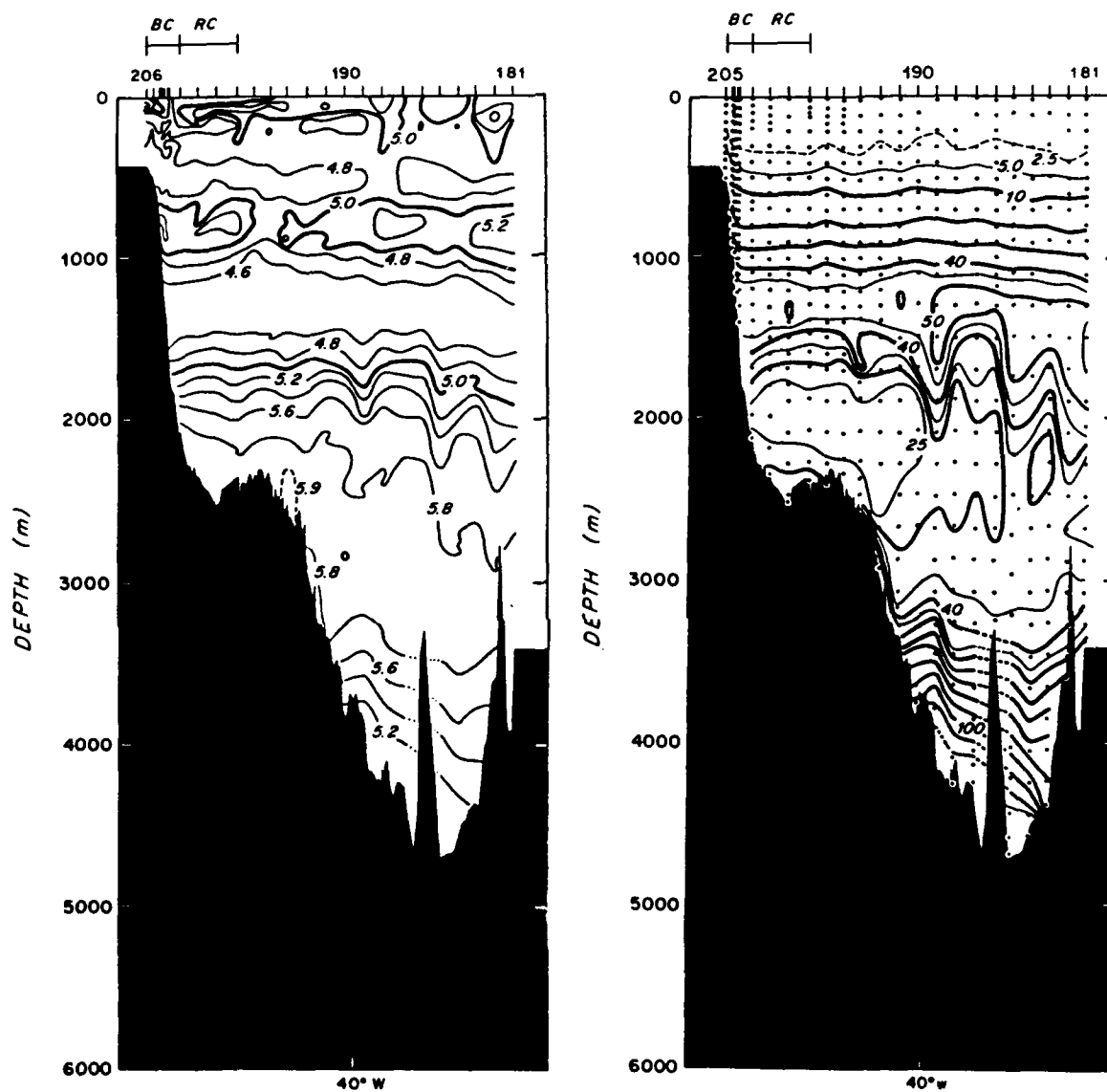


Figure 2.11: Sections of (c) oxygen ( $\text{ml l}^{-1}$ ) and (d) silica ( $\mu\text{mole l}^{-1}$ ) for  $27^\circ \text{S}$ . From the Thomas Washington Marathon Cruise, Leg 9.

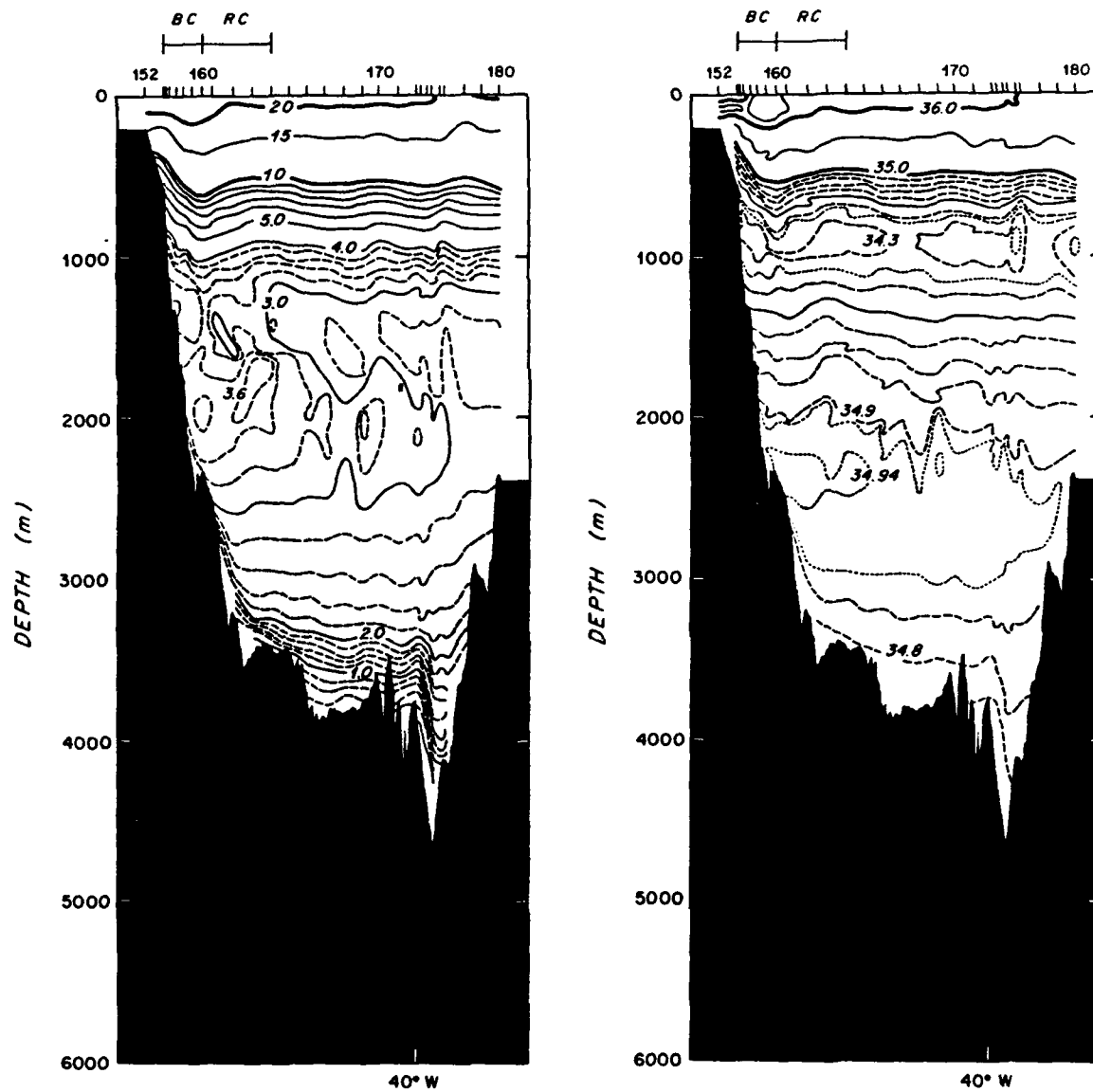


Figure 2.12: Sections of (a)  $\theta(^{\circ}\text{C})$  and (b) salinity (psu) for  $31^{\circ}\text{S}$ . From the Thomas Washington Marathon Cruise, Leg 9.

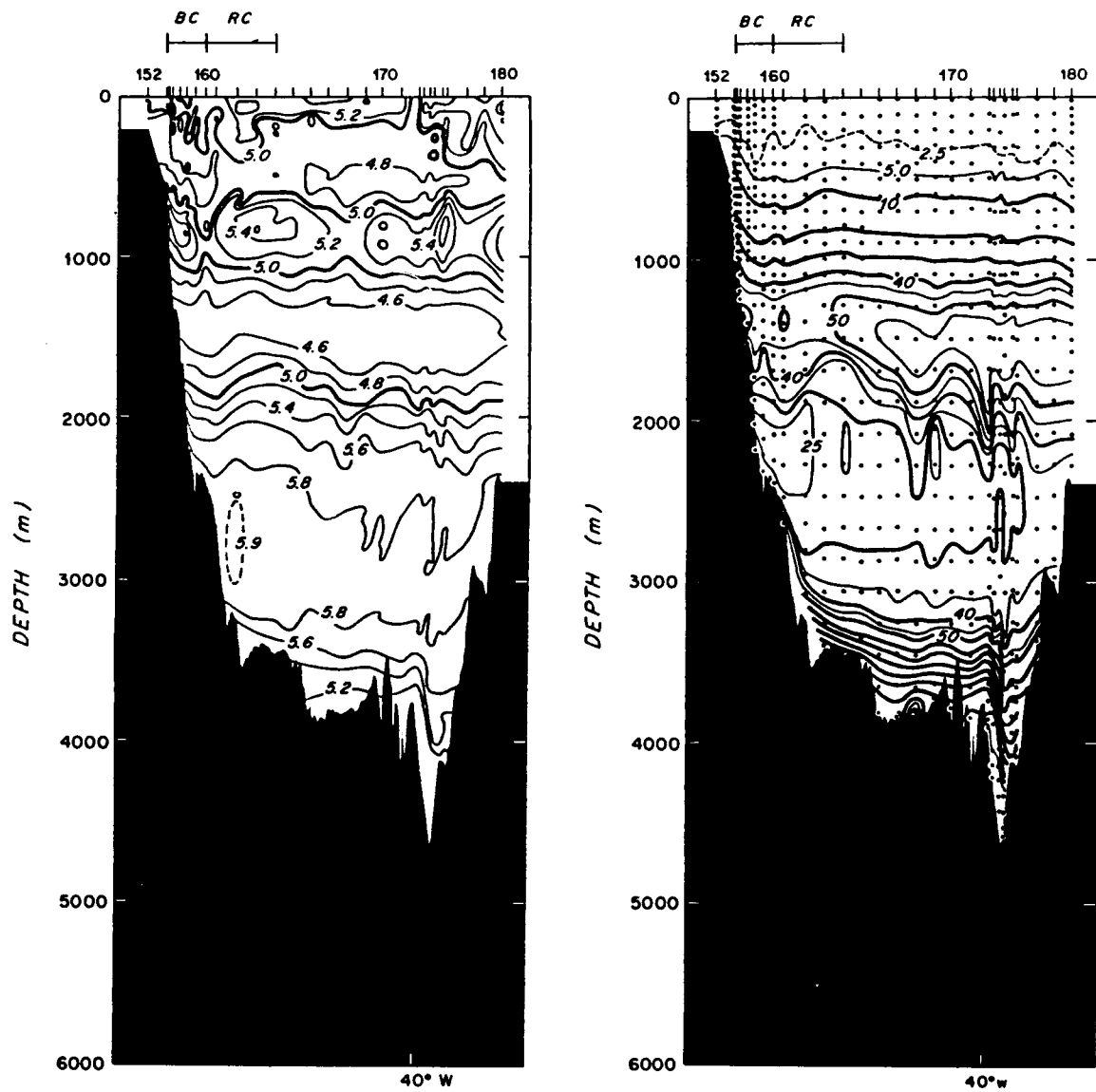


Figure 2.12: Sections of (c) oxygen ( $\text{ml l}^{-1}$ ) and (d) silica ( $\mu\text{mole l}^{-1}$ ) for 31° S. From the Thomas Washington Marathon Cruise, Leg 9.

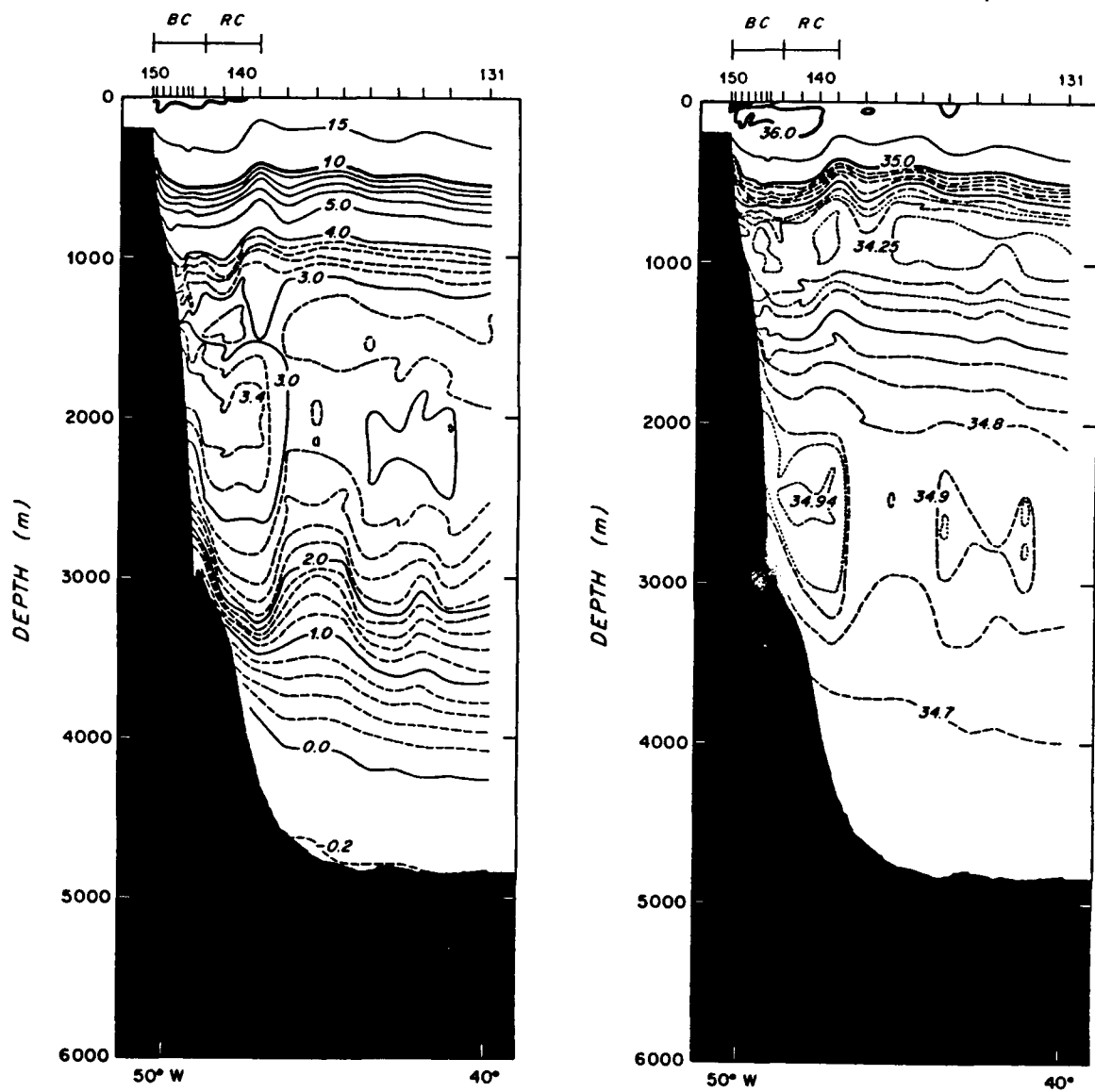


Figure 2.13: Sections of (a)  $\theta(^{\circ}\text{C})$  and (b) salinity (psu) for 34° S. From the Thomas Washington Marathon Cruise, Leg 9.

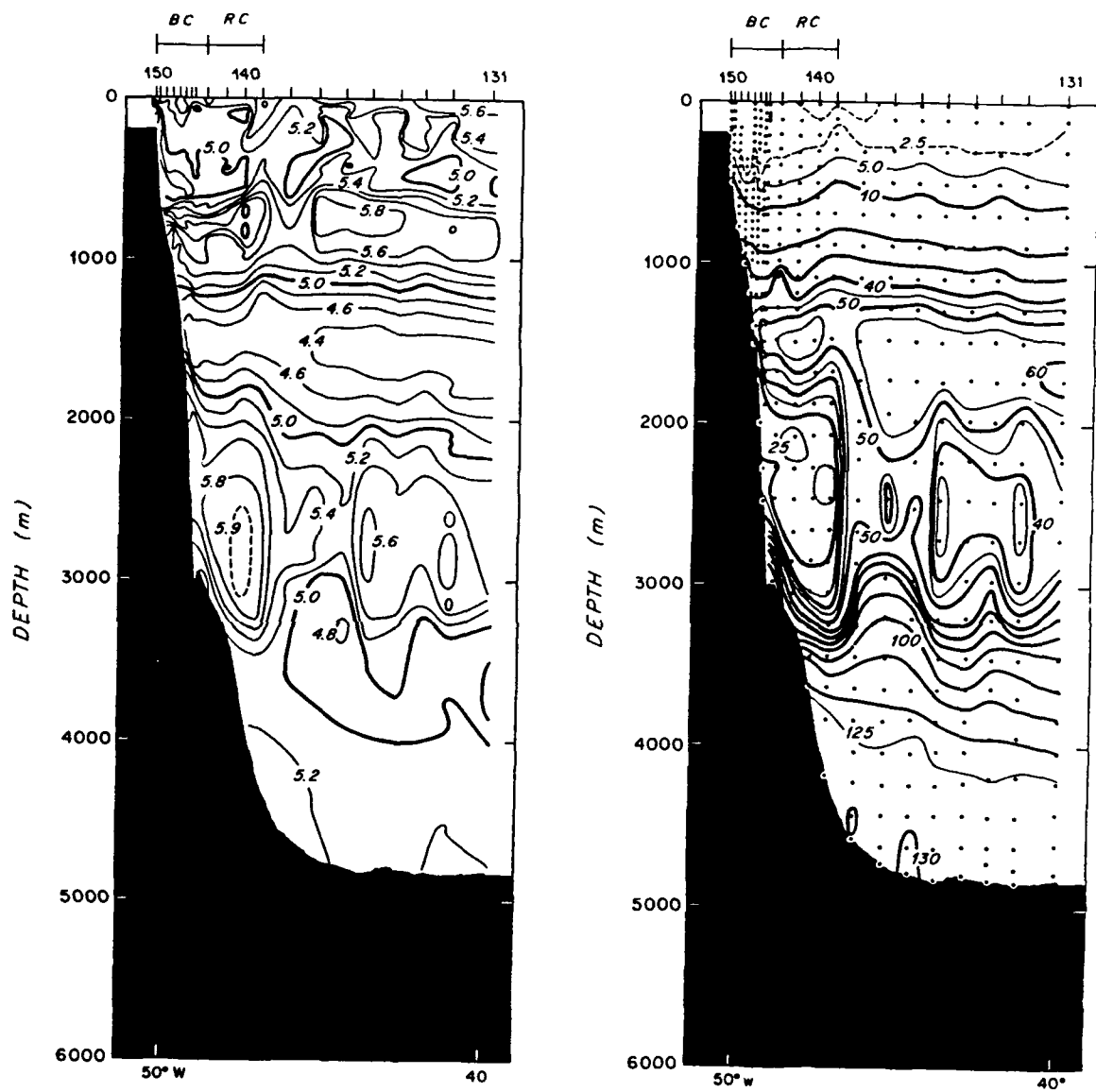


Figure 2.13: Sections of (c) oxygen ( $\text{ml l}^{-1}$ ) and (d) silica ( $\mu\text{mole l}^{-1}$ ) for 34° S. From the Thomas Washington Marathon Cruise, Leg 9.



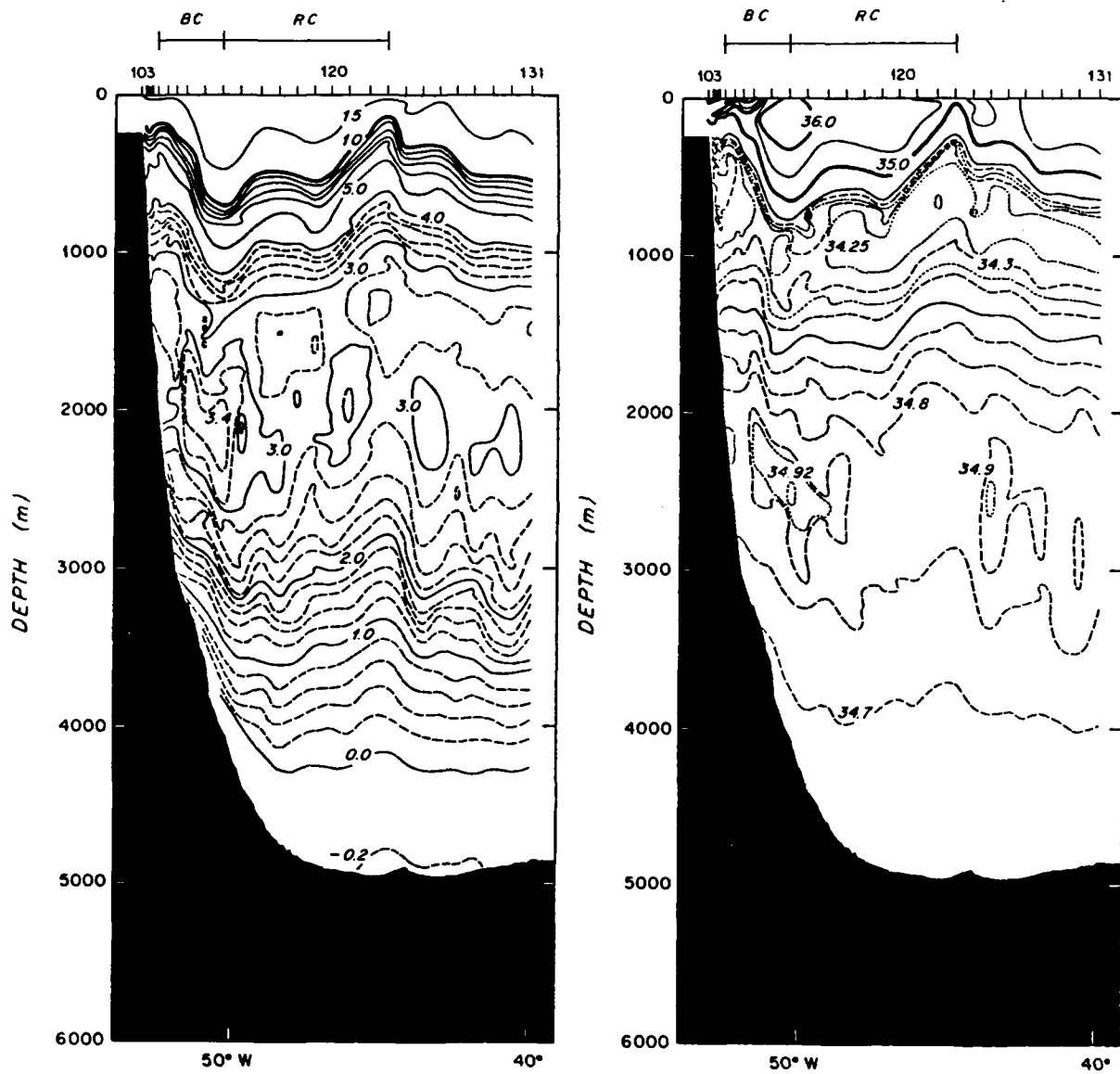


Figure 2.14: Sections of (a)  $\theta(^{\circ}\text{C})$  and (b) salinity (psu) for 36° S. From the Thomas Washington Marathon Cruise, Leg 9.

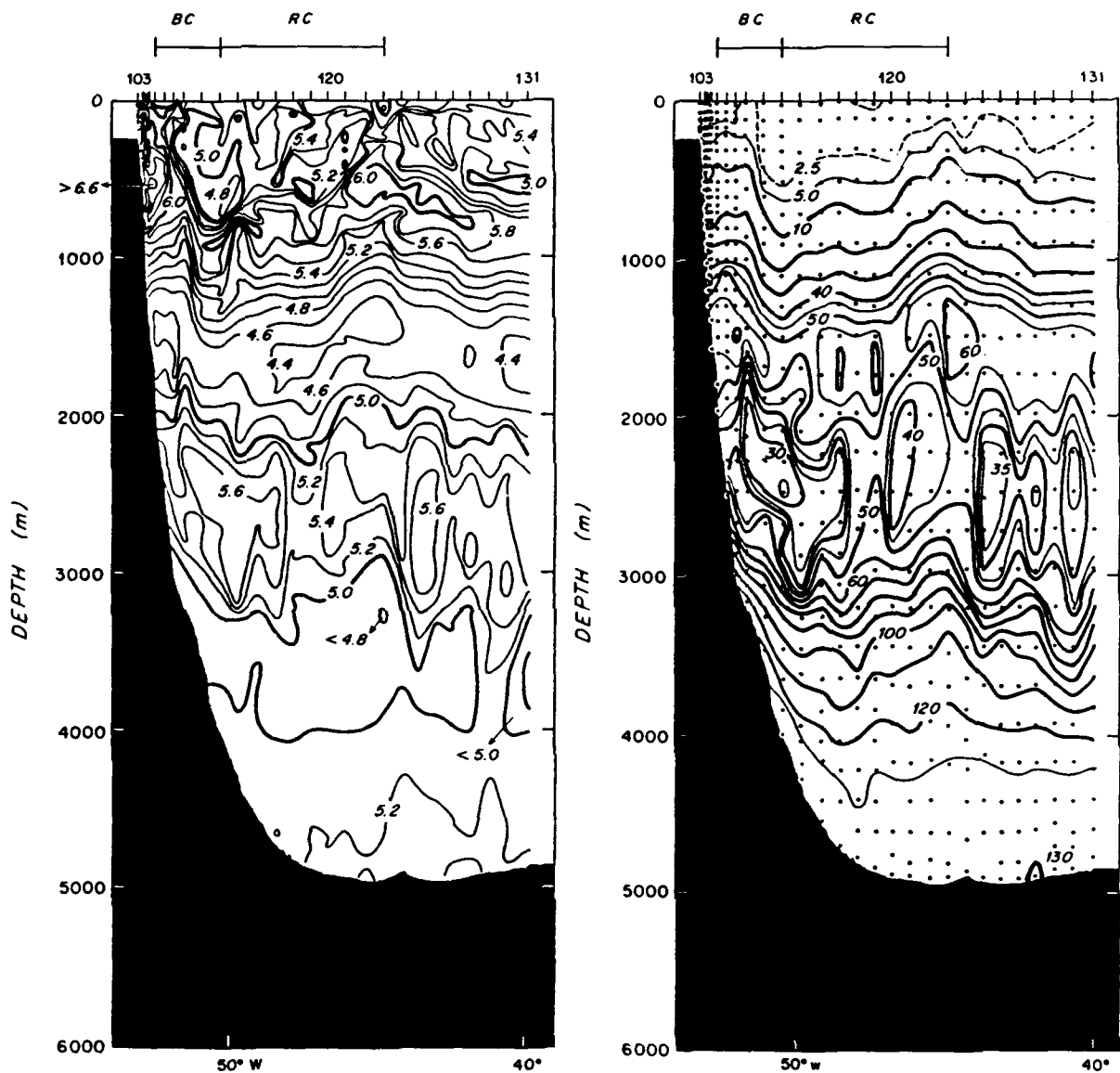


Figure 2.14: Sections of (c) oxygen ( $\text{ml l}^{-1}$ ) and (d) silica ( $\mu\text{mole l}^{-1}$ ) for 36° S. From the Thomas Washington Marathon Cruise, Leg 9.

surface water moving south, which is consistent with the Brazil Current flowing south.

### 2.3.2 Antarctic Intermediate Water

AAIW (found in the density range of 27.1 to 27.3  $\sigma_0$ ) is cold, fresh, and rich in oxygen. It can be seen at 27° S (fig 2.3) in cores of 34.3 psu in the salinity minimum layer (about 900 m), a small core right against the topography and a second larger one farther offshore. Similar cores of oxygen above 5.2  $ml\ l^{-1}$  are also found. At 31° S the 34.3 psu contour is almost continuous, with a larger core in line with the Brazil Current; it necks down, then enlarges offshore. The oxygen 5.2  $ml\ l^{-1}$  contour is still broken, but a 5.4  $ml\ l^{-1}$  contour emerges, again with a core under the Brazil Current and one offshore. At 34° S the 34.3 psu isohaline forms a wide band across the section, within which are pockets of 34.25 psu. Two pockets are found under the Brazil Current; two more are offshore. The oxygen shows a slightly different picture, with the inshore edge pinched off (although it now has a high of 5.8  $ml\ l^{-1}$ ) and the offshore showing the usual core, here reaching a value as high as 6.0  $ml\ l^{-1}$ . Finally the last section has the most extreme AAIW, with the 34.25 psu contour almost continuous across the section. Inshore, the oxygen concentration reaches values as high as 6.6  $ml\ l^{-1}$  under the Falklands Current and the inshore edge of the Brazil Current (sta. 105-109). Recall from the density section (fig 2.10) that the Falklands water is going north. The 6.6  $ml\ l^{-1}$  contour at the inshore edge of the Brazil Current is an indication of the Falklands water returning with the Brazil Current.

The path of AAIW through the subtropical South Atlantic has been a subject of controversy. Wust (1935) originally suggested that the water flows north under the Brazil Current, forming a subantarctic intermediate current. Others (Mirhanda and Filho (1981), Evans and Signorini (1985), Evans and Mascarenhas (unpublished)) have supported this idea. There is evidence for this in the small core of AAIW that

appears under the Brazil Current in all the sections except 34° S. However, when the Falklands and Brazil Currents meet, most of the AAIW appears to flow east with the confluence; also, the bowl of the subtropical gyre in dynamic topography maps reaches down to the AAIW. These features led Reid et al. (1977) and others (Gordon and Greengrove 1986, Buscaglia, 1971) to argue that the water flows east with the Brazil-Falklands confluence, enters the subtropical gyre, and comes south with the Brazil Current. The problem with this argument is that under the Brazil Current, the tracers associated with AAIW are clearly more extreme in the south than in the north, which suggests a flow direction from the source in the south towards the north. Another possibility is that AAIW flows north in the counterflow and comes back south with the current. However, the cores of AAIW under the current should then be slightly less fresh than those offshore in the counterflow, and this is not the case. Neither of these schemes accounts for the AAIW characteristics under the current.

As will be seen in the transport chapter, the majority of AAIW in the Brazil Current does flow southward. The following scenario, which is consistent with the data, has AAIW taking three pathways north, while still flowing south under most of the Brazil Current. Most AAIW goes east and enters the subtropical gyre. In addition, a small core of AAIW moves north in Wust's intermediate boundary current right against the topography, and some AAIW moves north with the recirculation. The last two form the extrema seen in the low salinity layer.

### **2.3.3 Upper Circumpolar Water**

The picture which emerges from UCPW in the sections can be confusing. UCPW (density range  $27.3 \sigma_0$  to  $36.7 \sigma_2$ ), of course, originates in the south, and some of the water appears to flow north with the counterflow. However, an extreme signal appears on the eastern side of the sections. Looking at maps of geopotential anomaly (Reid, 1989), one finds UCPW flowing east with the confluence, then

coming back west; thus, an extreme signal in the eastern part of the transects is not surprising.

UCPW is low in oxygen, and slightly higher in nutrients than the surrounding water of the same density. 27° S shows UCPW near 1200 m depth as an oxygen minimum band of  $4.6 \text{ ml } \ell^{-1}$  and silica maxima cores at  $50 \mu\text{mole } \ell^{-1}$ . The most extreme signal lies in the eastern part of the section. At 31° S there is still a band of  $4.6 \text{ ml } \ell^{-1}$  in oxygen; the silica section has a small core under the Brazil Current, one in the recirculation, and then a stronger band reaching higher than  $55 \mu\text{mole } \ell^{-1}$  on the eastern edge. The next section south shows the  $4.6 \text{ ml } \ell^{-1}$  oxygen contour pinched off under the Brazil Current. Offshore it widens, and a small band of  $4.4 \text{ ml } \ell^{-1}$  emerges. Silica also pinches off under the current, and reappears in the counterflow with a core of  $55 \mu\text{mole } \ell^{-1}$ . The  $55 \mu\text{mole } \ell^{-1}$  maximum is broken, then reestablished offshore, where it widens. At the eastern edge of the section lies a single bottle above  $60 \mu\text{mole } \ell^{-1}$ . At 36° S a  $4.4 \text{ ml } \ell^{-1}$  oxygen minimum is under the Falklands Current and the inshore edge of the Brazil Current; farther offshore are two more cores. Small patches of  $60 \mu\text{mole } \ell^{-1}$  silica water are across the section, lining up with the changes in shear.

Connecting the cores in the counter current through the two northern sections is questionable, as each is based on a single bottle value without a clear signal in oxygen. The connection between the two southern sections is better; the high silica value at 34° S is reinforced by a necking down in the oxygen (fig 2.9) suggesting a connection to the counterflow to the south.

### 2.3.4 North Atlantic Deep Water

NADW (with the density range of  $36.7 \sigma_2$  to  $45.85 \sigma_4$ ) splits the circumpolar water in two. It is relatively warm, causing a temperature inversion, low in nutrients, high in salinity and high in oxygen relative to the circumpolar waters. In the northern

section, there is a 34.94 psu core in salinity; it is widest where the bottom begins to deepen into the Vema Channel. Oxygen has a wide band of  $5.8 \text{ ml } \ell^{-1}$  across the section, with a small core of  $5.9 \text{ ml } \ell^{-1}$ . The silica section has a minimum core of  $25 \mu\text{mole } \ell^{-1}$  on the western side of the section, widening again as the bottom deepens. At  $31^\circ \text{ S}$  the salinity 34.94 psu core shrinks and moves away from the bottom, where there is a strong vertical shear (fig 2.5). Oxygen still shows a wide band of  $5.8 \text{ ml } \ell^{-1}$  across the section and a core of  $5.9 \text{ ml } \ell^{-1}$ , but silica has a reduced core of  $25 \mu\text{mole } \ell^{-1}$ , wider under the recirculation than under the Brazil Current. The  $34^\circ \text{ S}$  section shows the salinity core clearly separated from the topography, and lined up under the recirculation. A second core of 34.92 psu, offshore, aligns with variations in the shear field, which appears to be the Brazil Current meandering back through the section. The  $5.8 \text{ ml } \ell^{-1}$  oxygen is now a core against the western edge, still with a small maximum of  $5.9 \text{ ml } \ell^{-1}$ , and the silica  $25 \mu\text{mole } \ell^{-1}$  core reduces to three bottles on the western edge. Both oxygen and silica also show secondary cores in the Brazil Current meander. At the last section the 34.94 psu core shrinks to an isolated bubble right in the bowl of the current and recirculation. The maximum core of oxygen, reduced to a level of  $5.6 \text{ ml } \ell^{-1}$ , lies under the Brazil Current and recirculation; the  $5.6 \text{ ml } \ell^{-1}$  contour reappears offshore where the shear indicates meandering. Finally, the  $25 \mu\text{mole } \ell^{-1}$  silica core is a single bottle in the bowl, with the  $30 \mu\text{mole } \ell^{-1}$  contour primarily under the Brazil Current.

The southward flow of the core of NADW in the southern two section seems fairly clear; the cores are well defined, and the signature of the NADW is reduced from the northern two sections. The general trend of NADW flow in the northern sections is southward, but the absence of definitive cores in specific locations makes it difficult to determine where the flow might be northward. The silica and salinity sections give some indication, and information may be obtained from the other water masses.

### 2.3.5 Lower Circumpolar Water

LCPW ( $45.85 - 46.05 \sigma_4$ ), distinguished by its low oxygen, is only found in the southern two sections (water in this density range at the two northern sections does not have the low oxygen characteristics). The meridional section shown at the beginning of this chapter (fig 2.1) confirms that it does not extend farther north; maps of the entire basin show it flowing east (Reid, 1989). It is found in the two southern sections as a minimum core of  $5.0 \text{ ml } \ell^{-1}$  water, about 3500 m deep, concentrated on the eastern part of the section at  $34^\circ \text{ S}$ , and across the entire section at  $36^\circ \text{ S}$ . Both sections have a small bubble of  $4.8 \text{ ml } \ell^{-1}$  oxygen, which may be useful in confirming flow directions.

The water in the northern sections at this temperature range still has the low salinity and high nutrient characteristics of southern water, but it lacks the oxygen minimum signature of LCPW. Reid (1989) suggests this is the influence of vertical mixing in the water column. Interestingly, the thickness of the water column changes between the northern and southern sections (compare the separation of  $37.0 \sigma_2$  and  $45.9 \sigma_4$  contours in fig 2.7 - 2.10).

### 2.3.6 Antarctic Bottom Water

At the bottom of the water column is AABW ( $\sigma_4$  of 46.05 to bottom). It is cold, fresh and high in oxygen and nutrients. The high in oxygen is clearest in the southern two sections, clearly distinguishable from LCPW. In the northern sections the oxygen decays steadily from the NADW value to the AABW value.

At  $27^\circ \text{ S}$  AABW lies along the bottom of the section, characterized by the 34.7 psu salinity,  $5.2 \text{ ml } \ell^{-1}$  oxygen, and high silica of  $125 \mu\text{mole } \ell^{-1}$ . The  $31^\circ \text{ S}$  section shows the 34.7 psu salinity contour only in the Vema Channel, but the  $5.2 \text{ ml } \ell^{-1}$  oxygen contour extends out past the Channel. The silica maximum,  $125 \mu\text{mole } \ell^{-1}$ , is in the Channel. The next section south has a band of 34.7 psu water across the bottom of

the section. The  $5.2 \text{ ml } \ell^{-1}$  contour splits into two cores, one against the western edge, the other farther offshore. The  $125 \mu\text{mole } \ell^{-1}$  silica contour now extends across the bottom; two cores of  $130 \mu\text{mole } \ell^{-1}$  are on the western side of the section. At  $36^\circ \text{ S}$  the salinity still shows a wide band of 34.7 psu across the bottom. The oxygen core of  $5.2 \text{ ml } \ell^{-1}$  increases, and is slightly larger on the eastern part of the section. Silica has only a small bubble of  $130 \mu\text{mole } \ell^{-1}$ .

Based on the pattern of core strengths, AABW flows through the sections from south to north, but the path it takes to the Vema is unclear. It has been assumed to be a deep western boundary current, as seen in the southern sections, but there may be another interior path that water takes to get to the Channel. The southern sections do not extend far enough into the basin to determine this.

The water flow patterns suggested by each water mass can be summarized as follows:

- CW is most extreme in the north, with the tracer characteristics eroding away as the water flows south with the Brazil Current.
- Cores of AAIW are most extreme under the Brazil Current and counterflow, and erode to the north. They are suggestive of northward flowing water, perhaps in an older layer of AAIW coming south with the subtropical gyre.
- UCPW has cores under both the Falklands Current and the recirculation, which suggest northward flow, and the characteristics erode away to the north. The sections are dominated, however, by cores on the eastern edges, and the eastern influence complicates a determination of flow direction.
- NADW is most extreme in the north, with its signatures in salinity, oxygen and silica decaying to small cores in the south. The overall trends indicate flow from north to south.
- LCPW is only found in the southern two sections; the cores at  $34^\circ \text{ S}$  are less extreme than those at  $36^\circ \text{ S}$ , indicating northward flow.



●AABW cores erode from south to north, with the two northern sections showing AABW only in the Vema Channel. The indication of northward flowing water is fairly clear.

## **Chapter 3**

### **Transport of the Brazil Current**

Although estimates of the strength of the Brazil Current have existed for many years, the last decade has seen a resurgence of interest in the Brazil Current with several new studies completed. The recent experiments have clustered in two regions: 19 to 24° S, the nutrient rich fishing grounds off the coast of Brazil, and south of 37° S, the Brazil-Falklands confluence. A table summarizing the results shows the variation in transport estimates (table 3.1). Latitudinal variations are expected and found, but the variation at any single latitude is significant. The variations, as discussed in the introduction, result from different references for the velocity profiles, the definition of the Brazil Current and real temporal variations. Whether the Brazil Current is only a surface current or is all the southward flow, is discussed in the introduction. The second definition is favored here, but results are presented so that changes in the surface current can be observed separately from what happens below. The focus in this chapter is the reference choice for the velocity profiles.

The reasons given for the velocity references in table 3.1 are various. Some choose a zero velocity surface (ZVS) between the SW and AAIW surfaces so that AAIW flows north (Signorini, 1978; 23° S of Stramma, 1989). Stramma also uses Defant's level of no motion at 33° S. Defant chose a ZVS at the shallowest depth without shear (in or below the thermocline); the resulting ZVS is generally deeper than that

found using AAIW. Miranda and Filho (1981) use the layer of minimum oxygen concentration. One paper gives no reason for the choice of ZVS, although the value used follows the historical idea of a shallow current (Evans, Signorini, and Miranda, 1983). Two of the sections at 38° S, where one might expect the largest growth of the Brazil Current, are analyzed with a ZVS chosen primarily for convenience. Gordon and Greengrove (1986) give the following explanation of their choice (*italics mine*):

“ The 1400 m reference level allows higher horizontal resolution as it employs the full set of hydrographic data (only 40 percent of the stations reach beyond this depth to the sea floor). The sea surface dynamic height calculated relative to 1400 m represents on average 63 percent of the sea surface dynamic height relative to the deep reference level at 3000 m. Thus the 0/1400 m map serves as a *useful representation* of the overall thermocline geostrophic flow.”

The Brazil Current is being sampled as if it is only at the surface, even though this results in a loss of 37 percent of the signal. Peterson (1990) uses the same data set with a deeper ZVS determined by water mass information to obtain a significantly higher Brazil Current transport. Garzoli and Garraffo (1989) use 800 m as a ZVS at 38° S, and report that the results represents seventy-five percent of the transport reported by Gordon and Greengrove, and so captures most of the Brazil Current. Thus, Garzoli and Garraffo capture a little less than half the signal relative to 3000 m. This is particularly distressing since Roden (1986) reports Brazil Current signatures down to 4000 m in the confluence region just east of these studies. Peterson's new analysis of the data suggests that deep signatures are also found at 38° S. Finally, the two PEGASUS results use absolute velocities. The PEGASUS transports reported at 31° S are rough because of a number of problems with that survey: the transport estimate comes from only one realization of the current; there is still southward flow at the bottom of one of the PEGASUS drops (at 800 m), and

the survey does not resolve the outside edge of the stream.

Lat. (°S)	Zero Reference	Transport ( $\times 10^6 m^3 s^{-1}$ )	Source
19	26.8 $\sigma_0$	6.5	Miranda and Filho (1981)
20.5	500 m	3.8	Evans, Signorini and Miranda (1983)
20.5	1000 m	6.8	Evans, Signorini and Miranda (1983)
23	PEGASUS	11.0	Evans and Signorini (1985)
23	600 m	10.2	Stramma (1989)
24	500 m	4.1	Evans, Signorini and Miranda (1983)
24	600 m	9.4	Signorini (1978)
24	1000 m	7.8	Evans, Signorini and Miranda (1983)
31	800 m	11.2	Evans and Mascarenhas (unpublished)
31	PEGASUS	17.0	Evans and Mascarenhas (unpublished)
33	1600 m	17.5	Stramma (1989) <sup>1</sup>
38	1400 m	19.0	Gordon and Greengrove (1986)
38	~3000 m	70.0	Peterson (1990)
38	800 m	8.5	Garzoli and Garraffo (1989)
38	IES <sup>2</sup>	11.0	Garzoli and Garraffo (1989)

**Table 3.1: Historical Brazil Current Transports**

Several points emerge from this survey of recent experiments in the Brazil Current.

First, few transport estimates exist for the region examined here, 27 to 36° S.

Second, when transports are computed for the region, the appropriate ZVS needs to be chosen carefully. The only physically based ZVS for geostrophic transports in the previous list are Peterson's 38° S estimate and those using the AAIW argument (as was pointed out in chapter two the argument has been questioned). Finally, comparisons between various transport estimates at different locations must be

<sup>1</sup>data from the 1972 CATO expedition

<sup>2</sup>Inverted echo sounder

made with attention to what quantity is being measured; understanding of the Brazil Current system will not be furthered with murky definitions.

### 3.1 Transport Calculations

The transports presented in this section are calculated using the geostrophic method. Appendix B provides the details of the calculation, which is fairly straightforward. However, the complexity of the interwoven water masses of northern and southern origin brings zest to the job of choosing an appropriate ZVS. In general, the reference can be any velocity at a given depth. In practice, the reference chosen here is usually zero velocity for a specific density isopleth. If a velocity other than zero is inferred it will be indicated.

Choosing a ZVS for the shear profiles consists of several steps. As was described in chapter 2, the method used here centers on the extrema in water mass characteristics. These two way extrema- isolated blobs defining the core of a water mass- are required to move in the expected direction of the water mass. The expected direction is determined by the erosion of water mass characteristics away from its source. A single core will constrain the ZVS to fall between two surfaces; a second core in the water column further constrains the choice. Changes in the  $\theta$ -S and  $\theta$ -O<sub>2</sub> curves help to define the limits of a water mass and focus the ZVS choice. In some cases no well defined extremum exists in the water column. If other data exist (e.g. moored current meter records), they may be used to set the ZVS, although the records need to be examined to see if they exhibit a high degree of variability. In places where a reference choice is ill-defined, the ZVS from the surrounding stations is used. Finally, transports of the water masses are balanced and reference velocities are adjusted to conserve mass in closed boxes.

This method is more clearly applicable in some parts of the transects than others. Each transect of the Brazil Current has several extrema which constrain the ZVS

choice. Offshore from the current extrema are less frequent and, because of possible eastern sources, their implied flow direction sometimes ill-defined. Where well-defined extrema do exist they determine the ZVS. In the Vema Channel current meter measurements are used to help set the ZVS. As stated before, in the absence of clear information the ZVS is not changed from the surrounding stations, unless such a change is required to conserve mass. Closed boxes are formed by the two northern sections and the two southern sections. In the northern box, transport is not estimated across the gap connecting the two sections (sta. 180-184). Mass balances are computed for several water mass layers. The lowest layer, which is closed by the sections and topography, balances within 1 Sv; the others balance within 4 Sv. In the southern box, mass balances in each layer to within 3 Sv, with overall mass balance within 4 Sv. The imbalances may reflect errors in the ZVS choice, incorrectly estimated bottom triangle transports or flow occurring inshore of the shallowest stations. Note that the last two items in that list are not necessarily small. The current flows over the continental slope, so transports in the bottom triangles may be significant, and large estimates of shallow water transport exist.

The accuracy of the above approach depends on several points: an ability to pinpoint the core of the water mass; the knowledge of the direction a particular water mass should flow, and the validity of the assumption that the water in a core should flow in consonance with the water mass characteristics.

### **3.2 Reference Choices for each Section**

This section describes the specifics of applying this method to the four Brazil Current transects. The analysis of the water masses and their expected flow direction is presented earlier (chapter 2). Each transect will be discussed separately and a ZVS choice made for that transect. The effect of altering that choice is then explored in section 3.3. To simplify the presentation of the results, transport values are presented in four layers, with the UCPW combined with AAIW and LCPW

combined with AABW. This is done for two reasons: first, the oxygen minimum of LCPW is only found in the two southern sections, and so is not easily distinguished from AABW in the two northern sections, and second, both Reid (1989) and Rintoul (1988) suggest that the flow patterns for AAIW and UCPW are the same, as are those of LCPW and AABW. The four new density layers are these: CW, extending from the surface down to  $27.1 \sigma_0$  ( $36.2 \sigma_2$ ); second are AAIW and UCPW, from  $36.2 \sigma_2$  to  $36.7 \sigma_2$ ; next is NADW, from  $36.7 \sigma_2$  to  $37.05 \sigma_2$ ; and finally, LCPW and AABW, from  $37.05 \sigma_2$  to the bottom.

### 3.2.1 Section I. $27^\circ$ S

At  $27^\circ$  S, there are two water mass cores in the Brazil Current stations (sta. 199-206), CW, flowing south, and AAIW (sta. 200-202), flowing north. The shear reverses sign at the AAIW core (fig 2.7). A ZVS only slightly above the AAIW core sends it north at  $10 \text{ cm s}^{-1}$ , with Brazil Current surface velocities as high as  $50 \text{ cm s}^{-1}$  to the south. A shallower ZVS results in AAIW velocities of  $30 \text{ cm s}^{-1}$  northward (unrealistically large), with equally high bottom velocities. A deeper ZVS sends the AAIW core south, conflicting with the core information. Thus use of the  $27.2 \sigma_0$  surface as a ZVS is consistent with both water mass cores; it also agrees fairly well with the historical idea of a shallower Brazil Current to the north. Offshore, in the counterflow stations (sta. 197-199), a second core of fresh AAIW goes north, with southward flowing NADW below. Extending the ZVS of  $27.2 \sigma_0$  through this region is consistent with both these constraints. Farther offshore the most extreme NADW is found (sta. 193-194). For this water to go south the ZVS has to be deeper. Somewhat farther offshore (sta. 191) AABW is found, which flows north. A ZVS between NADW and AABW—  $45.85 \sigma_4$  — satisfies both requirements and is consistent with the Hogg et al. (1982) measurements of a ZVS at 3500 m in the Vema Channel (about 300 km to the south). Those stations too shallow to reach the  $45.85 \sigma_4$  contour have bottom velocities set (maximum of 1

$cm\ s^{-1}$ ) to aid in balancing mass.

The final ZVS choices for this section are the  $27.2\ \sigma_0$  surface through the Brazil Current and counterflow; the  $45.85\ \sigma_4$  surface the rest of the way. The resulting velocity section (fig 3.1) has the Brazil Current flowing south with a small (less than one sverdrup) northward intermediate current below. The counterflow to the east is limited to the upper layer; velocities in the rest of the section are low except in the Vema Channel. The resulting transports, divided into the layers and regions described, are presented in table 3.2.

layer transport (Sv)	location				Net
	BC	RC	Int.	VC	
CW	-11.7	4.2	-3.7	4.6	-6.6
AAIW/UCPW	0.5	-0.5	-2.1	-.6	-2.7
NADW	-0.2	0.2	-7.2	-2.5	-9.9
LCPW/AABW	0.0	0.0	-0.7	4.1	3.4

**Table 3.2:** Transports across the section at  $27^\circ\ S$ . The columns are the transports in each layer in the Brazil Current (BC), the recirculation (RC), the Interior (Int.) and the Vema Channel (VC).

### 3.2.2 Section II. $31^\circ\ S$

Like the section to the north, the stations in the Brazil Current (sta. 153-160) have cores of both CW and AAIW. The shear reversal at the AAIW core (sta. 156-157) is weaker (fig 2.8), so a shallower ZVS is necessary to send it north. A core of NADW is found offshore of the AAIW core, still in the Brazil Current stations and extending into the counterflow. Inshore of the NADW a shallow ZVS of  $27.1\ \sigma_0$  sends the AAIW north at about  $10\ cm\ s^{-1}$ , and the CW south with a maximum velocity of  $70\ cm\ s^{-1}$ . The velocity of the AAIW is lower than PEGASUS data in the area ( $30\ cm\ s^{-1}$  from Evans and Mascarenhas, unpublished), but still reasonable



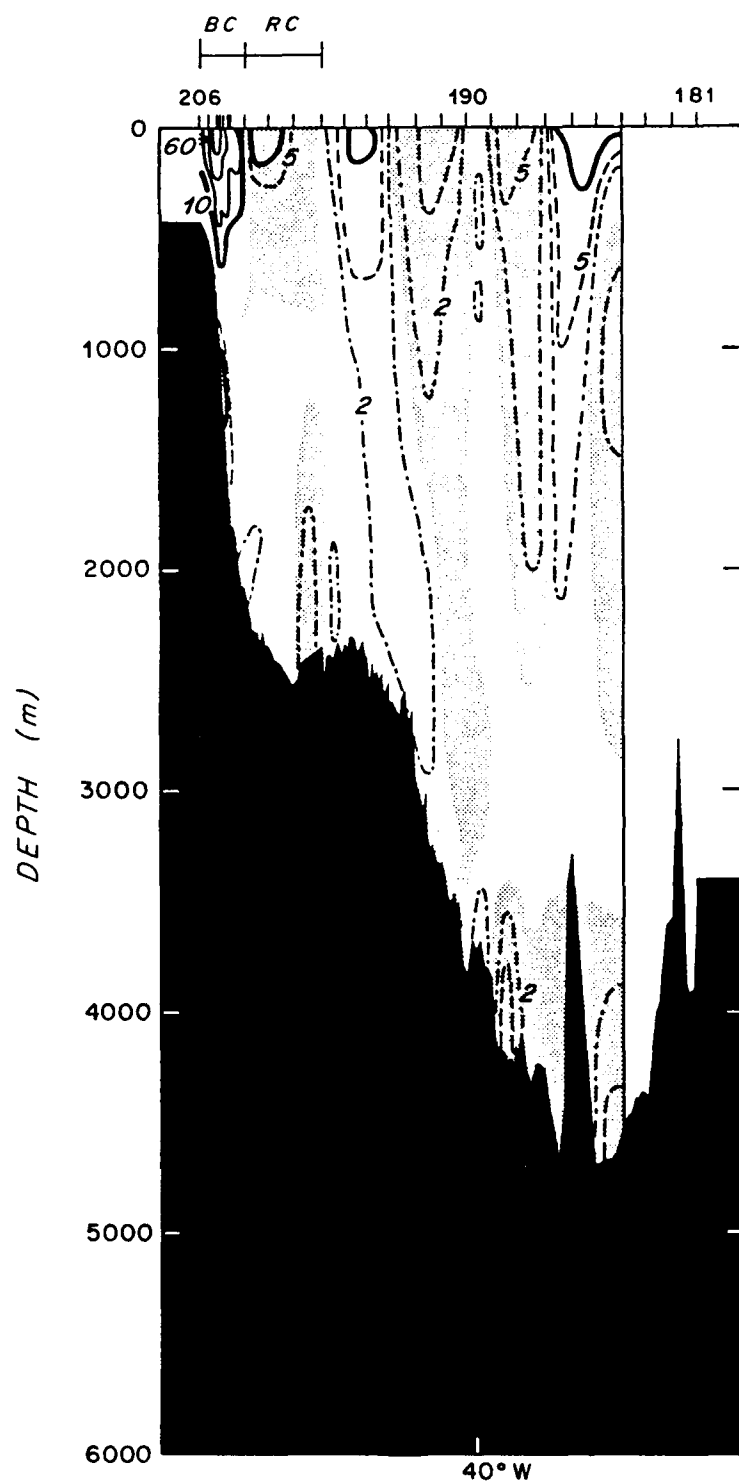


Figure 3.1: Velocity ( $\text{cm s}^{-1}$ ) section for  $27^\circ \text{ S}$ , stippling indicates northward flow.

since the PEGASUS data are instantaneous. A deep ZVS is needed to send the NADW core south, so the ZVS is dropped at station 159. The NADW core is slightly more extreme under the counterflow (sta. 162-163); below it, AABW is found, which should flow north. A deep ZVS consistent with both is  $45.85 \sigma_4$ . Farther offshore the strongest signal driving the reference choice is northward flowing AABW. The same ZVS still sends AABW north, so it is left unchanged. This ZVS is again consistent with the Hogg et al. (1982) current meter values in the Vema Channel, at approximately the same location.

The final ZVS choices for this section are the  $27.1 \sigma_0$  surface through most of the Brazil Current and the  $45.85 \sigma_4$  surface for the rest of the transect. The resulting velocity section (fig 3.2) shows the southward flowing Brazil Current with a stronger intermediate current (about  $2.5 \text{ Sv}$ ) below. The counterflow is deeper and faster than that at  $27^\circ \text{ S}$ . NADW below the counterflow reaches speeds of  $5 \text{ cm s}^{-1}$ . Large velocities are found at the top and bottom of the Vema Channel, both northward. The resulting transports are presented in table 3.3. The net imbalance between this section and the previous requires westward flow in all layers at the eastern edge of the box. This is obtained if the ZVS is between  $35.6 - 36.5 \sigma_2$ .

layer transport (Sv)	location				Net
	BC	RC	Int.	VC	
CW	-20.3	11.4	-6.8	3.0	-12.7
AAIW/UCPW	-2.5	1.5	-2.2	2.7	-0.5
NADW	-1.9	-5.6	-1.9	5.1	-4.3
LCPW/AABW	0.0	0.0	0.2	4.1	4.3

**Table 3.3:** Transports across the section at  $31^\circ \text{ S}$ . The columns are the transports in each layer in the Brazil Current, the recirculation, the Interior and the Vema Channel.

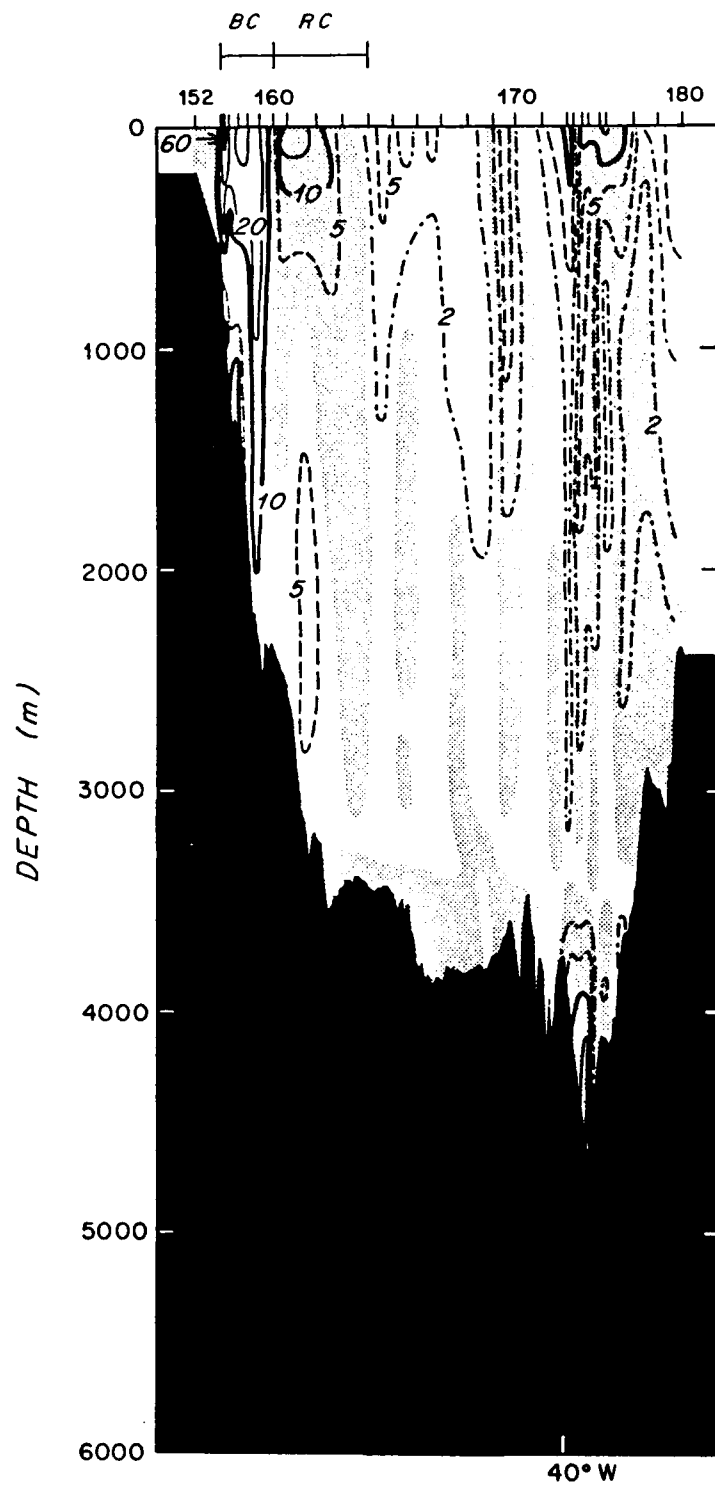


Figure 3.2: Velocity ( $\text{cm s}^{-1}$ ) section for  $31^\circ \text{ S}$ , stippling indicates northward flow.

### 3.2.3 Section III. 34° S

As was discussed in chapter two, the Brazil Current shear profile at 34° S is unusual (fig 2.9). It lacks the coherent vertical structure that exists both to the north and to the south. The result is a wobbly shear profile, making the reference choice more difficult. In addition, the baroclinic shear of the Brazil Current is weaker, with much of the shear occurring near the bottom (Note, for example, the western edge of 26.9 and 27.2  $\sigma_0$  and 36.7  $\sigma_2$ ).

The descriptive picture given at this section is of a Brazil Current with its inshore edge pinched off (section 2.2). The main core in the Brazil Current (sta. 142-150) is CW, with no AAIW core below; in fact, a high salinity core is found instead (fig 2.13). NADW is found on the offshore edge of the current. If the Brazil Current is to transport as much water as it did at 31° S, the ZVS must be deep; it is set at the bottom here to capture all of the baroclinic shear. The maximum surface velocity is then still low, 55  $cm\ s^{-1}$ , but the section may be oblique to the current; the transports are the critical numbers. This ZVS choice is actually conservative, because the NADW core under the stream is in an area of reversed shear. The result is that some NADW flows north (although the net is still southward); the northward flowing NADW can only be reversed by applying a southward bottom velocity (about 5  $cm\ s^{-1}$ ) and increasing the size of the Brazil Current, which has not been done. The counterflow (sta. 139-142) has cores of AAIW and NADW, which constrain the flow direction at those depths quite precisely, but the complicated shear profile makes it difficult to choose a single ZVS (e.g. a density isopleth) across the whole region. Instead the core constraints are met by setting the bottom reference velocity for each station pair. Offshore (sta. 131-139), LCPW flows north, along with AABW. This requires a ZVS above the LCPW core. The vertical shear throughout this region is monotonic top to bottom, but the sense of the shear changes across the section.

layer transport (Sv)	location			Net
	BC	RC	Int.	
CW	-24.2	13.2	-15.7	-26.7
AAIW/UCPW	-9.0	1.6	-5.8	-13.2
NADW	-4.6	-2.4	-3.0	-10.0
LCPW/AABW	0.0	1.3	3.7	5.0

**Table 3.4: Transports across the section at 34° S. The columns are the transports in each layer in the Brazil Current, the recirculation, and the Interior.**

This fluctuation is assumed to be a result of the edge of the Brazil Current meandering back through the section, so the ZVS is placed between LCPW and NADW, at  $45.85 \sigma_4$ . The resulting velocity section (fig 3.3) shows the southward flowing Brazil Current reaching to the bottom. High velocities reach as far inshore as was sampled, leaving the impression that the current continued onto the shelf. The recirculation is not as deep as it was at the previous section, although it is stronger in the top two layers. Beneath the counterflow is southward NADW. Farther offshore the flow changes direction several times, suggesting a meander through the section. The resulting transports are presented in table 3.4. Comparing these to the previous section one finds that an inflow of the top three layers, and an outflow of AABW, would be needed to balance mass. This sense of flow can be achieved between the eastern ends of the two sections with a ZVS near  $37.0 \sigma_2$ . An actual calculation is difficult because of the difference in depth between the two eastern edges.

### 3.2.4 Section IV. 36° S

The shear at 36° S is the most coherent, with most station pairs having monotonic shear top to bottom (fig 2.10). The northward flowing Falklands Current lies

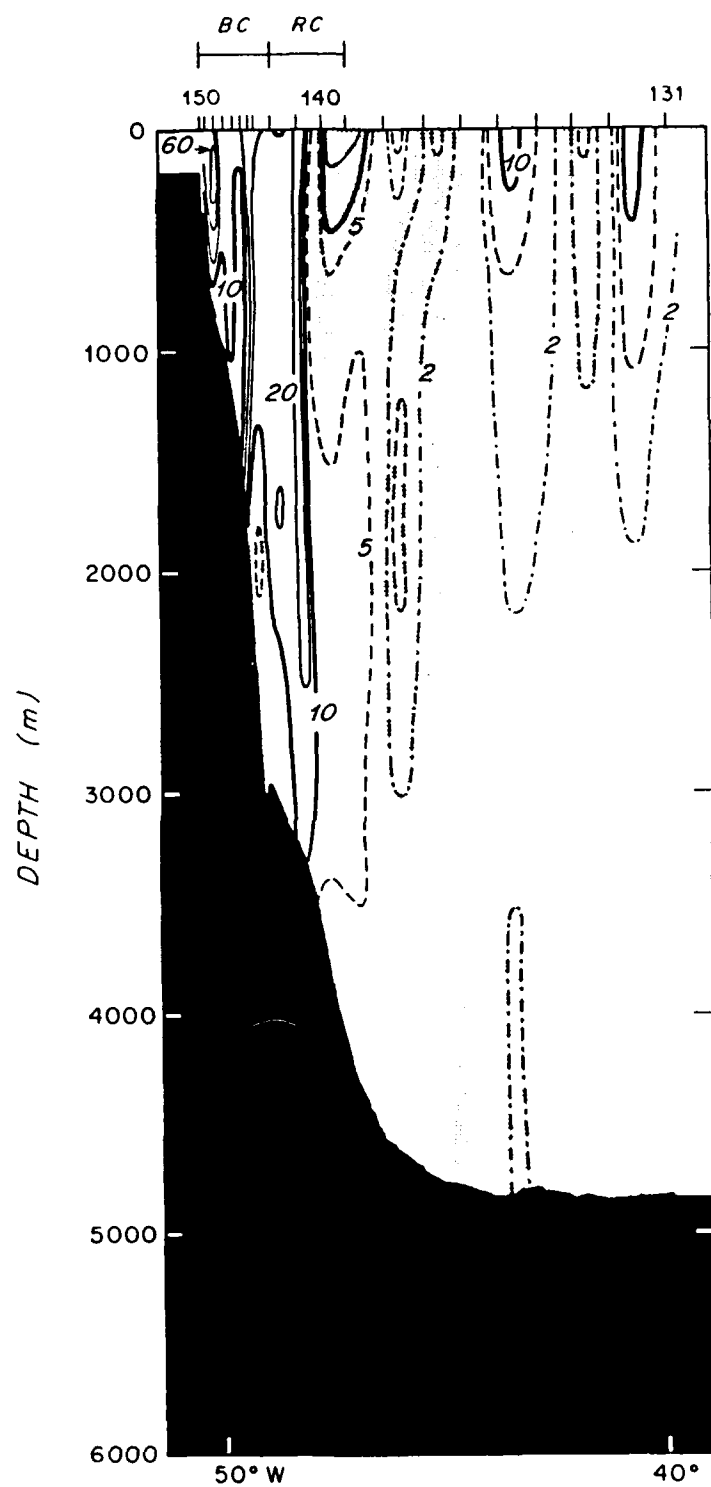


Figure 3.3: Velocity ( $\text{cm s}^{-1}$ ) section for  $34^\circ \text{S}$ , stippling indicates northward flow.

inshore of the Brazil Current (sta. 103-109). Since this water is clearly of southern origin, the ZVS is set at the bottom, sending the current north. The Brazil Current (sta. 109-114) is in deeper water with monotonic shear, top to bottom. Both the CW and NADW go south, requiring a ZVS below the NADW core. The LCPW below flows north, so the ZVS is placed between them, at  $45.8 \sigma_4$ . This choice results in a near-surface maximum southward velocity of  $100 \text{ cm s}^{-1}$ , larger than that found at the other sections (Gordon and Greengrove, 1986, found a maximum at  $38^\circ \text{ S}$  of  $70 \text{ cm s}^{-1}$  with a ZVS of 1400 m). The counterflow (sta. 114-116) has a deep shear reversal (between  $45.8$  and  $46.0 \sigma_4$ ); choosing the ZVS reference near the reversal ( $45.8 \sigma_4$ ) sends most of the water column north. Farther offshore the flow meanders back and forth. Again, this is treated as the meandering Brazil Current and a deep ZVS ( $45.85 \sigma_4$ ) sends the most extreme cores of AABW to the north.

The ZVS at  $36^\circ \text{ S}$  is the  $45.8 \sigma_4$  surface through the Brazil Current and counterflow and the  $45.85 \sigma_4$  surface for the rest of the transect. The velocity section (fig 3.4) has a strong deep Brazil Current extending down to include the southward NADW, and riding over northward LCPW. A strong recirculation flows north. Current meanders are found to the east, seen in the relatively high ( $40 \text{ cm s}^{-1}$ ) velocities. The transports are presented in table 3.5. Comparing these transports to those at  $34^\circ \text{ S}$  one finds no more than 1 Sv difference in any one layer.

layer transport (Sv)	location				Net
	FC	BC	RC	Int.	
CW	3.4	-51.4	25.8	-3.5	-25.7
AAIW/UCPW	1.5	-18.5	5.7	-1.1	-12.4
NADW	-0.2	-10.1	1.6	-0.4	-9.1
LCPW/AABW	0.0	2.1	3.7	0.1	5.9

**Table 3.5: Transports across the section at  $36^\circ \text{ S}$ . The columns are the transports in each layer in the Falklands Current, the Brazil Current, the recirculation, and the Interior.**

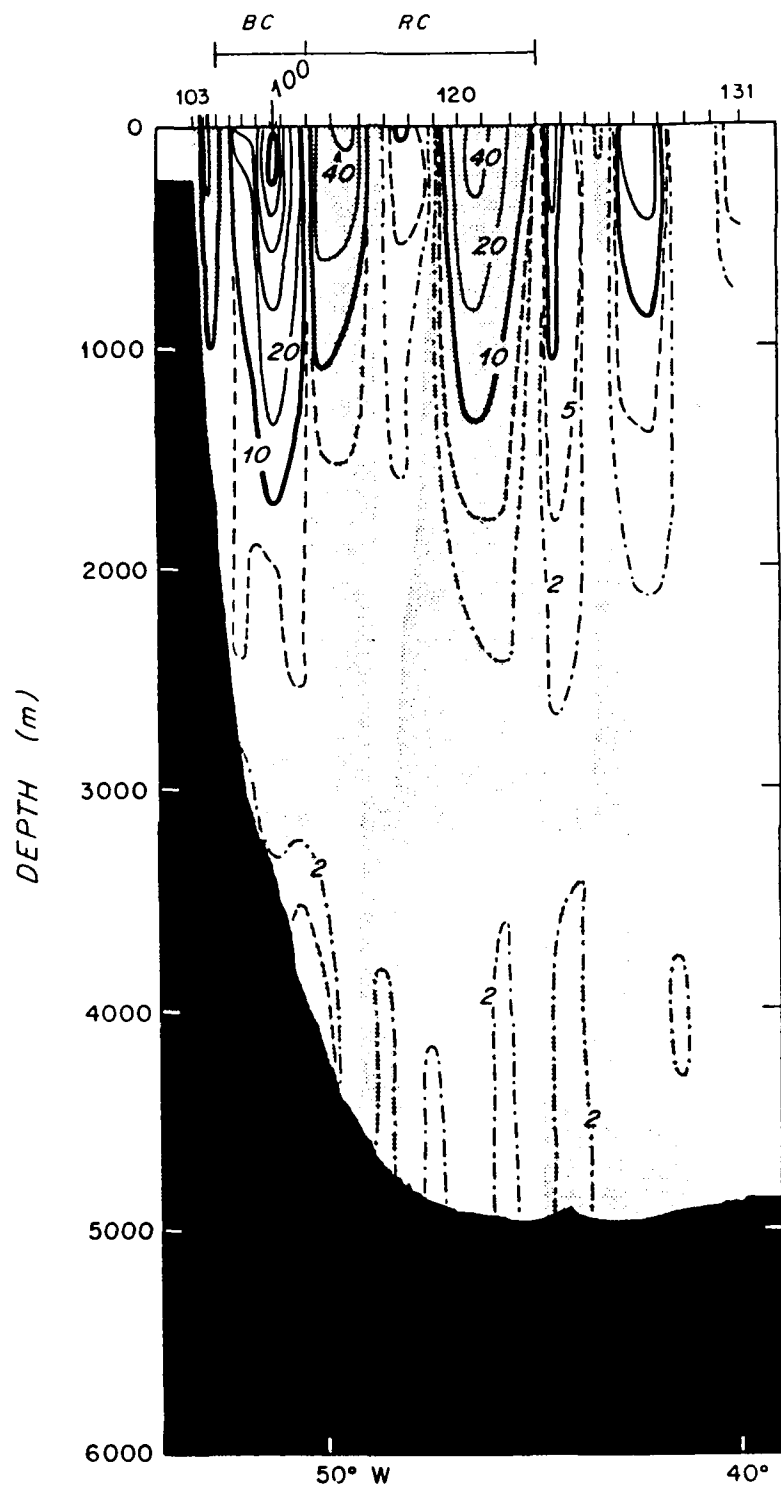


Figure 3.4: Velocity ( $\text{cm s}^{-1}$ ) section for  $36^\circ \text{ S}$ , stippling indicates northward flow.



### 3.3 Resulting Flow Patterns

The estimates of Brazil Current transports for each transect are presented in table 3.6. Regardless of how one defines the Brazil Current, significant growth occurs downstream. In his world ocean driven by a Sverdrup interior, Godfrey (1989) calculated the Brazil Current at 25° S to be 20 Sv, at 36° S to be 32 Sv and at 38° S, 110 Sv. The sudden jump in the calculated Brazil Current comes from the edge of South Africa being reached; the Brazil Current then closes the circulation for both the South Atlantic and Indian Oceans. The jump found in these sections at 36° S is not quite as extreme. In the surface layer, transport grows between 27 and 36° S at an average rate of about 20 percent per 100 km, although the growth at 34° S is low compared to the others. The rate is higher than the 5 percent growth reported by Gordon and Greengrove (1986); it is also higher than the 6 percent growth found in the Gulf Stream (Knauss, 1969). A fair portion of this growth comes from the counterflow immediately offshore from the Brazil Current. This recirculation forms a much tighter recirculation bowl than that found in either the Gulf Stream or the Kuroshio. It starts at 4 Sv at 27° S and reaches a maximum of 26 Sv at 36° S.

layer transport (Sv)	location			
	27	31	34	36
CW	-11.7	-20.3	-24.2	-51.4
AAIW/UCPW	—	-2.5	-9.0	-18.5
NADW	—	-1.9	-4.6	-10.1
LCPW/AABW	—	—	—	—
Net	-11.7	-24.7	-37.8	-80.0

**Table 3.6: Transport of the Brazil Current across each section.**

If instead the net southward transport is used to define the Brazil Current, the growth is from 11.7 to 80 Sv. Below the surface layer, the AAIW and UCPW layer changes from heading slightly north to strongly south; the inshore (northward)

AAIW current is too small to dominate the total transport. The recirculation in this layer is weaker, although strongest to the south. Increases in the layer in the Brazil Current at 34° S are too large to be accounted for by just the recirculation; additional water must be brought in from the east. This picture is consistent with that found in Reid (1989, his fig. 19). Below, NADW flows south in all the transects. Its net transport under the Brazil Current increases greatly, primarily a result of the NADW shear aligning with the current as it moves from north to south. The only section with any NADW recirculating is 36° S, the farthest to the south.

The general pattern of the Brazil Current is similar to other western boundary currents. The Brazil Current grows rapidly as it moves south. Its shear signature deepens, and more water is drawn in via a recirculation cell on the offshore side of the current. The recirculation is poleward intensified, growing stronger and deeper in the south. In addition, some water enters the Brazil Current system on the inshore edge, via the Falklands Current.

Extending our focus beyond the Brazil Current, we can construct circulation cartoons for each layer (fig 3.5-3.8). These show visually the southward increase in strength and depth of the recirculation. The nearshore current of AAIW is found at 27° and 31° S. NADW comes down the coast in a fairly uniform current; the water in this density range that flows north through the Vema is coming from east of the sections. The northward LCPW and AABW layer starts out around 6 to 7 Sv; by the time it reaches the Vema Channel it shrinks to 4 to 5 Sv, consistent with the Hogg et al. (1982) estimate. The excess water may continue north via a path to the east of the Rio Grande Rise (Reid, 1989, his fig. 29). The core of NADW coming south through all the sections is fairly constant, at about 10 Sv. The AAIW and UCPW layer moves south, supplied by both the UCPW coming in from the east and the older AAIW in the subtropical gyre, coming from the north. Some AAIW does flow north, both in a small current trapped against the coast (about 1 Sv) and in the recirculation. These currents provide the freshest cores of AAIW in the salinity minimum layer, and they are consistent with the AAIW scenario described

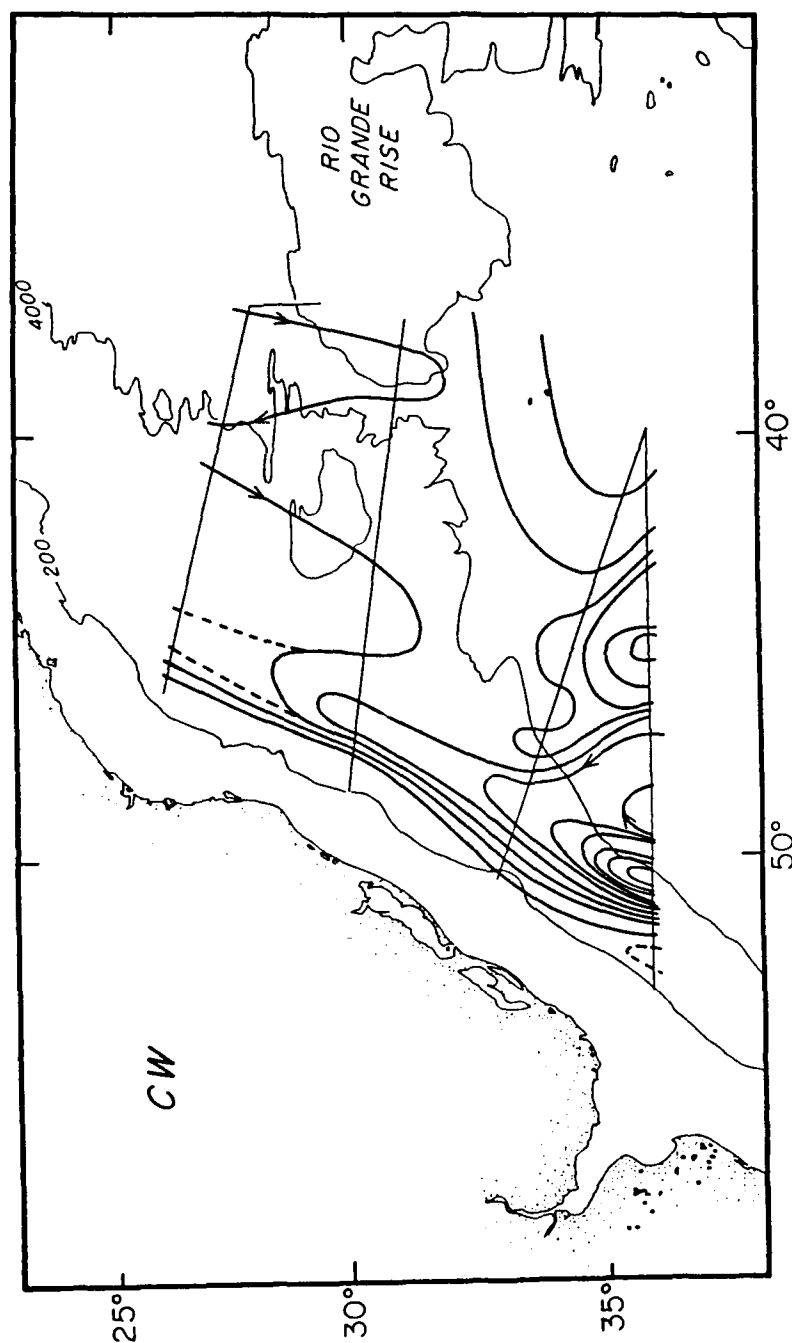


Figure 3.5: Transport cartoon for the central water layer. Each solid line represents approximately 5 Sverdrups, with dashed lines indicating flows below that level.

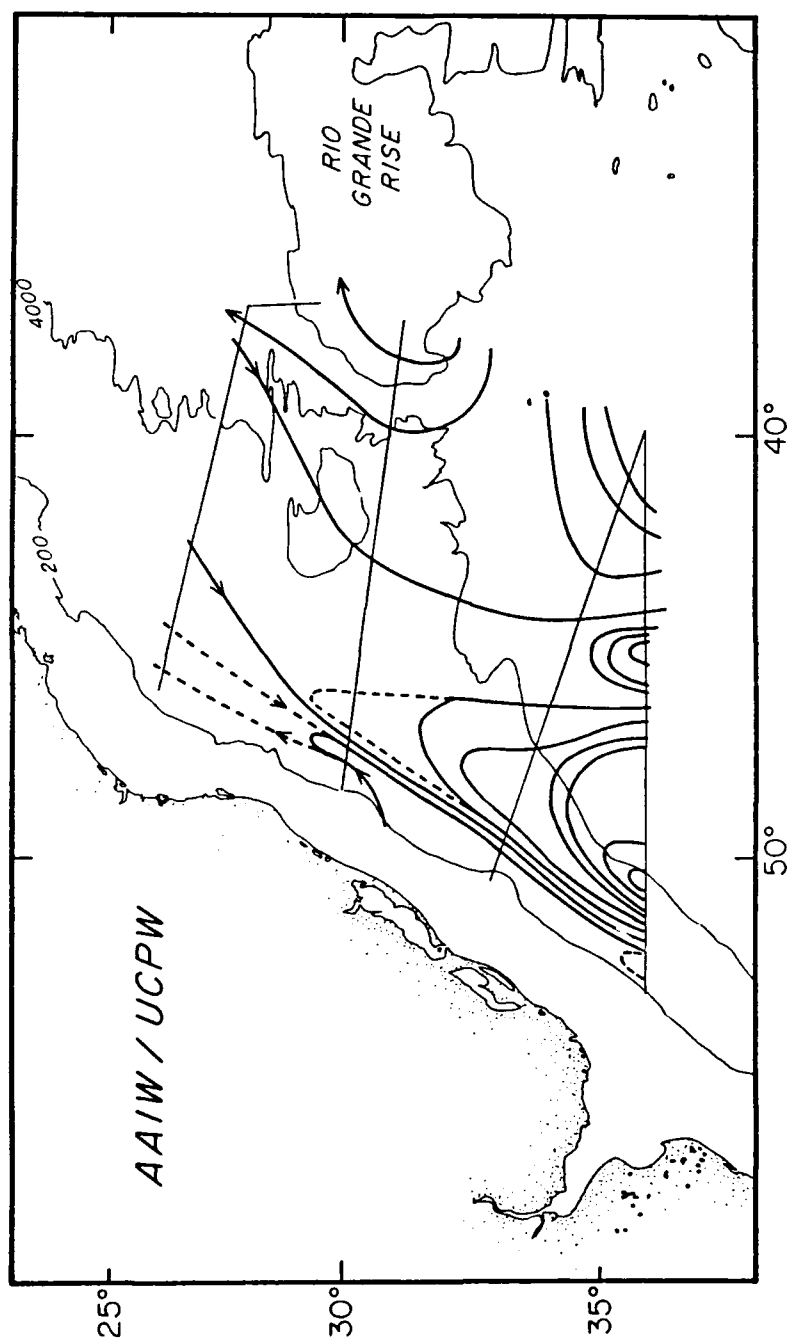


Figure 3.6: Transport cartoon for the AAIW/UCPW layer. Each solid line represents approximately 2 Sverdrups, with dashed lines indicating flows below that contour level.

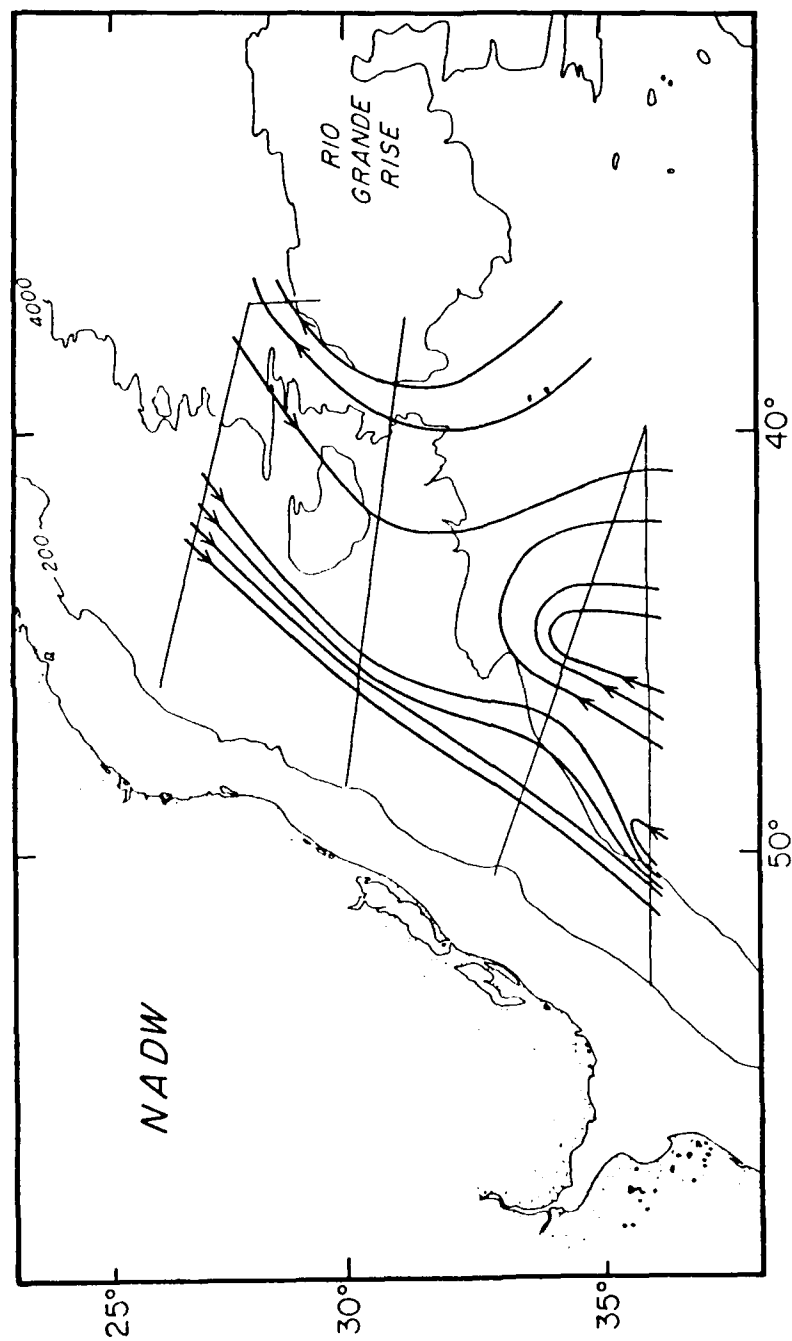


Figure 3.7: Transport cartoon for the NADW layer. Each solid line represents approximately 2 Sverdrups.

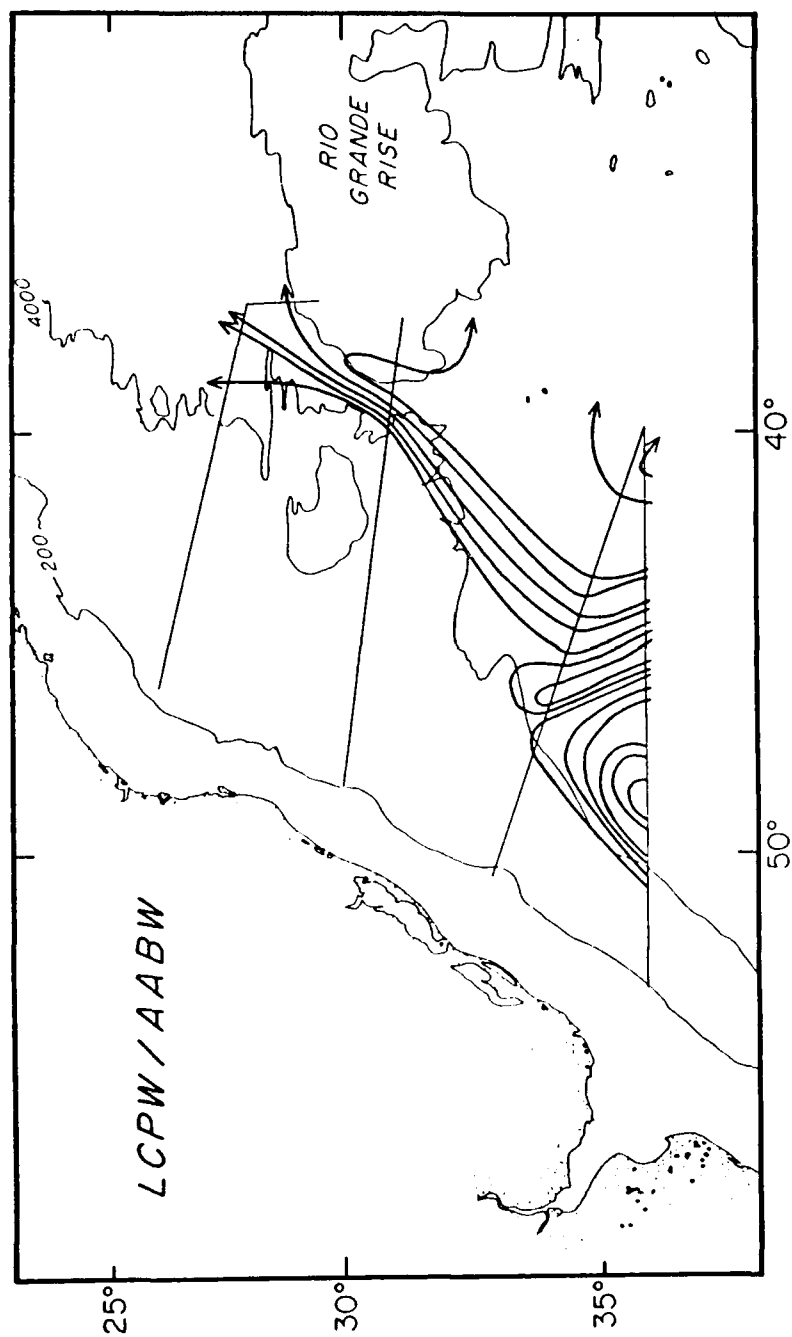


Figure 3.8: Transport cartoon for the AABW/LCPW layer. Each solid line represents approximately 1 Sverdrup.

in section 2.3.

### 3.4 How Good are the Results?

As was discussed at the beginning of the chapter, the choice of a ZVS for the Brazil Current is not something all authors agree on. To examine the effect of changing the ZVS on the transport estimates, the transports are recalculated with other choices of ZVS. The validity of the ZVS choices may then be explored, and the transports can be compared with historical estimates. The results are described below.

At 27° S (table 3.7), a shallower ZVS of 500 m sends the NADW in the wrong direction, although not critically so. The difference between this and our reference is not significant, although it results in a very strong inshore current of AAIW flowing north. Moving the ZVS deeper to Defant's 1300 m has little effect, primarily because the bulk of the current is over topography shallower than the reference surface.

layer transport (Sv)	ZVS		
	500 m	27.2 $\sigma_0$	1300 m
CW	-7.1	-11.7	-13.9
AAIW/UCPW	3.0	0.5	-0.6
NADW	0.9	-0.2	-0.2
LCPW/AABW	0.0	0.0	0.0

**Table 3.7: Transport of the Brazil Current at 27° S with various ZVS choices.**

At 31° S (table 3.8), the shallower ZVS— 500 m — results in a large AAIW current and an unreasonable NADW current of 9 Sv flowing north. Moving the reference deeper, to Defant's ZVS of 1500 m, has little effect on the CW, although it reverses the NADW. The bulk of the current lies over topography shallower than 1500 m. The Brazil Current transport compares favorably with that measured by PEGASUS

at 31° S (Evans and Mascarenhas, unpublished), particularly since the PEGASUS results did not span the entire current.

layer transport (Sv)	ZVS		
	500 m	27.1 $\sigma_0$ and bot	1500 m
CW	-4.3	-20.3	-21.1
AAIW/UCPW	9.2	-2.5	-2.5
NADW	8.6	-1.9	1.9
LCPW/AABW	0.0	0.0	0.0

**Table 3.8: Transport of the Brazil Current at 31° S with various ZVS choices.**

At 34° S (table 3.9) two shallower ZVS are given for the Brazil Current. The 700 m ZVS results in NADW flowing north, as does the 1700 m ZVS. The problem here, as explained above, is that most of the shear lies at the bottom of the stations. The only possible change that would be consistent with the water masses is adding southward bottom velocities to the current; this also boosts the growth of the CW to be in line with the other sections. The results are shown in the fourth column, with  $-2 \text{ cm s}^{-1}$  added to each station pair. The CW and AAIW/UCPW transports are acceptable, but too much NADW now comes through the section compared with the other sections. It is probably possible to adjust some of the bottom velocities for a reasonable Brazil Current, but a reference of zero bottom velocity in the current seems the best.



layer transport (Sv)	ZVS			bottom v -2 cm s <sup>-1</sup>
	700 m	1700 m	bottom	
CW	-8.0	-16.9	-26.8	-36.2
AAIW	.2	-3.3	-10.7	-17.4
NADW	5.1	4.2	-5.0	-17.2
AABW	1.0	1.1	0.7	-0.5

**Table 3.9: Transport of the Brazil Current at 34° S with various ZVS choices.**

Finally, at 36° S, two shallower and one deeper ZVS are given (table 3.10). The two shallow references (1400 m was the reference used by Gordon and Greengrove (1986)) result in huge northward flowing NADW currents, indicating that a deep ZVS is required at this section. The bottom reference sends AABW the wrong direction, and there is no source for the bottom water north of the section.

layer transport (Sv)	ZVS			
	1400 m	1800 m	45.8 $\sigma_4$	bottom
CW	-35.6	-41.0	-51.4	-60.0
AAIW/UCPW	-3.7	-8.8	-18.5	-25.8
NADW	16.3	7.1	-10.1	-23.3
LCPW/AABW	9.9	7.3	2.1	-2.9

**Table 3.10: Transport of the Brazil Current at 36° S with various ZVS choices.**

### 3.5 Summary

- At 27° S, the Brazil Current is shallow and weak, transporting less than 12 Sv south. This is consistent with values that have been obtained farther to the north.

- As the current moves south the transport in its upper layer increases to 50 Sv; in addition the current deepens. As the current moves offshore it is aligned over the southward moving NADW so that the total southward transport at 37° S is 80 Sv.

- Changing the ZVS to a shallower depth in the southern sections is inconsistent with the water mass information, as it results in NADW flowing north. The transport value here is comparable to that obtained by Peterson (1990), but significantly larger than other estimates to the south. Since Peterson's estimate is based on the same data as one of the other estimates, it must be concluded that the difference lies in the ZVS choice. Gordon and Greengrove's arbitrary use of a shallow ZVS results in artificially small transport values.

## Chapter 4

### A Simple Layer Model of the South Atlantic at 31° South

One of the limitations of the data used in this study is that they do not extend very far across the South Atlantic. This leads one to treat the Brazil Current as an isolated feature, instead of as an integral part of the subtropical circulation. This chapter explores the interplay of the Brazil Current with the over-turning modes of several of the water masses. The results of an inverse calculation of the South Atlantic (Rintoul, 1988) will be used to help set limits in the model.

Rintoul explored a variety of constraints in his inverse; the results we are interested in are the mass transports for the layers of surface water, intermediate water, deep water and bottom water (the inverse originally had thirteen layers, but these were grouped into four layers for the purpose of discussion). Rintoul found that the net transport across 32° S in each layer changed very little with different initial reference level choices, i.e. the constraints were strong enough to force the system to behave in a certain way. His "standard" model gave transports across 32° S of 8 Sv north of surface water, 5 Sv north of intermediate water, 17 Sv south of deep water, and 4 Sv north of bottom water. The net transport across the section is zero; thus these numbers can be thought of as exchanges among the different layers. The simple model constructed here will be asked to match the *sense* of the layer-to-layer exchanges found in Rintoul's inverse calculation.

Rintoul's net layer transports are used to constrain a simple model driven by

changes in layer thickness across the basin. This type of approach is explored by Stommel, Niiler and Anati (SNA, 1978) in the North Atlantic. SNA note that one of the strongest features in the North Atlantic is the change in depth of the  $10^{\circ}$  isotherm from east to west. They use this feature to divide the North Atlantic into a two layer system, and define three distinct regions in a cross section of the basin: the Gulf Stream, the recirculation, and an interior (fig 4.1). The geometry of the upper layer (defined by the  $10^{\circ}$  isotherm) is such that the western edge is thinner than the eastern edge; it is thickest in the bowl of the recirculation. SNA point out that the difference in height of the upper layer across the section suggests a warm to cold water conversion to the north. From the changes in layer thickness baroclinic transports are calculated for the upper layer. Because there is relatively little structure in the deep water, the baroclinic transport there has been set to zero. The two layers are allowed to exchange mass in the north. The system is constrained to have no interior barotropic transport. Based on an assumed layer-to-layer exchange, *barotropic transports for the Gulf Stream and recirculation* are computed to balance mass across the section. The net result is that the amount of overturning, or layer-to-layer exchange, is tied to the strength of the recirculation. This does not specifically set the strength of the barotropic transport for either the Gulf Stream or the recirculation; rather, it specifies limits on the barotropic transports based on what is known about the exchange between the layers to the north.

A similar approach is taken here for the South Atlantic, however, it is important to note that the two oceans are distinctly different. First, the net meridional heat flux in the South Atlantic is toward the equator. This manifests itself in the geometry of the  $10^{\circ}$  isotherm (fig 4.2), which is shallower at the eastern edge than western edge at  $31^{\circ}$  S; the reverse is found in the North Atlantic. Second, the deeper layers show a great deal more structure than is seen in the North Atlantic. The impact of these differences on the results will be examined as we try to understand the relationship between the large scale balances in the South Atlantic and the Brazil Current.

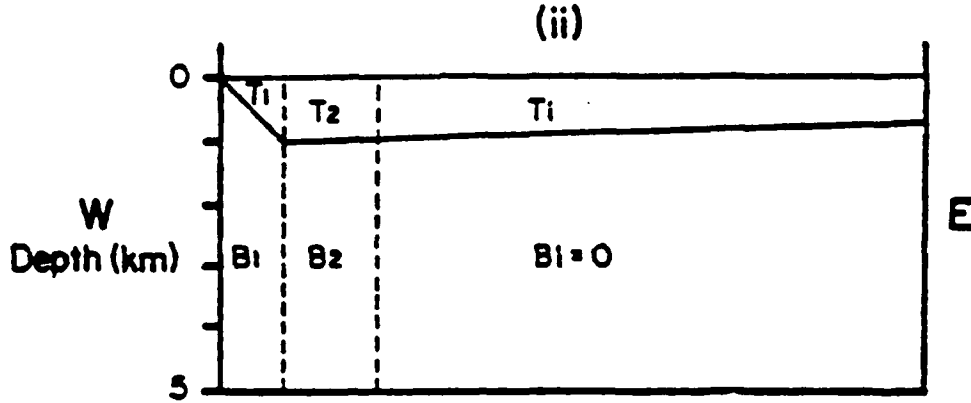


Figure 4.1: Schematic diagram of a two layer model of the Gulf Stream. The geometry is set by the 10° isotherm. from Stommel, Niiler and Anati (1978).

#### 4.1 Construction of the Layer Systems

This chapter contains results for two, three and four layer systems, so the geometry is described in terms of a generalized multilayer system. The first step in constructing the system is the calculation of baroclinic transports from the geometry described by the data (fig 4.4). A schematic of the four layer model is shown in figure 4.3.

The baroclinic velocity,  $v$ , in each layer is independent of depth; the change in velocity between layers is determined by the slope of the interface dividing the two layers (such an approach is described in chapter 6 of Pedlosky, 1982).

$$v_{i,j} - v_{i-1,j} = \frac{g}{f\rho_o} \frac{\Delta\rho}{\Delta x} \Delta h = \frac{g}{f\rho_o} \frac{\Delta\rho}{\Delta x} (h_{i,j+1} - h_{i,j}) \quad (4.1)$$

where  $i$  identifies the layer and  $j$ , the region.  $\rho_o$  is an average density for the ocean; the  $h$ 's are the thicknesses of each layer. The baroclinic velocity in the lowest layer is generally set to zero, following the example of SNA. The baroclinic transport,  $t$ , is determined by multiplying the velocity by the width and average height for that section

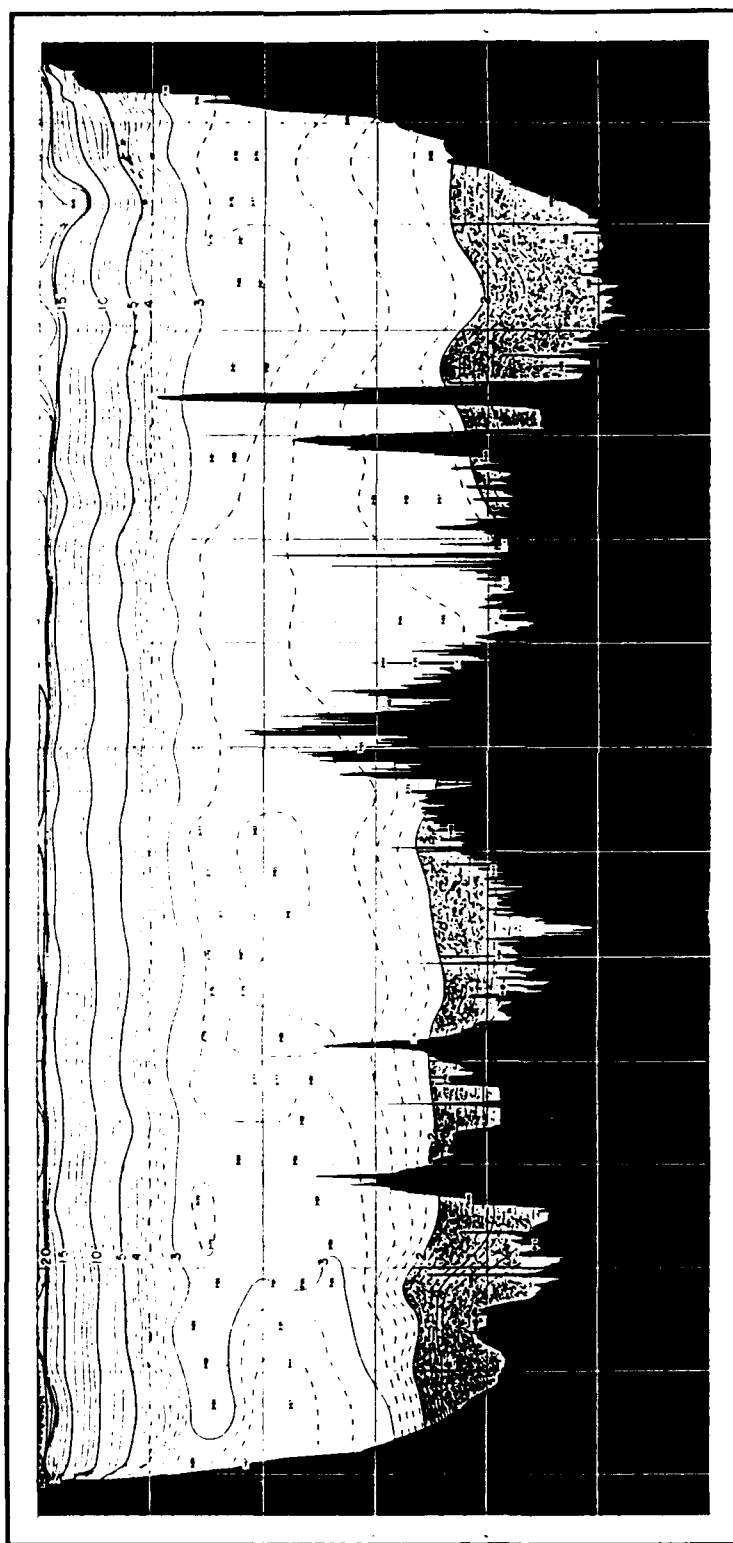


Figure 4.2: Temperature section across 32° S. from Fuglister (1960).



$$\begin{aligned}
t_{i,j} &= v_{i,j} * \bar{h}_{i,j} * \Delta x \\
&= v_{i-1,j} + \frac{g}{f\rho_o} \frac{\Delta\rho}{\Delta x} (h_{i,j+1} - h_{i,j}) \frac{h_{i,j+1} + h_{i,j}}{2} \Delta x \\
&= v_{i-1,j} + c_i (h_{i,j+1}^2 - h_{i,j}^2)
\end{aligned} \tag{4.2}$$

$$c(i) = \frac{g\Delta\rho_i}{2f\rho_o} \tag{4.3}$$

The barotropic transport contributes a weighted amount to each layer's mass balance. The weighting,  $p$ , is determined by the average height of that layer, i.e.

$$p_{i,j} = \frac{\bar{h}_{i,j}}{H_j} \tag{4.4}$$

$$H_j = \sum_i \bar{h}_{i,j} \tag{4.5}$$

The resulting mass balance for layer  $i$  is then

$$\mathcal{T}_i + B_j p_{i,j} + F_i - F_{i-1} = 0 \tag{4.6}$$

or in matrix form for a three layer system

$$\begin{pmatrix} p_{1,1} & p_{2,1} & p_{3,1} & 1 & 0 \\ p_{1,2} & p_{2,2} & p_{3,2} & -1 & 1 \\ p_{1,3} & p_{2,3} & p_{3,3} & 0 & -1 \end{pmatrix} \begin{pmatrix} B_1 \\ B_2 \\ B_3 \\ F_1 \\ F_2 \end{pmatrix} = - \begin{pmatrix} \mathcal{T}_1 \\ \mathcal{T}_2 \\ \mathcal{T}_3 \end{pmatrix} \tag{4.7}$$

$$\mathcal{T}_i = \sum_j t_{i,j} \tag{4.8}$$

$\mathcal{T}$  is the net baroclinic transport in a layer across the section. The  $B$ 's are the barotropic transports associated with different regions of the flow; the layer-to-layer



exchange is given by  $F$ . Another way of thinking of the  $F$ 's is as *a measure* of the net transport of the layer across the section. For example, if  $F_1$  Sv are converted from layer two to layer one, then layer one must have a net northward transport of  $F_1$  to balance mass; for layer two, the transport north is  $F_2$  minus  $F_1$ . From the model's perspective, positive flow always indicates flow into the layer or box; thus an  $F_1$  transferring water up into layer one is positive, and a southward flowing Brazil Current sending water into the layer is positive. These equations can be adapted to any number of layers and regions, and several cases will be discussed.

The sensitivity of the model to the various input (the layer depths, the net water column depth and the density difference parameters) has been explored, and some of the results are shown below. The model proved to be most sensitive to the layer geometry on the eastern boundary. Given the above equations, this sensitivity should come as no surprise. The difference between the eastern and western boundaries yields the net baroclinic imbalance in each layer; any significant change in this imbalance alters the final solutions. Changes in the water column depth and the density parameters had to be extreme before they impacted the solutions significantly.

## 4.2 Two Layer Systems

The two layer system is used here to explore how the South Atlantic works with this model. The ocean is initially treated as two layers, having a configuration similar to that used by SNA. SNA obtained solutions by setting the interior barotropic transport to zero. Because the South Atlantic has a great deal of deep water structure, this step is likely to give poor results. The effect of such an assumption can be easily checked with the two layer system, by testing the sensitivity of the results to different applications of the barotropic transports. In addition, different choices can be made for the isotherms defining the layers. SNA used the  $10^\circ$  isotherm because it varies in depth a great deal across the basin in the North

Atlantic. Equally interesting in the South Atlantic is the 3.4° isotherm, near the boundary of the AAIW and NADW water masses. Since it separates northward and southward flowing water masses it might be a more appropriate choice. Both possibilities are explored with the two layer system: first, the effect of setting the barotropic transport to zero in the interior, and second, the effect of different layer choices.

The two layer system has two constraints. First is overall mass conservation:

$$T_1 + B_1 + B_2 = 0 \quad (4.9)$$

and conservation of mass in the upper layer

$$T_1 + p_{1,1}B_1 + p_{2,1}B_2 + F_1 = 0 \quad (4.10)$$

The other constraint that is required for a solution to be deemed acceptable is for the layer-to-layer conversion,  $F_1$ , to be positive, i.e. a cold to warm overturning mode.  $F_1$  can be specified as a fraction of the total baroclinic transport across the section

$$F_1 = \gamma T_1 \quad (4.11)$$

This artifice allows the barotropic transports to be written as a function of  $\gamma$ , yielding a simple equation for the barotropic Brazil Current,

$$B_1 = T_1 \frac{1 + \gamma - p_{2,1}}{p_{2,1} - p_{1,1}} \quad (4.12)$$

If  $p_{1,1}$  and  $p_{2,1}$  are equal the two equations are degenerate and no unique solution can be found. If the difference between them is small, then  $B_1$  will be correspondingly large. Finally, note that the sign of  $B_1$ , the barotropic Brazil Current will be determined by which of the two weighting factors is larger.

To see how a zero barotropic interior affects the results, the two layer system is divided into three region, as in SNA. In the first run the interior has no barotropic

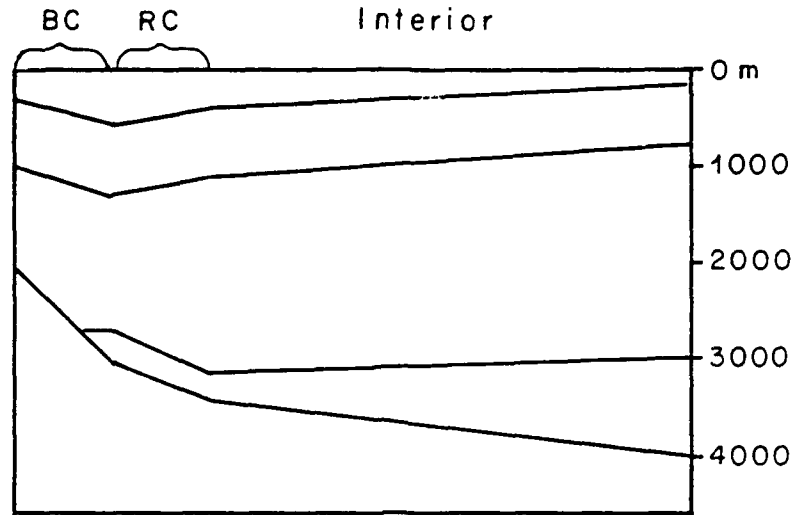


Figure 4.4: Geometry of a multilayer model of the Brazil Current. The geometry is set by the 2.6, 3.4 and 10° isotherm.

transport, but a barotropic transport is allowed for the recirculation; this is analogous to the SNA treatment. The second run treats the recirculation as part of the interior, with one barotropic transport for the entire interior (this changes the effective height over which the barotropic transport is spread in each layer). The two runs differ only by changing the weighting  $p_{2,1}$ :

$$p_{2,1} = \frac{h_{2,1}}{H_2} \quad \text{Barotropic recirculation}$$

$$p_{2,1} = \frac{h_{2,1} + h_{4,1}}{H_2 + H_4} \quad \text{Barotropic interior}$$

The data used to determine the thermocline heights are a combination of the 31° S section across the Brazil Current and Fuglister's IGY data from 32° S (fig 4.2), both of which will now be referred to as 31° S. The two layers are separated by the 10° isotherm, shown by the top line in fig 4.4.

The constant,  $c$ , representing the density difference between the two layers, is set using the data from the modern 31° S section;  $c$  is chosen to give the same baroclinic transport in the Brazil Current as is measured at 31° S, assuming a 10° C ZVS (the baroclinic Brazil Current is approximately 15 Sv, with an baroclinic interior transport of 20 Sv). This results in a  $c$  of 80, which corresponds to a density

difference of approximately  $.7 \text{ kgm}^{-3}$ . The range of  $\gamma$  is chosen in all models so that  $F_1$  has a range of 0 to 20 Sv, with the sense being that of upper water being formed in the south (this is the opposite of the North Atlantic). Thus all the solutions presented for this case satisfy the requirement on  $F_1$ . Since the upper layer is thinner in the east than in the west,  $\gamma$  must be negative. Rintoul's standard model has an  $F_1$  of 8 Sv.

The results (fig 4.5) indicate that the treatment of  $B_2$  is critical to the solution (the first run, with no barotropic interior, is the solid line; the second run is the dashed line). When the interior barotropic transport is constrained to zero, the resulting barotropic Brazil Current and recirculation are large. When the barotropic transport is spread over the interior, the magnitude of the barotropic terms is smaller. More importantly, the sign of the barotropic transport is reversed. The treatment of  $B_2$  radically changes the result.

Part of the difference between the two runs is caused by the choice of the  $10^\circ$  isotherm as a layer boundary. When the barotropic transport is ascribed to the recirculation,  $p_{2,1}$  (.208) is greater than  $p_{1,1}$  (.195); the reverse is true when the barotropic transport is spread across the interior and  $p_{2,1}$  (.111) is reduced. The reversal would not happen in the North Atlantic, as the eastern edge of the  $10^\circ$  isotherm is deeper than the western edge.

The same two runs are done using the  $3.4^\circ$  isotherm to divide the two layers, with the geometry given by the second layer shown in fig 4.4. When a different isotherm is used to separate the layers, the size of the baroclinic Brazil Current (23 Sv) and sizes of the weighting factors ( $p_{1,1}$  is now .45 and  $p_2$  is .4) are altered. As a result, comparing the two cases is not simple. In addition  $F_1$  is now a layer-to-layer exchange between different layers; Rintoul's value for this combination, 13 Sv, is still within the range explored. The figure labeled as the Brazil Current for each run is only the transport in the upper layer in the Brazil Current region,

$$BC = B_1 * p_{1,1} + t_{1,1} \quad (4.13)$$

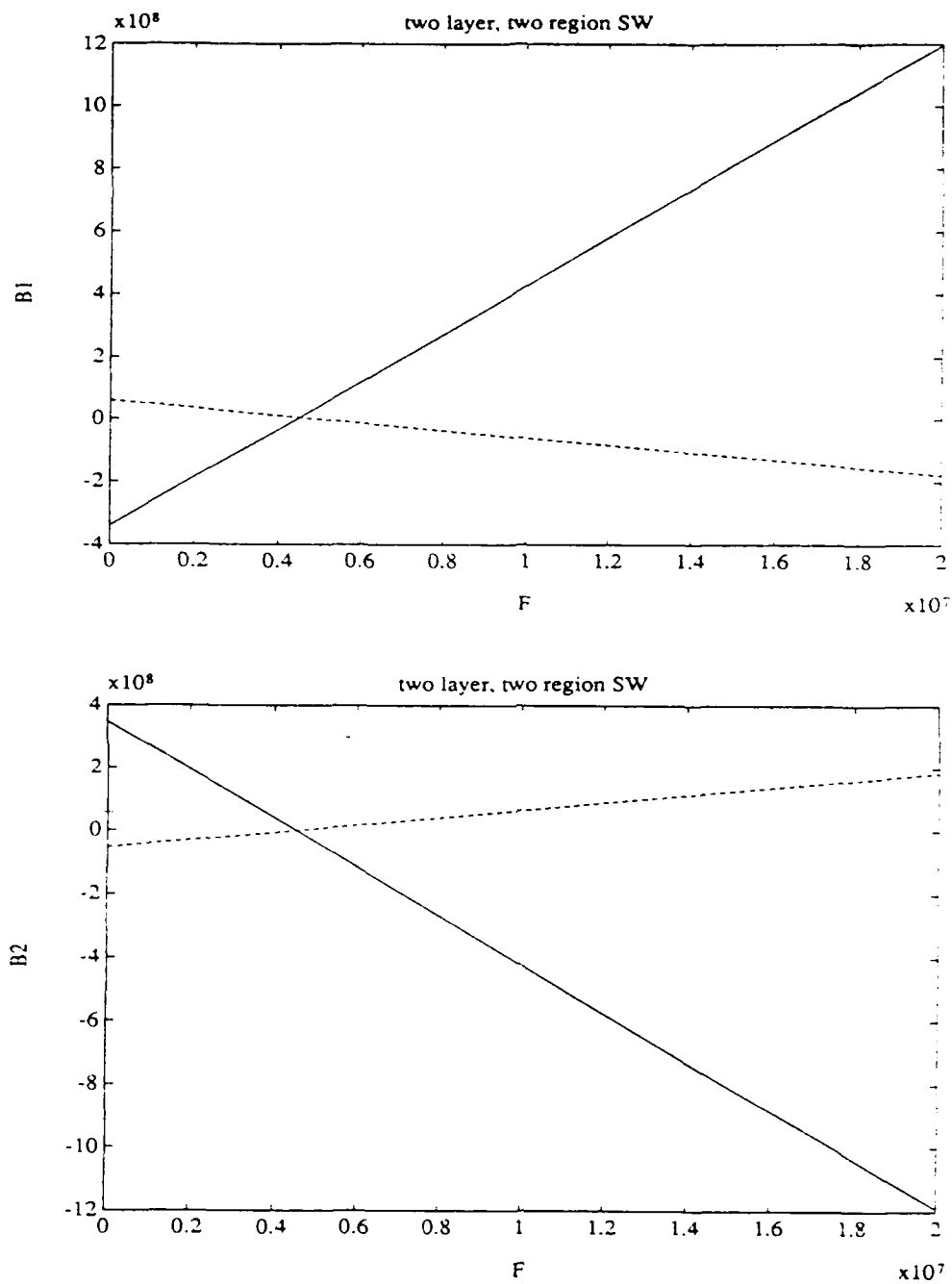


Figure 4.5: The results from the two layer, two region model which uses the  $10^\circ$  isotherm to separate the two layers. (a) is the barotropic transport ( $m^3s^{-1}$ ) in the Brazil Current; (b) is the barotropic transport for either the interior with no recirculation (---) or the recirculation with no interior (—).

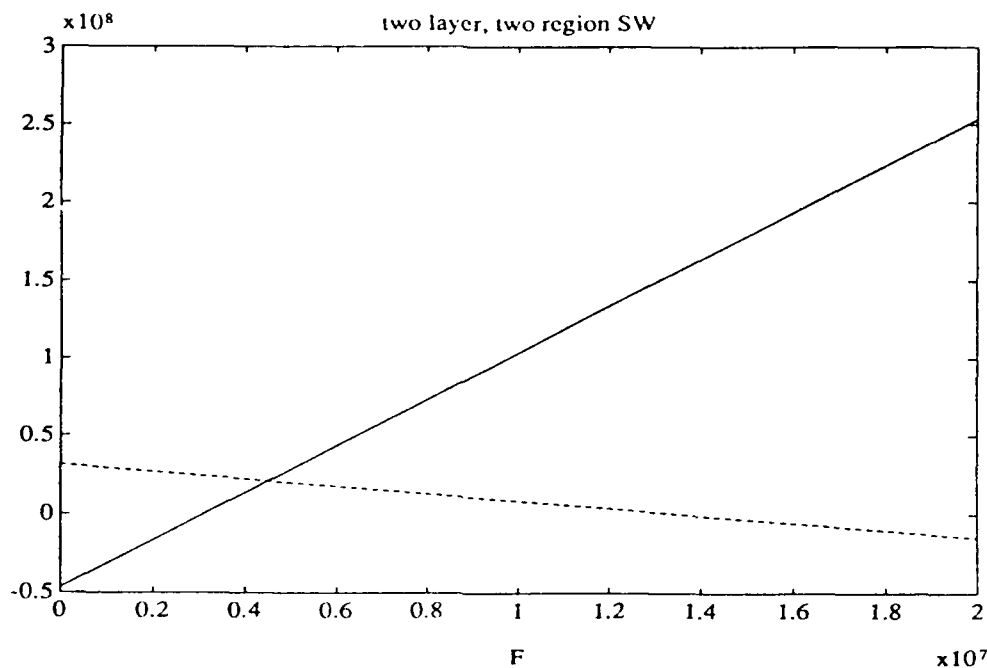


Figure 4.5: The results from a two layer, two region model which uses the  $10^\circ$  isotherm to separate the two layers. (c) is the net Brazil Current transport in the upper layer.

The most important change is that this geometry is not as sensitive to where  $B_2$  is applied (fig 4.6). The sign of the barotropic transports, regardless of where  $B_2$  is applied, is the same, however, the magnitudes of the barotropic transports are different by more than a factor of two.

Instead of setting the barotropic transport in the interior to zero, all three regions can be included so that both the recirculation and the interior have barotropic transport terms. By allowing barotropic transport in all three regions, another unknown is introduced,  $B_3$ , without adding any constraints. Results can be obtained if the barotropic recirculation,  $B_2$ , is represented parametrically,

$$B_2 \approx \alpha B_1 \quad (4.14)$$

Initially no assumption will be made about the sign of  $\alpha$ . The two layer, three region case is run for the second geometry, described above. The magnitudes of the barotropic transports are reduced (the maximum barotropic Brazil Current is reduced from 200 to 80 Sv), suggesting that the system does not have to work as

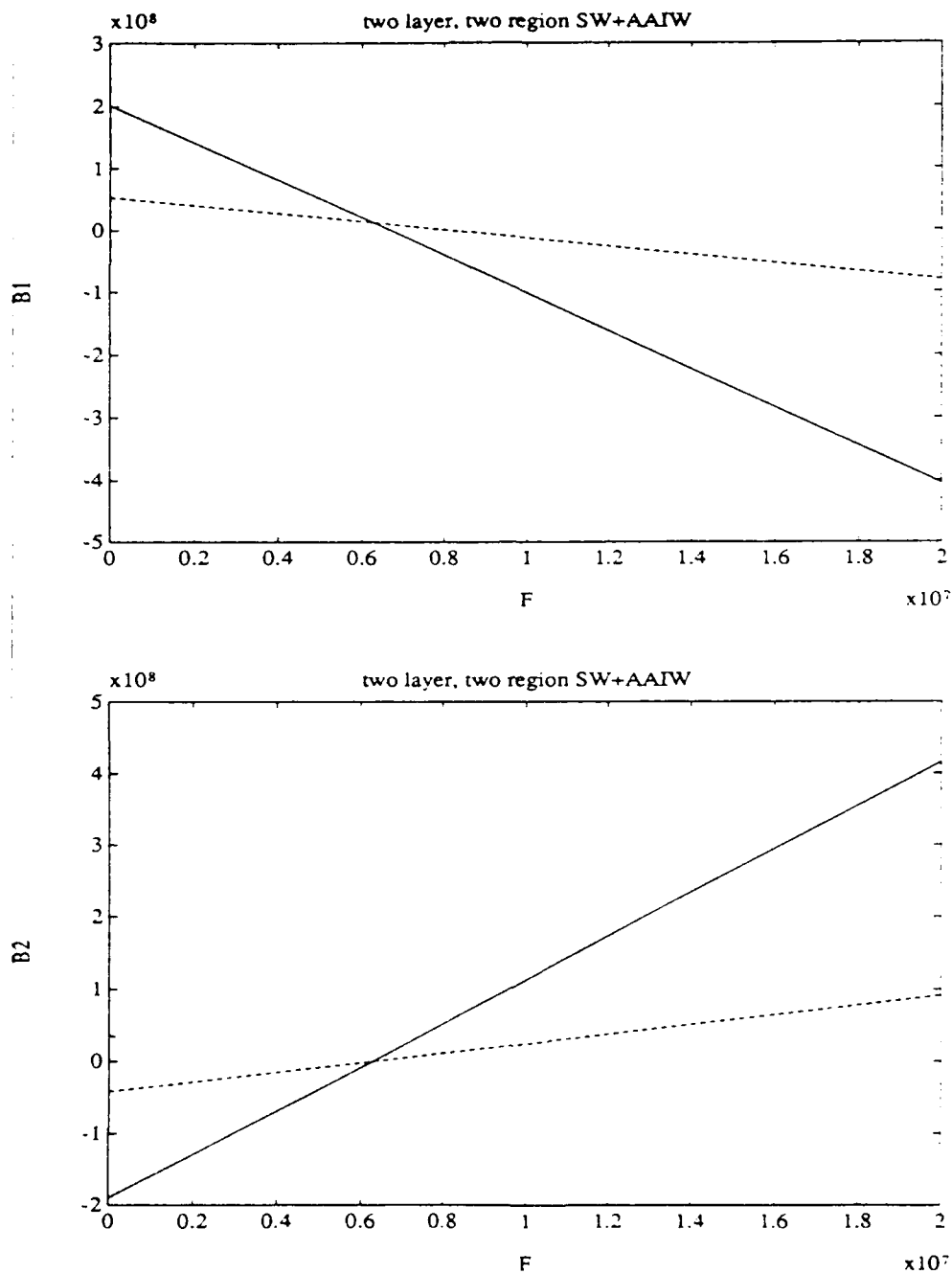


Figure 4.6: The results from the two layer, two region model which uses the  $3.4^\circ$  isotherm to separate the two layers. (a) is the barotropic transport ( $m^3s^{-1}$ ) in the Brazil Current; (b) is the barotropic transport for either the interior with no recirculation (---) or the recirculation with no interior (—).

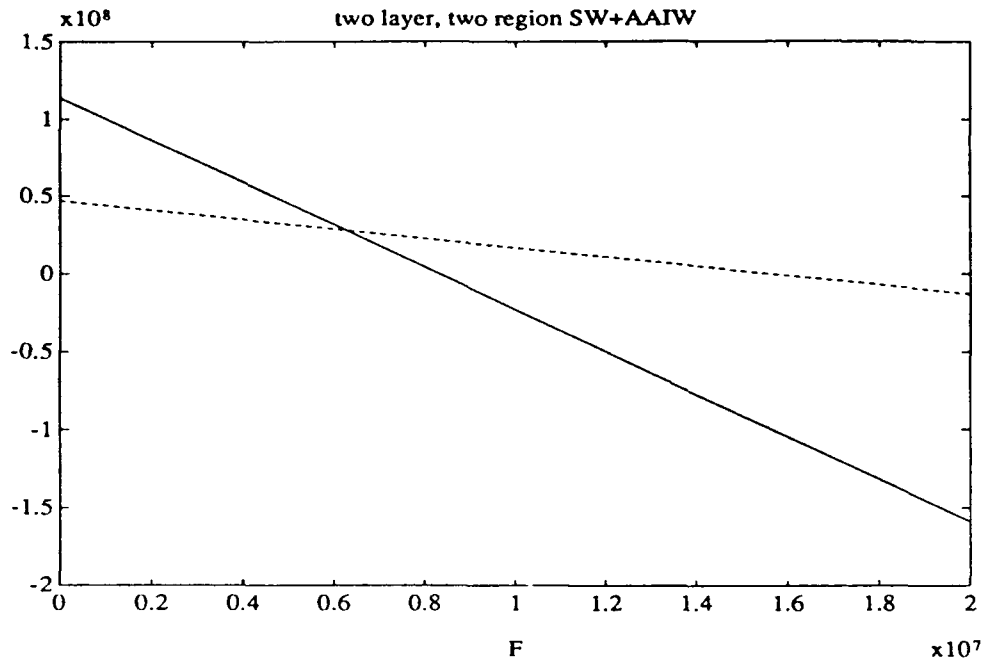


Figure 4.6: The results from a two layer, two region model which uses the  $3.4^{\circ}$  isotherm to separate the two layers. (c) is the net Brazil Current transport in the upper layer.

hard to achieve a balance (fig 4.7). This is encouraging; however, we know a two layer system cannot hope to represent realistically even the gross details of the region. Clearly three layer or more layers will better be able to represent these details. In addition, the inclusion of a third layer will introduce another requirement on the sense of the overturning modes: that some of the southward flowing NADW be balanced by northward flowing bottom water.

### 4.3 Three Layer Systems

In the three layer system, the top layer is defined to be a combination of the CW and AAIW, above the  $3.4^{\circ}$  isotherm. The second layer is NADW, and the third is a combination of LCPW and AABW, below the  $2.6^{\circ}$  isotherm. The IGY section across  $31^{\circ}$  S shows a good deal of variation in the thickness of these layers. Adding a third layer adds a constraint, since mass must be balanced within the new layer; another



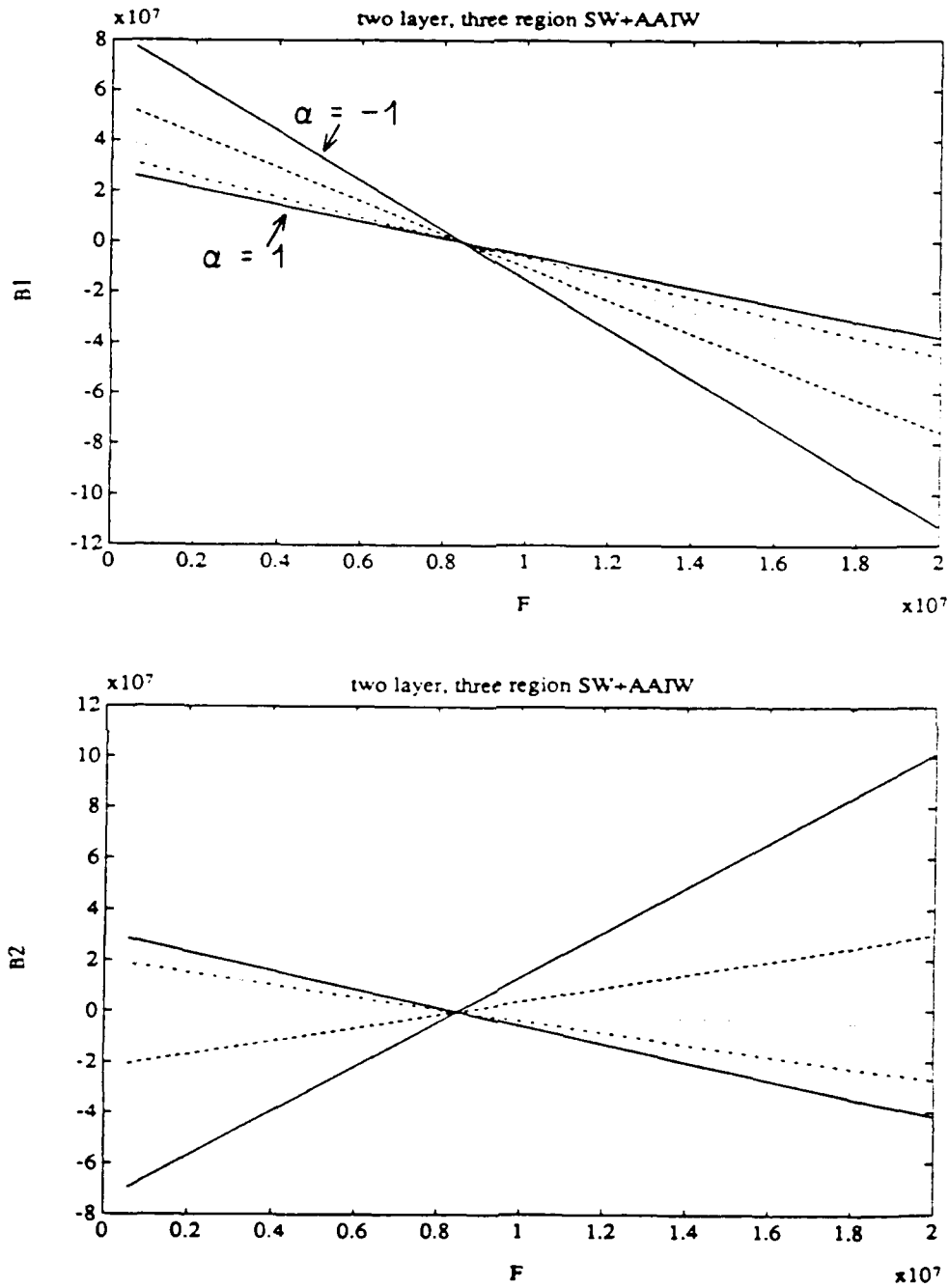


Figure 4.7: The results from the two layer, three region model. The different lines are the results for varying  $\alpha$  between  $\pm 1$ , as indicated. (a) is the barotropic transport ( $m^3 s^{-1}$ ) in the Brazil Current; (b) is the barotropic transport for the recirculation.

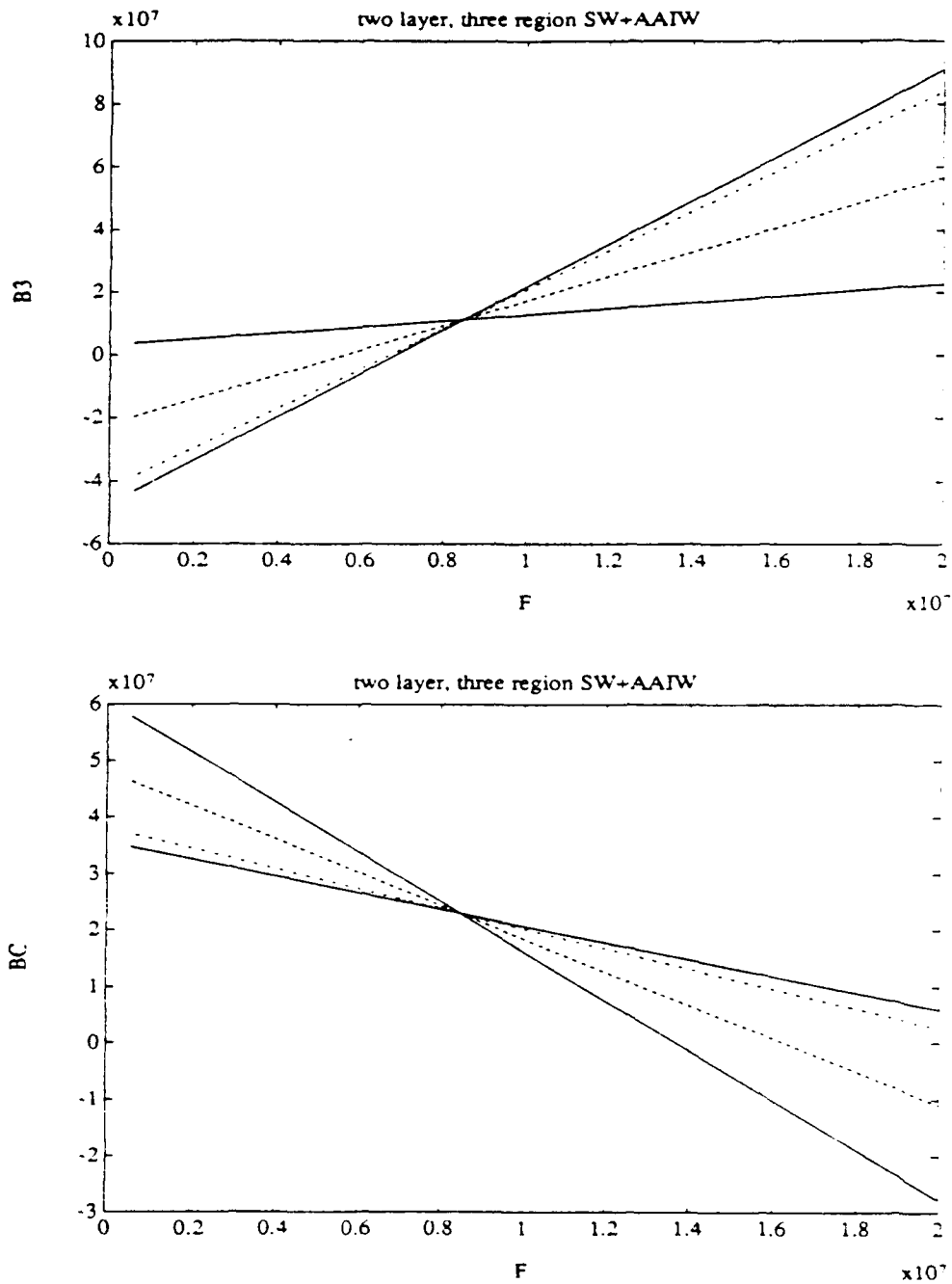


Figure 4.7: The results from the two layer, three region model. The different lines are for varying  $\alpha$  as indicated previously. (c) is the barotropic transport ( $m^3s^{-1}$ ) for the interior; (d) is the Brazil Current transport in the upper layer.

unknown is also added, namely, a second layer-to-layer conversion,  $F_2$ . AABW should be formed in the south, implying the sign of  $F_2$  should be negative. Rintoul's work indicates that the sign of  $F_1$  should be positive; his value for this case is 13 Sv.

As in the two layer runs, baroclinic transport in the bottom layer is set to zero and the baroclinic transport in the top two layers is computed from changes in layer thickness. The constants,  $c_1$  and  $c_2$ , are set for both layers by matching the transports to those computed from the 31° S transect using a reference level between NADW and AABW (a southward flowing Brazil Current of about 30 Sv and southward flowing NADW of about 10 Sv). The sensitivity of the model to various  $c$ 's is explored in the first case, which is a three layer, two region system (fig 4.8). Once again, this run shows the difference between  $B_2$  applied generally across the interior or to the recirculation. The range in  $c_1$ , from 40 to 120, corresponds to a change in  $\Delta\rho$  from 0.315 to 0.946  $kgm^{-3}$ . Qualitatively the solutions are similar, suggesting the model is not overly sensitive to reasonable choices for  $c$ .

The next step is to run the full three layer, three region system. The parameters are the same as those for the two layer, three region case,  $\alpha$  and  $\gamma$ . Put into matrix form this yields three equations and three unknowns in addition to the two parameters:

$$\begin{pmatrix} p_{1,1} + \alpha p_{2,1} & p_{3,1} & 0 \\ p_{1,2} + \alpha p_{2,2} & p_{3,2} & 1 \\ p_{1,3} + \alpha p_{2,3} & p_{3,3} & -1 \end{pmatrix} \begin{pmatrix} B_1 \\ B_3 \\ F_1 \end{pmatrix} = - \begin{pmatrix} T_1(1 + \gamma) \\ T_2 - \gamma T_1 \\ T_3 \end{pmatrix} \quad (4.15)$$

We would like to limit the range of  $\alpha$  explored. To determine what might be physically meaningful values for  $\alpha$ , the model is run for a large range of layer-to-layer transports, with  $F_1$  varying between 0-20 Sv and  $F_2$  between minus 0-9 Sv (estimates of AABW production are about 4 Sv).  $B_1$  and  $B_2$  are computed separately, and then a plot of  $\alpha$  (fig 4.9) is obtained by dividing  $B_2$  by  $B_1$ . When  $F_1$  is large,  $F_2$  alters  $\alpha$  only slightly;  $\alpha$  is constant at about -1.5. As  $F_1$  decreases, discontinuities occur in the  $\alpha$  plots as  $B_1$  passes through zero. When  $B_1$  changes

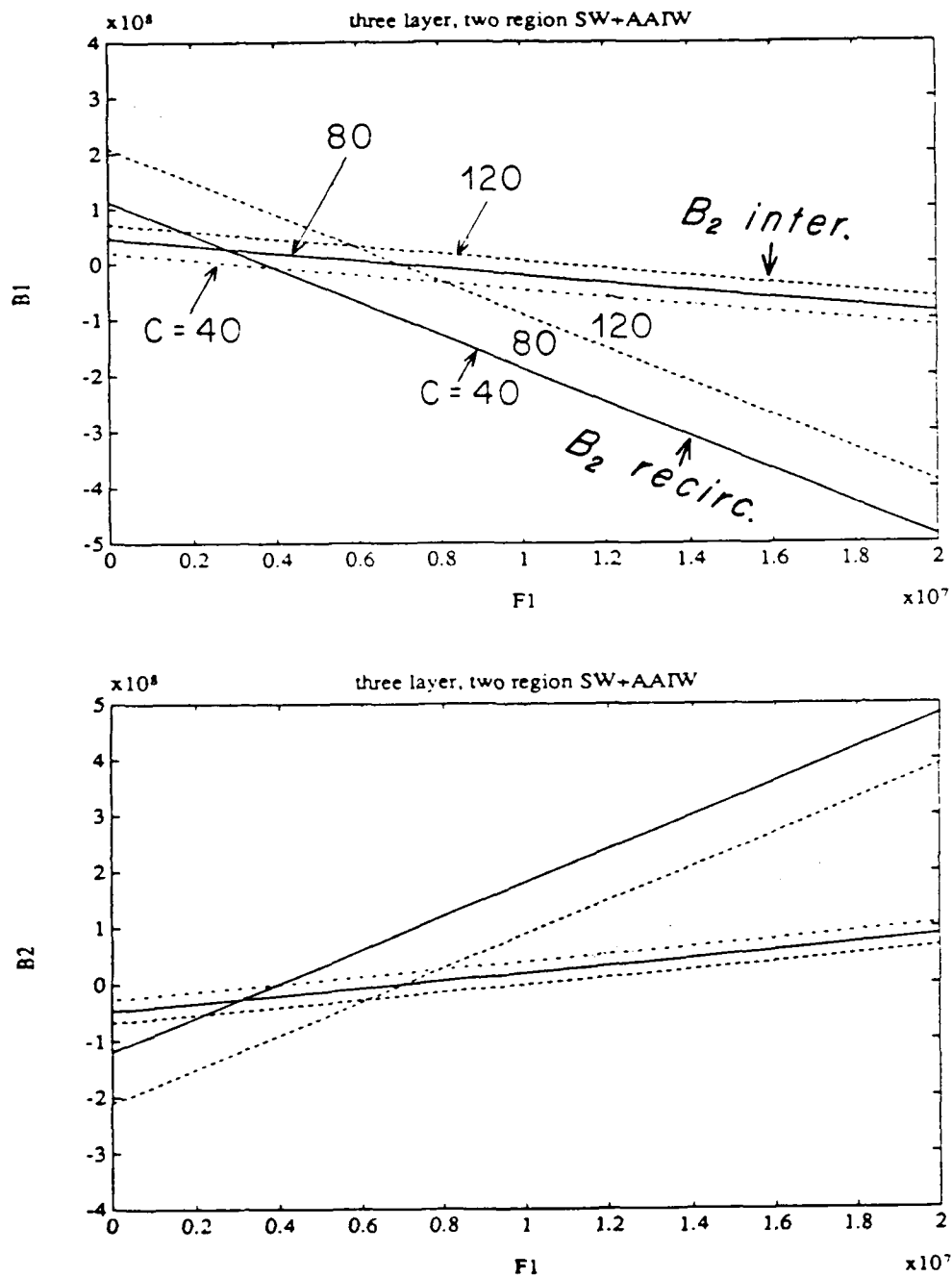


Figure 4.8: The results from the three layer, two region model.  $c_1$  has values of 40, 80 and 120. The two sets of runs are as described in figure 4.4. (a) is the barotropic transport ( $m^3 s^{-1}$ ) in the Brazil Current; (b) is the barotropic transport for the recirculation.

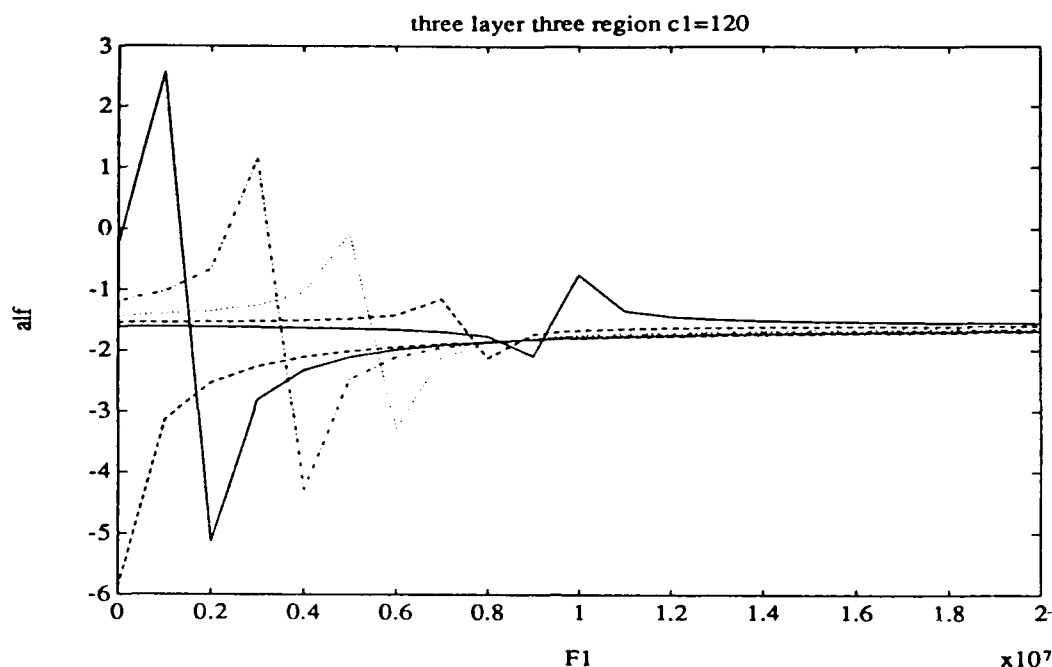


Figure 4.9: Plot of the ratio of the barotropic transports of the Brazil Current to that of the recirculation for a range of  $F_2$  between 0 to 9 Sv.

sign  $\alpha$  becomes positive, but  $B_2$  is close in magnitude to  $B_1$ ; once  $B_2$  passes through zero  $\alpha$  once again falls near -1.5. The solution region in which  $B_1$  and  $B_2$  are virtually zero will be ignored, and  $\alpha$  will be limited to the range of -1.75 to 0.  $\alpha$  between -1.75 and -1 corresponds to the magnitude of  $B_2$  being larger than that of  $B_1$ ; the reverse is true between -1 and 0. In all cases the signs of the two barotropic transports are opposite.

The case run uses  $c_1=120$  (fig 4.10), with a baroclinic Brazil Current of about 33 Sv (with a net upper layer baroclinic transport of -12 Sv). The two runs with the magnitude of  $B_2$  greater than that of  $B_1$  ( $\alpha$  of -1.75 and -1.5) have much larger ranges for  $B_1$  and  $B_2$  than the other runs.  $B_3$  and  $F_2$  also have different responses in these two runs. At an  $F_1$  of about 10 Sv the solutions converge with  $B_1$  and  $B_2$  both zero (i.e., the value of  $\alpha$  does not matter). For  $F_1$  less than this,  $B_1$  increases the strength of the Brazil Current and  $F_2$  is generally negative, that is, NADW is converted to bottom water. For larger  $F_1$ , the Brazil Current is decreased until it eventually reverses, and bottom water is converted to NADW.

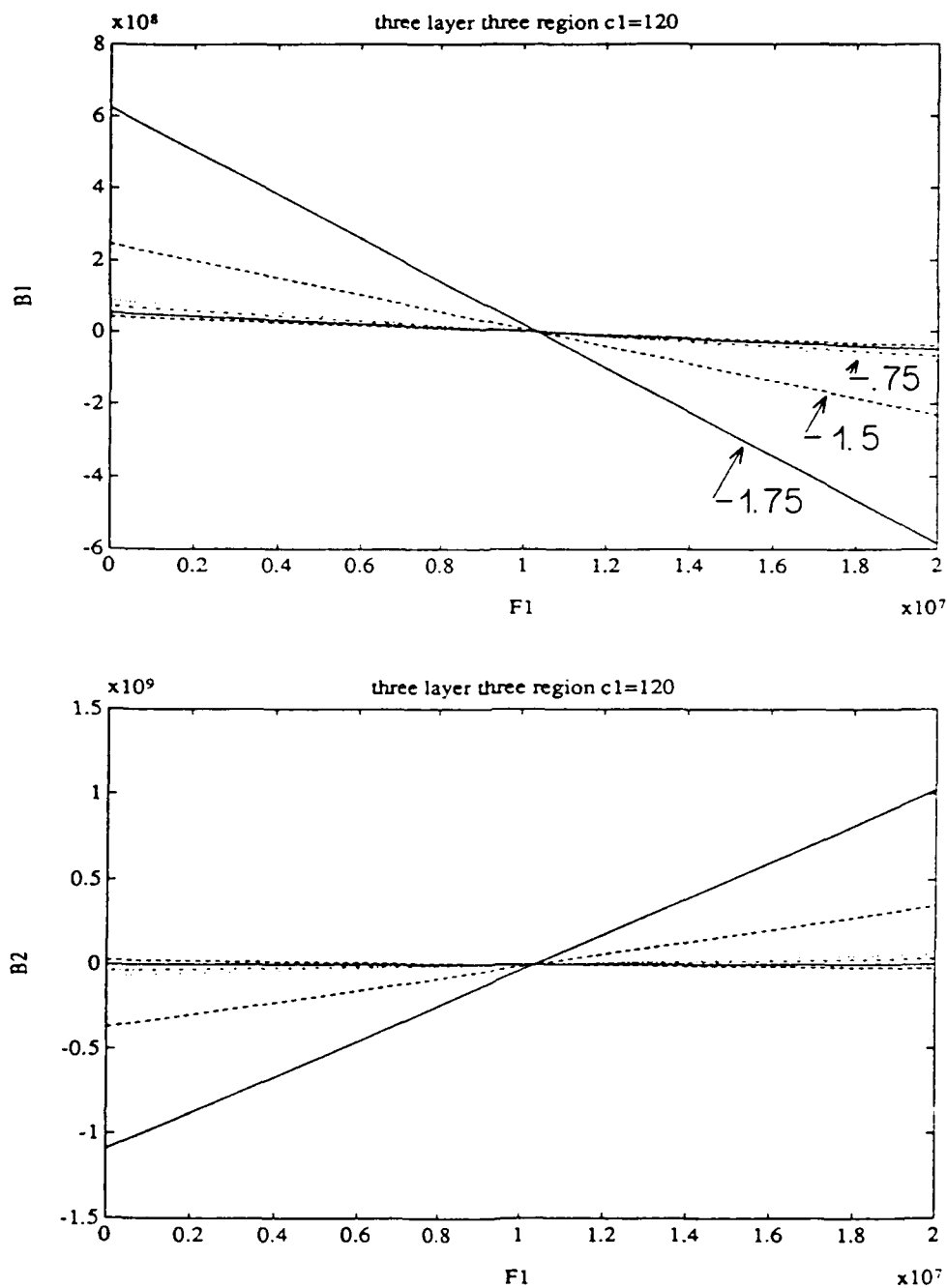


Figure 4.10: The results from the three layer, three region model. The different lines are the results for varying  $\alpha$  between 0 and -1.75, as indicated. (a) is the barotropic transport ( $m^3s^{-1}$ ) in the Brazil Current; (b) is the barotropic transport for the recirculation.

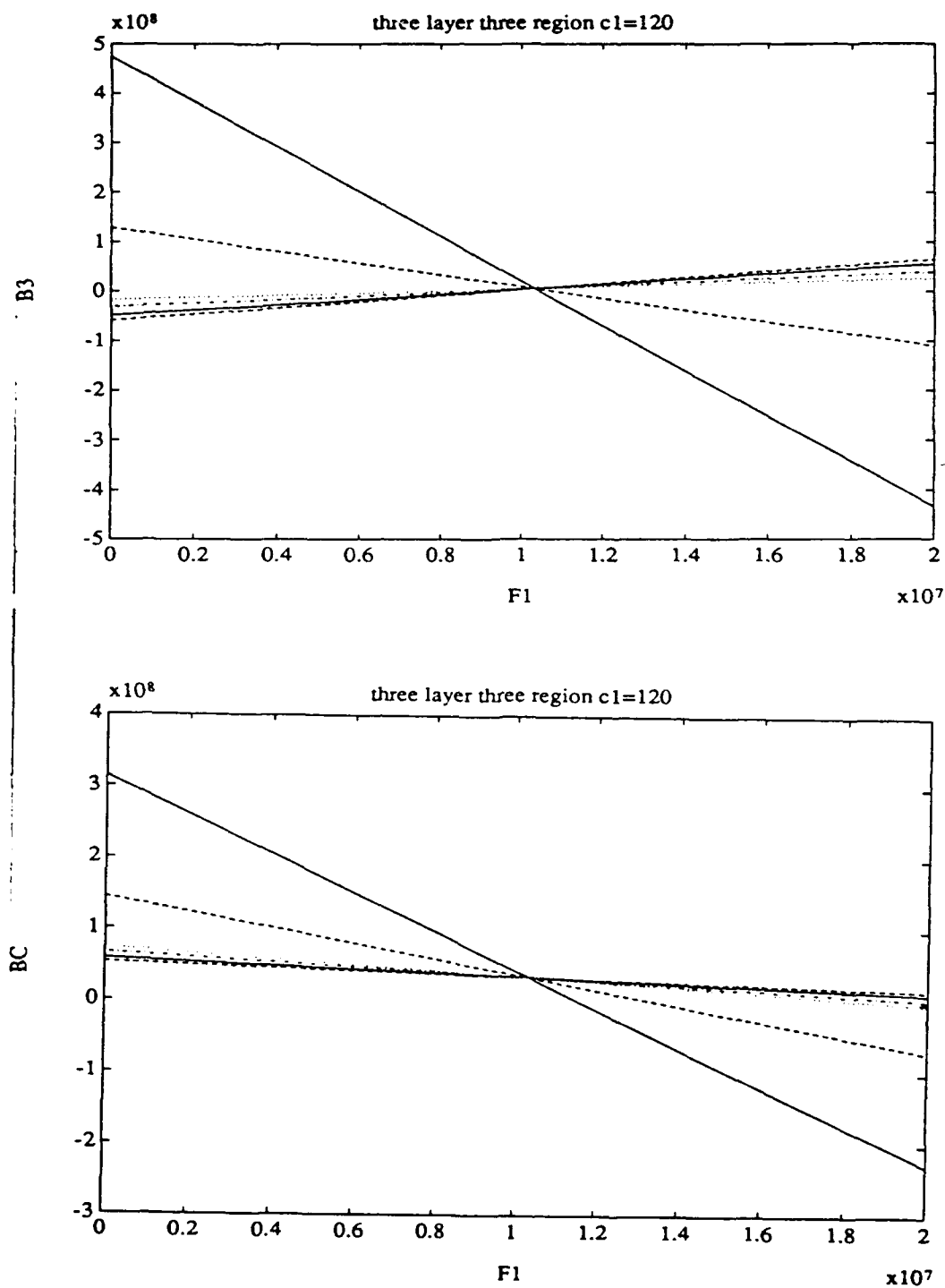


Figure 4.10: The results from the three layer, three region model. The different lines are for varying  $\alpha$  as indicated previously. (c) is the barotropic transport ( $m^3s^{-1}$ ) for the interior; (d) is the Brazil Current transport in the upper layer

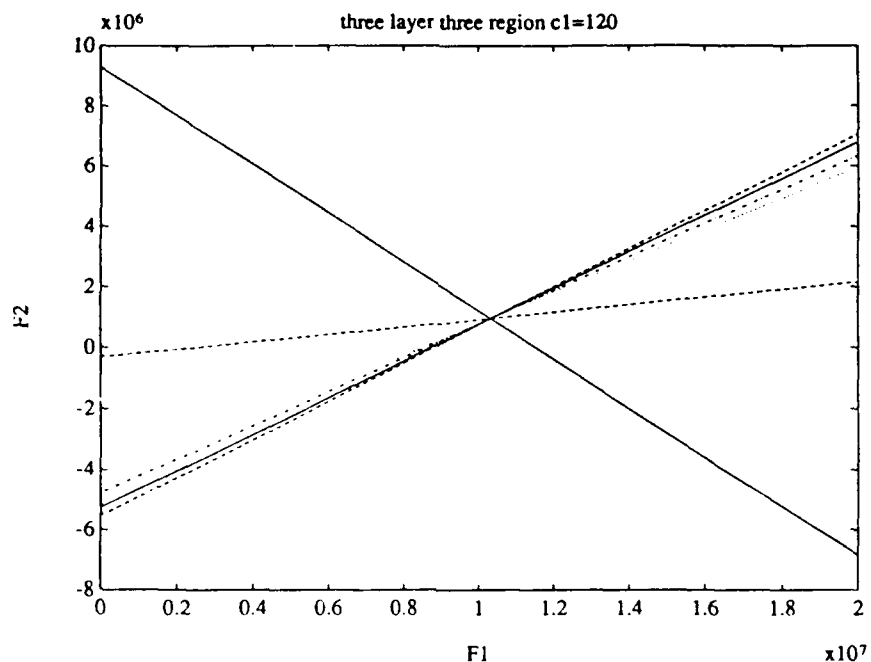


Figure 4.10: The results from the three layer, three region model. The different lines are for varying  $\alpha$  as indicated previously. (e) is the layer-to-layer transport ( $m^3 s^{-1}$ ) between the NADW and the AABW layers; a negative value indicates flow from NADW to AABW.

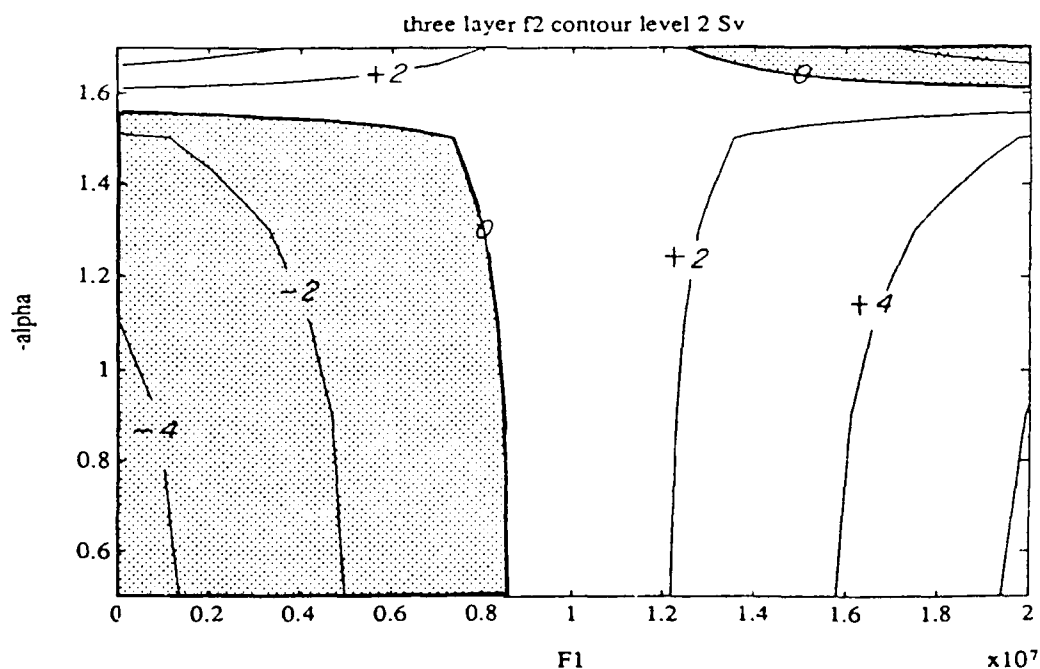


Figure 4.11: Contours of  $F_2$ , the layer-to-layer exchange between NADW and AABW, mapped on a grid of  $\alpha$  and  $F_1$ . Contour level is 2 Sv, and the stippled region indicates negative  $F_2$ .



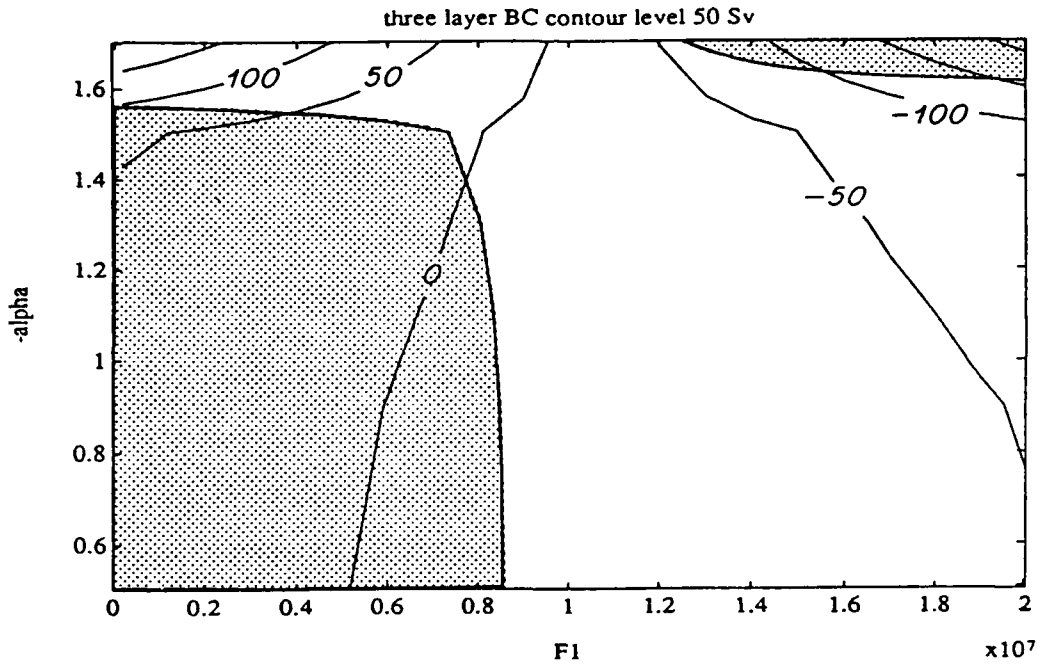


Figure 4.12: The Brazil Current transport mapped on a grid of  $\alpha$  and  $F_1$ . Contour level is 50 Sv, and the heavy line indicates the zero contour. The stippled region indicates negative  $F_2$ .

By mapping the results onto a grid of  $\alpha$  and  $F_1$ , the acceptable solution regions can easily be indicated. Figure 4.11 shows  $F_2$  contoured for the entire parameter range; the stippling indicates negative  $F_2$ , or the formation of AABW. By mapping the zero  $F_2$  contour onto the Brazil Current solution (fig 4.12), one sees that the Brazil Current is usually less than 50 Sv in the region with negative  $F_2$ . There are, however, regions in which the Brazil Current has northward flow. The three layer, three region system shows some sensitivity to the physical constraints. Instead of pursuing this case further, however, a four layer model is developed in the next section that better represents the South Atlantic.

#### 4.4 Four Layer System

In the four layer system, the top layer is the CW, defined by the  $10^\circ$  isotherm. The second layer is the AAIW, defined by the  $3.4^\circ$  isotherm. Third and fourth are

NADW and AABW; all are shown in fig 4.4. Adding a fourth layer adds another constraint, mass balance in the fourth layer, and an unknown, a third layer-to-layer conversion. Rintoul's estimates for these conversion terms are 8, 13, and -4 Sv for  $F_1$ ,  $F_2$ , and  $F_3$ , respectively. Note that  $F_3$  now represents the exchange between NADW and AABW;  $F_2$ , the exchange between NADW and AAIW, and  $F_1$ , that between CW and AAIW.

As in the three layer runs, baroclinic transport in the bottom layer is set to zero and the baroclinic transports in the top layers are computed from changes in layer thickness. The values of the constants  $c$  are again set by matching the model baroclinic transports to those computed from the 31° S transect using a reference level between NADW and AABW ( $c_1$  is set by a surface Brazil Current of about 20 Sv;  $c_2$ , by an AAIW transport of about 10 Sv, and  $c_3$ , by a NADW transport of 10 Sv in the recirculation). The baroclinic transports in each region are

	B.C.	Recirc.	Int.	Net
CW	20.1	-7.1	-18.5	-5.5
AAIW	8.8	-2.4	-8.5	-2.1
NADW	0.0	9.6	-3.1	6.5
AAIW	0.0	0.0	0.0	0.0

Once again the range for  $\alpha$  is explored; the results are similar to the three layer case except that  $\alpha$  asymptotes to a value slightly less than negative one, which means that the barotropic Brazil Current has a larger magnitude than the barotropic recirculation (fig 4.13). Runs were made with  $\alpha$  varying from -1.5 to -.5.

Instead of showing the runs for various  $\alpha$ 's, the data are again mapped onto a grid of  $\alpha$  and  $F_1$ . The first two plots show the layer-to-layer exchanges,  $F_2$  and  $F_3$  (fig 4.14 and fig 4.15). The zero contours for both are on each plot, showing that the satisfactory solution region—where  $F_2$  is positive and  $F_3$  is negative—is fairly small. This “solution region” is indicated on the maps of the other variables

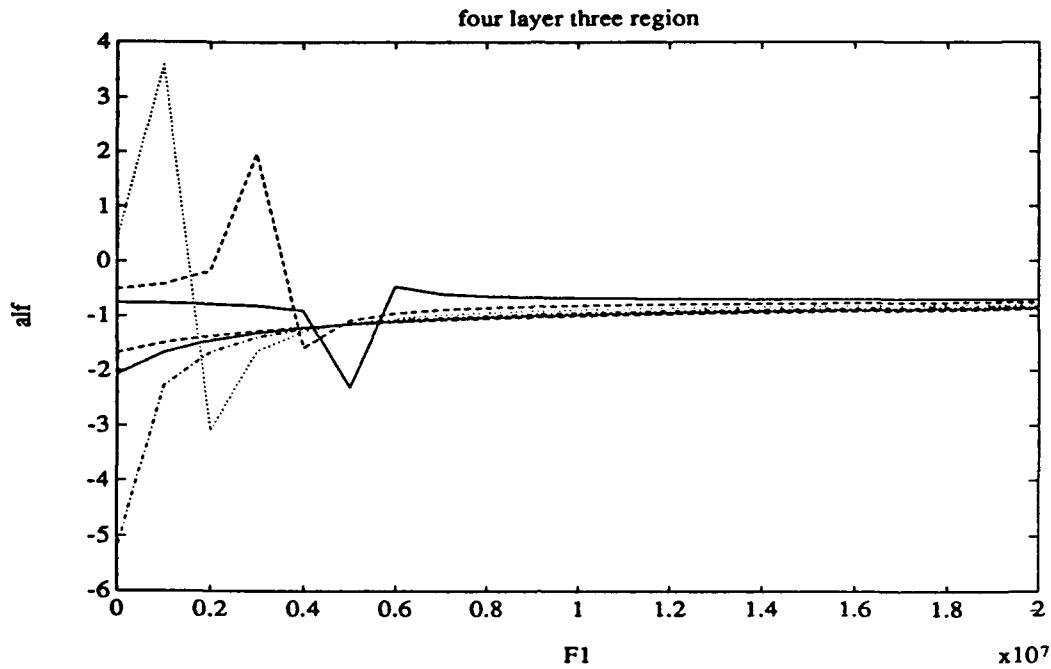


Figure 4.13: Plot of the ratio of the barotropic transports of the Brazil Current to that of the recirculation for the four layer, three region system, with a  $F_3$  varying from 0 -9 Sv.

(fig 4.16- 4.19). The zero lines for  $B_1$  and  $B_2$  lie quite near the  $F_3$  zero. Even though  $B_1$  does have some negative values in the solution region, BC is always positive (fig 4.19). Although BC does not change value much in the solution region, the  $B_3$  map shows that different balances obtain. To discuss the different balances the approximate weightings for each region are given below. Note that in the fourth layer the balance is basically between  $B_2$  and  $B_3$ , and in the third layer all barotropic transports have the same weighting.

	B.C.	Recirc.	Int.
CW	.2	.2	.1
AAIW	.3	.2	.2
NADW	.5	.5	.5
AAIW	.0	.1	.2

In the region where  $\alpha$  is between -1.2 and -1.5 (the magnitude of  $B_2$  is greater than that of  $B_1$ )  $B_3$  has the same sign as  $B_1$  to balance the larger  $B_2$ . To the left of the

solution region,  $F_1$  is not big enough to balance the net baroclinic flow;  $B_2$  balances the rest<sup>1</sup>, and is thus positive.  $B_3$  is not large enough to compensate in the lowest layer; as a result  $F_3$  is positive, and AABW is converted to NADW in the south. In the solution region, the magnitude of  $F_1$  is larger than that of the net baroclinic flow, driving  $B_2$  to reverse sign;  $F_3$  also reverses sign, and AABW is made in the south. To the right of the solution region  $B_2$  must get much larger to compensate the larger  $F_1$ , and  $B_1$  and  $B_3$  cannot compensate the larger  $B_2$  in the NADW layer, so AAIW is converted to NADW ( $F_2$  is negative).

In the next  $\alpha$  region, -.9 to -1.2,  $B_1$  and  $B_2$  are approximately equal in strength. In the area to the right of the solution region  $B_3$  is too small to balance  $B_2$  in the bottom layer, so a large negative  $F_3$  is needed to balance that layer. As a result the NADW layer is out of balance; a negative  $F_2$  provides the balance. In the solution region  $B_2$  and  $B_3$  are approximately in balance in the bottom layer, so  $F_3$  is small and  $F_2$  reverses. To the right of the solution region the balance between the baroclinic transports and  $F_1$  reverses sign, and the signs of  $B_1$ ,  $B_2$ ,  $B_3$  and  $F_3$  also reverse.

In the last  $\alpha$  region, -.5 to -.9, the magnitude of  $B_1$  is greater than that of  $B_2$ ; as a result  $B_3$  has the same sign as  $B_2$ . To the left of the solution region the large  $B_1$  brings more AAIW south than the other two barotropic terms can balance, so some is converted to NADW ( $F_2$  is negative). As  $F_1$  increases it takes up some of the excess AAIW and less  $B_1$  is needed to balance the upper layer. To the right of the solution region, where  $F_1$  is larger than the net baroclinic imbalance in the top layer,  $B_1$  changes sign to compensate the larger  $F_1$ , causing  $B_2$ ,  $B_3$  and  $F_3$  to follow suit.

Treating the acceptable solutions as three different  $\alpha$  regimes, we find the first two to have similar balances: the small net imbalance between  $F_1$  and the baroclinic transports is compensated by  $B_1$  and  $B_3$ , both of which are positive. The small

---

<sup>1</sup>In discussing the results I frequently say that A causes B; it could just as easily be said that B causes A. The equations are solved simultaneously, and one thing does not cause the other, but I find this way of thinking about the results convenient.

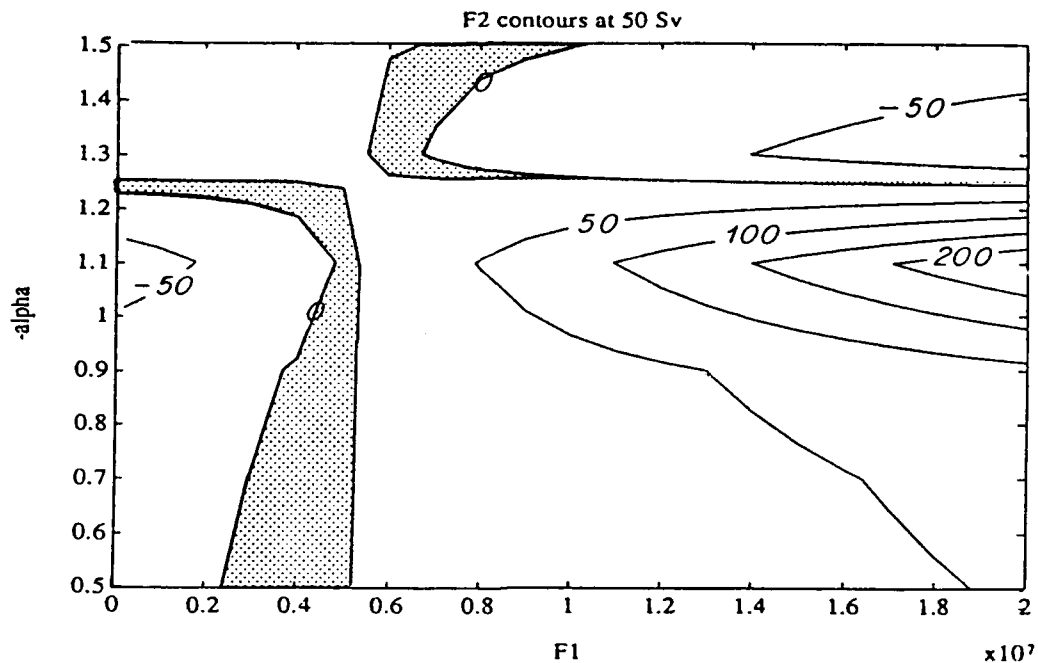


Figure 4.14: Contours of  $F_2$ , the layer-to-layer exchange between AAIW and NADW mapped on a grid of  $\alpha$  and  $F_1$ . Contour level is 50 Sv, and the stippling indicates the overlapping region between positive  $F_2$  and negative  $F_3$ .

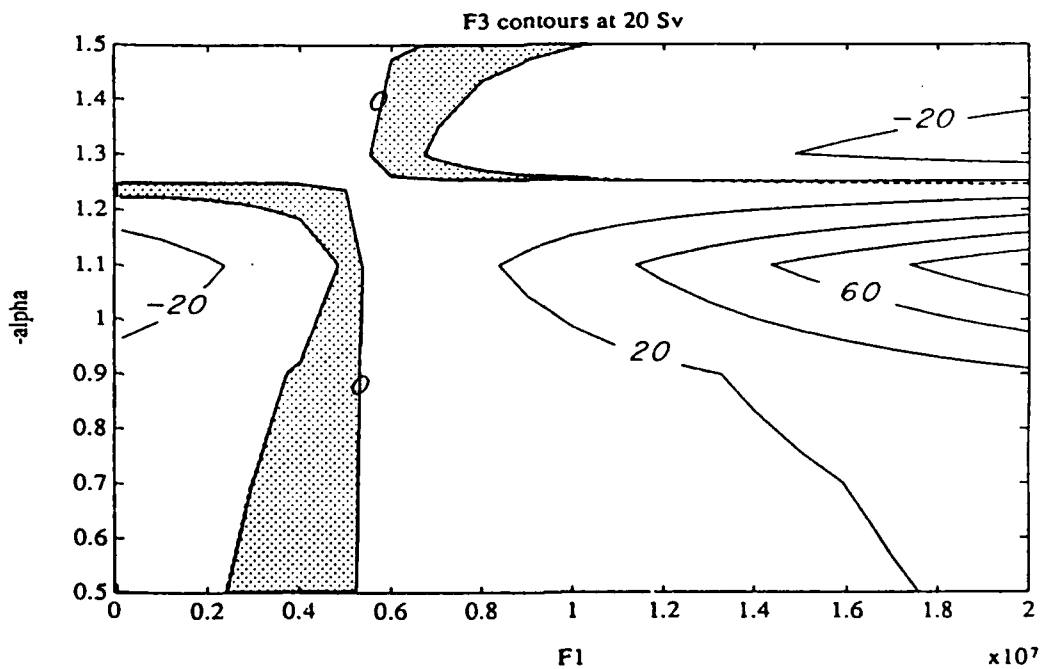


Figure 4.15: Contours of  $F_3$ , the layer-to-layer exchange between NADW and AABW mapped on a grid of  $\alpha$  and  $F_1$ . Contour level is 20 Sv, and the stippling indicates the overlapping region between positive  $F_2$  and negative  $F_3$ .

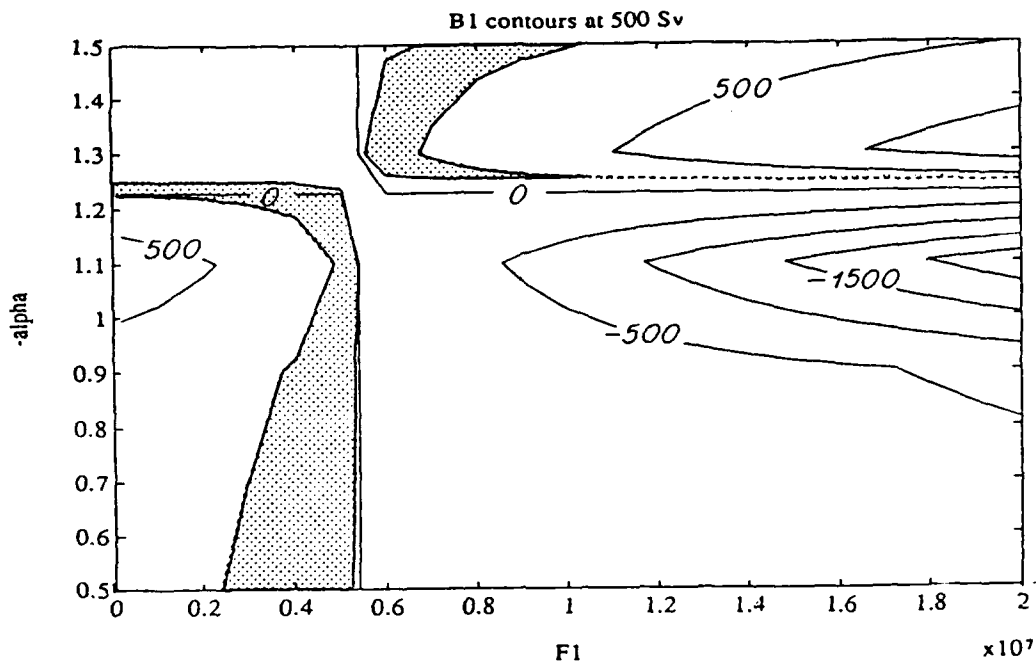


Figure 4.16: Contours of  $B_1$ , the barotropic transport in the Brazil Current, mapped on a grid of  $\alpha$  and  $F_1$ . Contour level is 500 Sv; the stippling indicates the overlapping region between positive  $F_2$  and negative  $F_3$ .

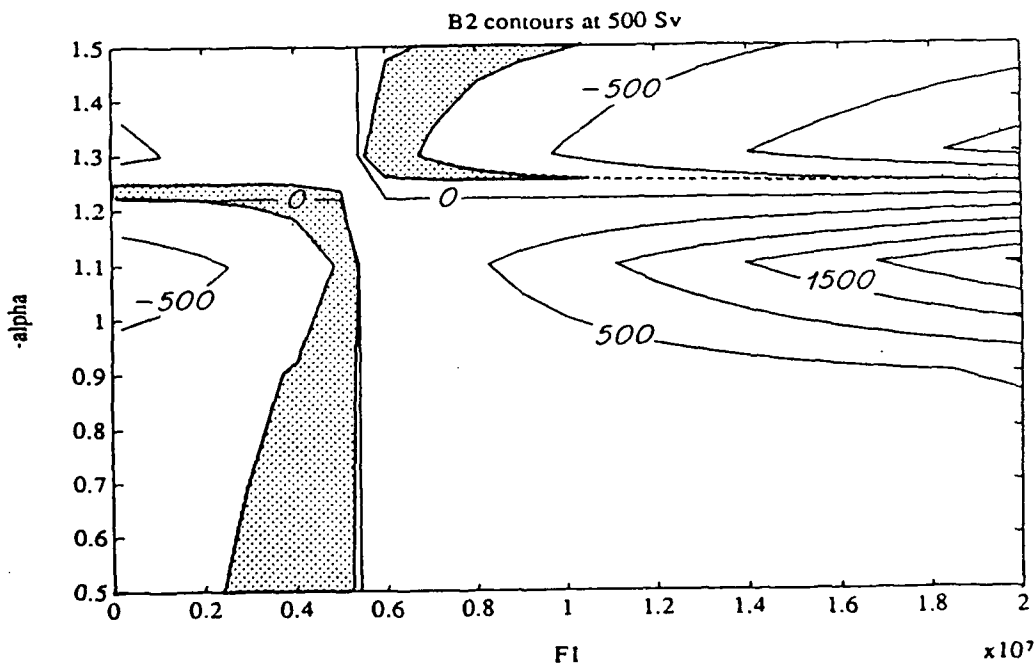


Figure 4.17: Contours of  $B_2$ , the barotropic transport in the recirculation, mapped on a grid of  $\alpha$  and  $F_1$ . Contour level is 500 Sv; the stippling indicates the overlapping region between positive  $F_2$  and negative  $F_3$ .

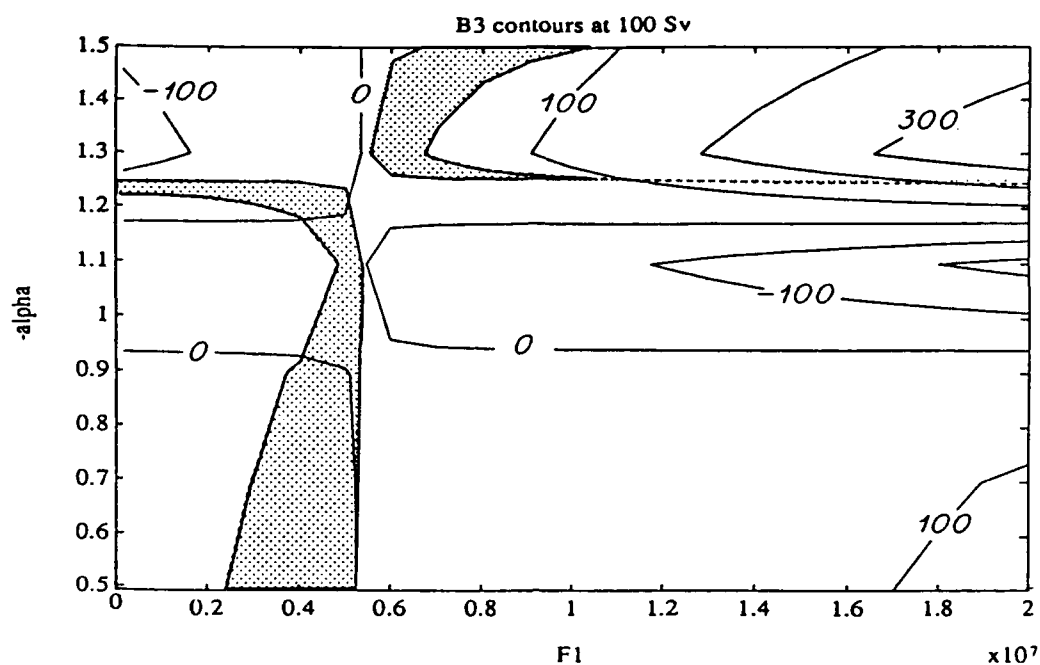


Figure 4.18: Contours of  $B_3$ , the barotropic transport in the interior, mapped on a grid of  $\alpha$  and  $F_1$ . Contour level is 100 Sv; the stippling indicates the overlapping region between positive  $F_2$  and negative  $F_3$ .

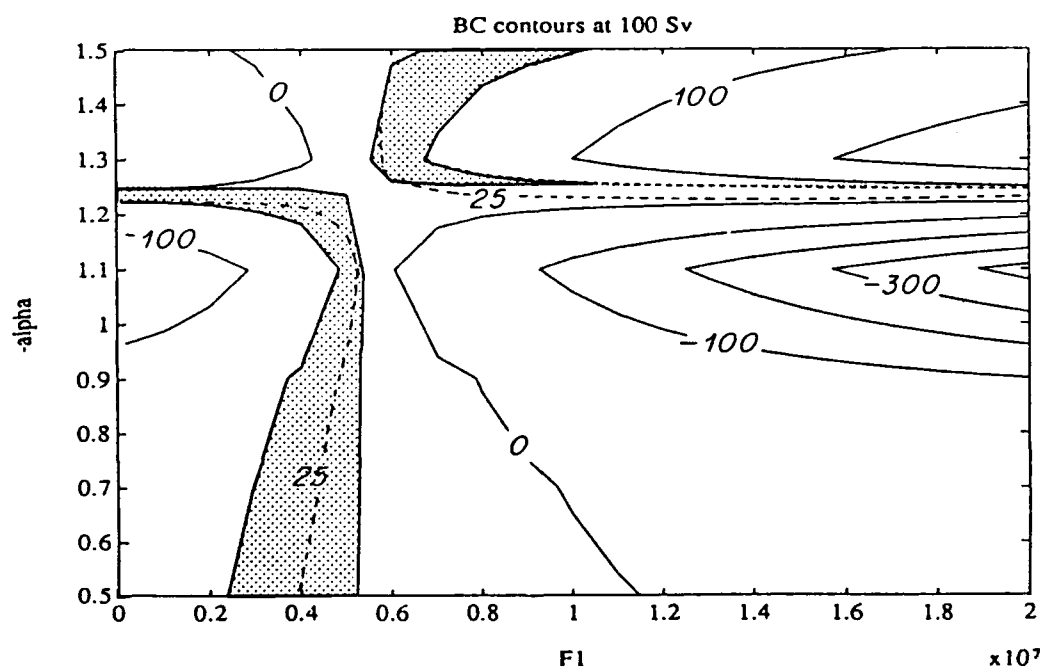


Figure 4.19: Contours of BC, the total transport of the upper layer of the Brazil Current, mapped on a grid of  $\alpha$  and  $F_1$ . Contour level is 100 Sv; the stippling indicates the overlapping region between positive  $F_2$  and negative  $F_3$ .

differences between  $B_3$  and the negative  $B_2$  result in small, negative  $F_3$ 's. In the third region  $B_1$  is stronger than  $B_2$  and can compensate for the surface layer imbalance by itself.  $B_3$  then works with  $B_2$  to balance the large barotropic Brazil Current in the other layers. Since  $B_2$  and  $B_3$  are both negative,  $F_3$  is larger than in the other regions. Shown below is an example of the net transports in each region from the acceptable solution region (the specific numbers for the Brazil Current and recirculation can be compared to those found in Table 3.3). The solution below is neither a best nor worst case, although its Brazil Current transport in the upper layer is on the lower end. The range of transports in the upper layer of the Brazil Current in the solution region is from 20 to 33 Sv. Converting the numbers in the sample solution to net layer transports across the section, one finds 5 Sv of surface water flowing northward, 1.4 Sv of intermediate water flowing northward, 6.7 Sv of NADW flowing southward and .3 Sv of bottom water flowing northward. Although all the magnitudes are smaller than those computed by Rintoul in his standard case, they do have the same flow direction.

**Sample Solution  $\alpha = -.5$**

$$\begin{array}{rcl}
 21.4 & -7.7 & -18.7 \\
 & & 5.0 \uparrow \\
 10.6 & -3.0 & -8.9 \\
 & & 6.4 \uparrow \\
 3.3 & 7.8 & -4.3 \\
 & & 0.3 \downarrow \\
 0.5 & -0.4 & -0.4
 \end{array} \tag{4.16}$$

## 4.5 Summary

The models progress from a two layer, two active regions version (no barotropic transport is applied to the third region) to the final four layer, three region version.



In all cases the system is underdetermined. The first step towards obtaining a solution is to set  $F_1$  (0 to 20 Sv); when only two regions are active, setting the one parameter is sufficient to obtain a solution. When all three regions are active (requiring three barotropic transports) another parameter is required to find a solution. By setting the conversion to bottom water (0-9 Sv), results are obtained that show the ratio of  $B_1$  to  $B_2$  is fairly insensitive to changes in the fixed layer-to-layer conversions. Thus the ratio,  $\alpha$ , is used as the additional parameter, leaving  $B_1$ ,  $B_3$ ,  $F_2$  and  $F_3$  to be determined by the system equations.

General features, and not specific transport values, are the most important results of the layer models. The incremental development of the three models elucidates physical features in the circulation pattern and illustrates constraints of the system. Attempting to model the South Atlantic with the two layer system resulted in very large barotropic adjustments, which suggests that such a model is insufficiently sophisticated to capture the essential physics of the system. Also, the single overturning mode did not constrain the range of solutions. The addition of one or two layers allows the basic features of the system to be represented and provides a limited range of solutions. The four layer system, with very basic, realistic constraints on layer exchanges, results in remarkably consistent barotropic transports for the Brazil Current and recirculation. Attempting to make the Brazil Current very large or very small results in layer-to-layer exchanges in the opposite direction of that expected from physical intuition.

## Chapter 5

### Potential Vorticity in the Brazil Current

In the previous chapters, the data were examined using a classical approach, the use of tracers to determine a ZVS from which transport estimates can be made. The data can also be used to calculate potential vorticity<sup>1</sup>, which can be used as both a tracer and a dynamic tool.

The value of potential vorticity as a tracer has only recently been exploited, although static stability, which is proportional to planetary potential vorticity ( $\mathcal{P}$ ), has frequently been used as a tracer in the past. Low values of  $\mathcal{P}$ , found in convectively formed mode waters, have been used to trace those water masses and track their formation rate (Talley and McCartney (1982) and Talley and Raymer (1982)). Bower, Rossby and Lillibridge (1985) used the difference in  $\mathcal{P}$  between Sargasso Sea Water and Slope Water as a measure of the amount of mixing which occurs cross stream. Using the Gulf Stream 60 data, they found a “wall” or front of  $\mathcal{P}$  in the upper water located partway across the stream; the persistence of the wall downstream suggested that no mixing took place across it. The presence of the wall was confirmed in other tracer data. Deeper,  $\mathcal{P}$  was homogenized across the stream,

---

<sup>1</sup>This section assumes the reader is familiar with the basics of potential vorticity ( $Q$ ), namely, that it has planetary ( $\mathcal{P}$ ) and relative ( $\mathcal{R}$ ) components

$$Q = \mathcal{P} + \mathcal{R}$$

suggesting that mixing could occur. This work was extended by Leaman, Johns and Rossby (1989) using  $Q$  calculated from PEGASUS data. Looking at three cross sections of the Gulf Stream, they also found the wall of  $Q$  persisted in the upper layers of each section. The  $Q$  contour dividing the "wall region" from the rest of the stream was the same in each crossing. Bennett (1988) in her analysis of the Agulhas retroflection, also found a wall of  $P$  against the coast. The wall — or front — of  $P$  is present in sections using  $\sigma_0$  as a vertical coordinate; thus any parcel trying to conserve both its density and potential vorticity will be unable to cross the wall.

Of course, potential vorticity is not limited to use as a tracer, but is dynamically important as well. Ertel (1942) shows that  $Q$  is conserved along the fluid path in the absence of mixing and dissipation (a complete discussion can be found in Gill, 1982). Once a relationship is established between the stream function ( $\Psi$ ) and  $Q$ , the ocean circulation is determined. Some simple western boundary current models assume a uniform  $Q$ - $\Psi$  relationship; the conservation of this relationship drives the evolution of the current. Others have used somewhat more complicated  $Q$ - $\Psi$  relationships (for instance Fofonoff, 1954, used a linear relationship), but one needs to question whether a western boundary current is an appropriate place to assume potential vorticity is conserved. Besides interaction with the atmosphere there may be dissipation along the wall and mixing in the high velocity current. The effect of dissipation on the potential vorticity in a western boundary current is explored in a recent paper by Lozier and Riser (1989).

Lozier and Riser explore dissipation along the wall with a multilayer, quasi-geostrophic, eddy-resolving model. The model has three layers of which only the uppermost is wind forced. Each has a dissipative boundary regime on the western edge; in these  $Q$  increases downstream with the change in Coriolis force (fig 5.1). The dissipative boundary in the upper layer is 17 km wide for a 70 km wide current. These dissipative boundary regimes are similar to what one would find in a traditional frictional model (e.g. Stommel, 1948, using bottom friction and Munk, 1950, using lateral friction). The layers can be distinguished outside the

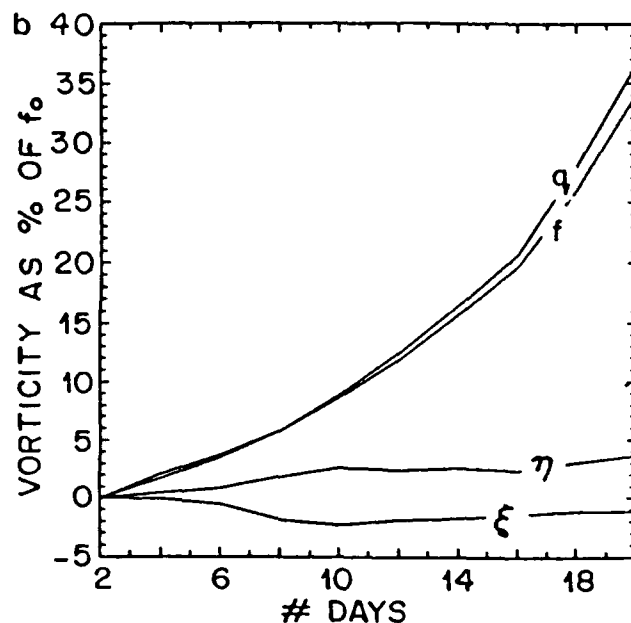


Figure 5.1: The change in potential vorticity as a float moves downstream in the frictional boundary regime.  $f$  is the planetary term,  $\eta$  is stretching,  $\xi$  is the relative term. From Lozier and Riser (1989).

dissipative boundary regime by the type of potential vorticity balance they achieve. In the upper layer, the inertial regime outside the dissipative regime conserves  $Q$  by balancing the increase in Coriolis force<sup>2</sup> with negative  $\mathcal{R}$  (fig 5.2). In this layer,  $Q$  would increase downstream on the inshore edge and be conserved across the rest of the current. In the second layer, the inertial regime conserves  $Q$  by balancing changes in the Coriolis force with stretching;  $\mathcal{R}$  is important only in the dissipative boundary regime. The third layer has no mean inertial regime. The different regimes in these layers may be useful in interpreting the potential vorticity profiles obtained from the sections.

Previous studies using potential vorticity follow one of two paths: they use hydrographic data to calculate  $\mathcal{P}$ , or they measure absolute velocities (from

<sup>2</sup>LR divide  $Q$  into three components: the changes in  $Q$  resulting from changes in Coriolis force, stretching and relative vorticity. In the lexicon used here  $\mathcal{P}$  is a multiplicative combination of the first two, and  $\mathcal{R}$  is a multiplicative combination of the last two. This means that at a given section, changes in  $\mathcal{P}$  represent stretching, but downstream changes in  $\mathcal{P}$  probably reflect changes in  $f$ .

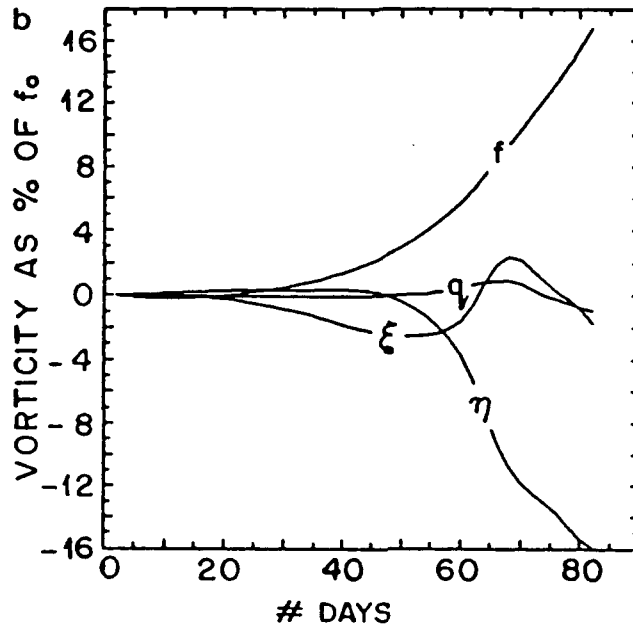


Figure 5.2: The change in potential vorticity as a float moves downstream in the inertial boundary regime.  $f$  is the planetary term,  $\eta$  is stretching,  $\xi$  is the relative term. From Lozier and Riser (1989).

moorings or PEGASUS) to calculate  $\mathcal{R}$ , and then  $Q$ . Hydrography has a sampling advantage, since a dense array stations of the entire water column are easily, and relatively cheaply, obtained. Also, in most parts of the ocean,  $\mathcal{P}$  is an adequate substitute for  $Q$ . Unfortunately,  $\mathcal{P}$  and  $Q$  are not the same in western boundary currents, which gives absolute velocity measurements the advantage. This might be overcome with good station spacing if one were confident of her ZVS choice.

There are several problems involved with calculating  $Q$  from hydrographic data; these are addressed in the next section. Section 5.2 uses the calculated  $Q$  to look at water mass characteristics. Section 5.3 uses layer averages to look for a  $Q$ - $\Psi$  relationship in the current, whether it is conserved on streamlines, or whether it reflects some of the changes suggested by Lozier and Riser. In addition, the results are examined to see what effect including or excluding  $\mathcal{R}$  has, both qualitatively and quantitatively.

## 5.1 Calculating Potential Vorticity from Hydrographic Data

The first step in estimating  $Q$  in the Brazil Current is determining what terms are expected to be important. The expression for potential vorticity is

$$Q = \frac{1}{\rho_0} \left[ \left( \underbrace{f}_1 + \underbrace{\frac{\partial V}{\partial x} - \frac{\partial U}{\partial y}}_{R_o} \right) \frac{\partial \lambda}{\partial z} + \frac{\partial U}{\partial z} \frac{\partial \lambda}{\partial y} - \underbrace{\frac{\partial V}{\partial z} \frac{\partial \lambda}{\partial x}}_{R_g^2} \right] \quad (5.1)$$

where  $U$  is the cross stream velocity,  $V$  is along stream velocity, and  $\lambda$  is a conservative scalar (several choices can be made for  $\lambda$ ; here  $\sigma_2$  has been used). In the current,  $U$  is assumed to be much smaller than  $V$ , so terms involving zonal velocity may be neglected. The relative scaling of the remaining terms is given below the equation in terms of the Rossby number, which is roughly estimated here as

$$R_o = \frac{V}{fL} \approx \frac{100 \frac{cm}{s}}{7.3E-5 \frac{1}{s} 50km} \approx .30 \quad (5.2)$$

For the Brazil Current,  $\mathcal{R}$  can be expected to contribute about fifteen percent to  $Q$ . This is not large, but could affect the results obtained. In addition,  $\mathcal{R}$  changes sign across the current, enhancing  $\mathcal{P}$  on one side, diminishing it on the other. Outside the current  $\mathcal{R}$  is small, and  $\mathcal{P}$  should be an adequate estimate of  $Q$ .

The next step in estimating  $Q$  is estimating what horizontal resolution is needed to calculate  $\mathcal{R}$  from hydrographic data. Of course, the use of hydrographic data immediately implies no ageostrophic components of  $Q$  will be determined; these are included in current meter and PEGASUS measurements (however, Johns, Watts and Rossby, 1989, use PEGASUS measurements to conclude that the main structure of the Gulf Stream is geostrophic, with the largest ageostrophic component coming from curvature of the path). With hydrography, velocity is computed using the thermal wind relation, which yields the following  $Q$  equation

$$Q = \left( f + \frac{\Delta V_b}{\Delta x} + \frac{\Delta V_r}{\Delta x} \right) \frac{\Delta \sigma_2}{\Delta z} - \frac{\Delta V_b}{\Delta z} \frac{\Delta \sigma_2}{\Delta x} \quad (5.3)$$

where

$$V = V_r + \frac{g}{f\rho} \int_{z(r)} \frac{\partial \rho}{\partial x} dz = V_r + V_b \quad (5.4)$$

In the  $Q$  equation, the first term,  $\mathcal{P}$ , is easily calculated using modern hydrographic data, as it requires only the vertical derivative of density. The second term,  $\mathcal{R}$ , involves both the vertical and horizontal derivatives of density; the station spacing will directly impact its calculation. Evaluation of the third term is determined by the ZVS choices made in chapter two. The fourth term is not usually included in  $Q$  estimates because it is order  $R_o^2$ . It can be calculated directly from hydrographic data and is included for completeness; note that because it is the vertical derivative of  $V$ , only the horizontal derivative of  $\rho$  is needed to calculate it. Only the second term is strongly affected by the station spacing. Recall that two stations are needed to calculate velocity, and three to calculate vorticity. Widely spaced data gives a velocity averaged over a longer distance and the detailed structure of the current disappears (note that this is a problem for absolute velocity measurements also, except they will not be averages). One way to estimate the resolution needed is to assume adjustments will take place on the scale of the Rossby radius of deformation. The Rossby radius of deformation, scaled here for the Brazil Current thermocline, is

$$L_r = \frac{ND}{f_o} \approx \frac{.04 * 700}{7E - 5} = 40km \quad (5.5)$$

Because derivatives of velocity are being computed, measurements need to be made at about half the deformation radius, or 20 km. The three northern sections have average spacing through the current of 13.7, 17.4 and 19.4 km, but the fourth section has an average of 38.4 km.

A potentially bigger problem for calculating relative vorticity is whether the cruise track is perpendicular to the current. Transport calculations are unaffected by the

crossing angle. Velocity is reduced by the cosine, but  $\mathcal{R}$  goes down by  $\cosine^2$ . Nothing can be done to adjust for this when it is a problem, other than noting it as a possible cause for reduced values. This is one area where absolute velocity measurements have a big advantage, as the direction of flow is known.

For most people, the biggest concern with calculating  $\mathcal{Q}$  from hydrographic data is the ZVS. Error can be introduced in this term through relative errors between station pairs; if the same error in velocity choice were made at all stations, e.g. all were 2 cm/s too fast, no error would be introduced. There are two ways of examining this problem. If one assumed there was an arbitrary error of 5 cm/s in the opposite direction in adjacent station pairs separated by 20 km, this would introduce an error on the order of seven percent of  $\mathcal{P}$ . An error of the type described would do real violence to the flow directions of the water masses as described in chapter two. A more reasonable way of addressing this question is to calculate  $\mathcal{R}$  with different ZVS choices.

The components of  $\mathcal{Q}$  for the 36° S section are shown in fig 5.3 to 5.6. This section has the largest  $\mathcal{R}$  contribution, with the ratio of  $\mathcal{R}$  to  $\mathcal{P}$  reaching as high as one in the current (fig 5.6); across the rest of the section it contributes ten to twenty percent. The ratio of  $\mathcal{R}$  to  $\mathcal{P}$  is the same as the Rossby number; the earlier estimate of the relative importance of  $\mathcal{R}$  is quite conservative. This transect also has the largest contribution from the  $\frac{dv}{dz}$  term, with the ratio of it to  $\mathcal{P}$  reaching .4 (fig 5.8) in the current; it contributes very little to the rest of the section (The ratios for the other sections are in Appendix F.). The  $\mathcal{R}$  calculation was redone using a level ZVS, 1800 m, instead of a density surface; the two differ in depth by about 1000 m (Recall from chapter three this ZVS choice was shallow enough to send NADW north). A plot of the new  $\mathcal{Q}$  looks virtually the same as the old one, as the differences between the two (fig 5.9) are less than the contour interval. As long as the ZVS is even close to reasonable it should not have much effect on the results.

It appears that it should be possible to get good estimates of  $\mathcal{Q}$  from hydrographic



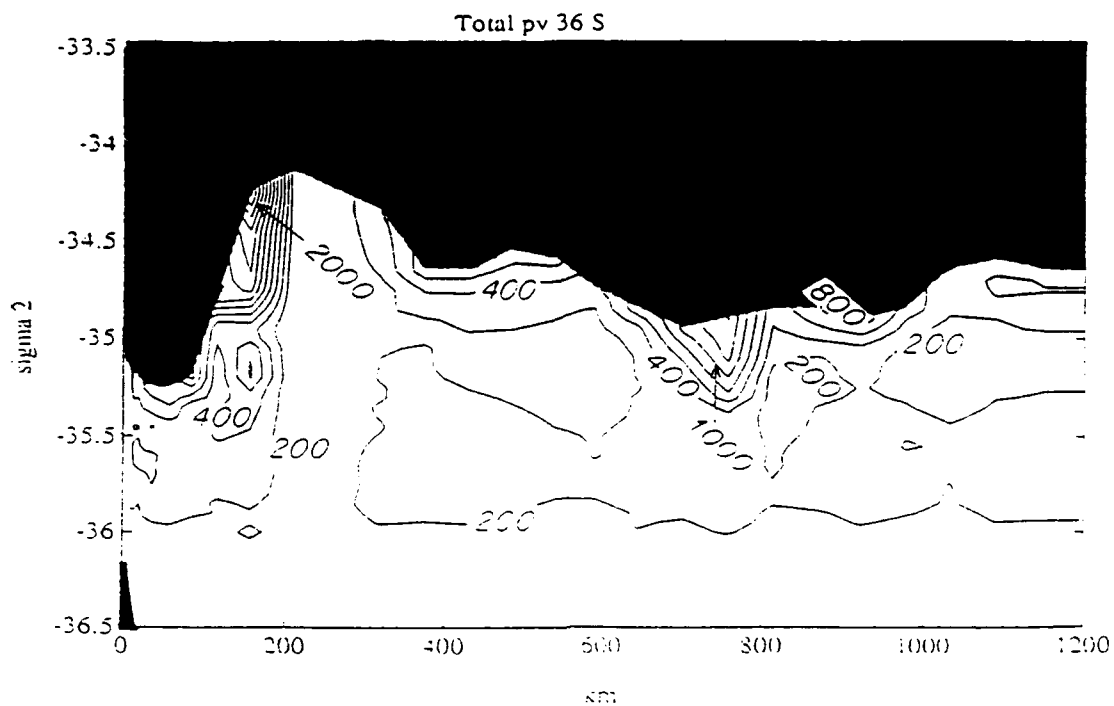


Figure 5.3: Contoured map of total potential vorticity at  $36^\circ$  S on a grid of distance (km) and density ( $\sigma_2$ ). The surface and bottom are indicated by the blackened areas. The contour interval is  $200 \text{ E-}9\text{m}^{-1}\text{s}^{-1}$ .

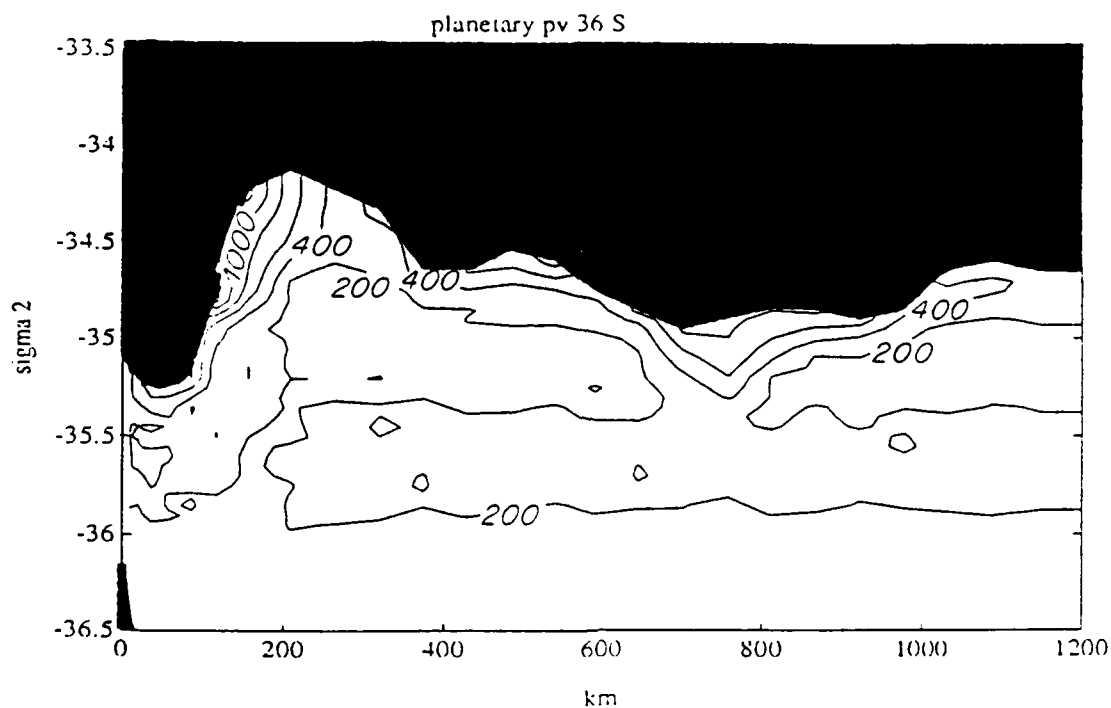


Figure 5.4: Contoured map of planetary potential vorticity at  $36^\circ$  S on a grid of distance (km) and density ( $\sigma_2$ ). The surface and bottom are indicated by the blackened areas. The contour interval is  $200 \text{ E-}9\text{m}^{-1}\text{s}^{-1}$ .

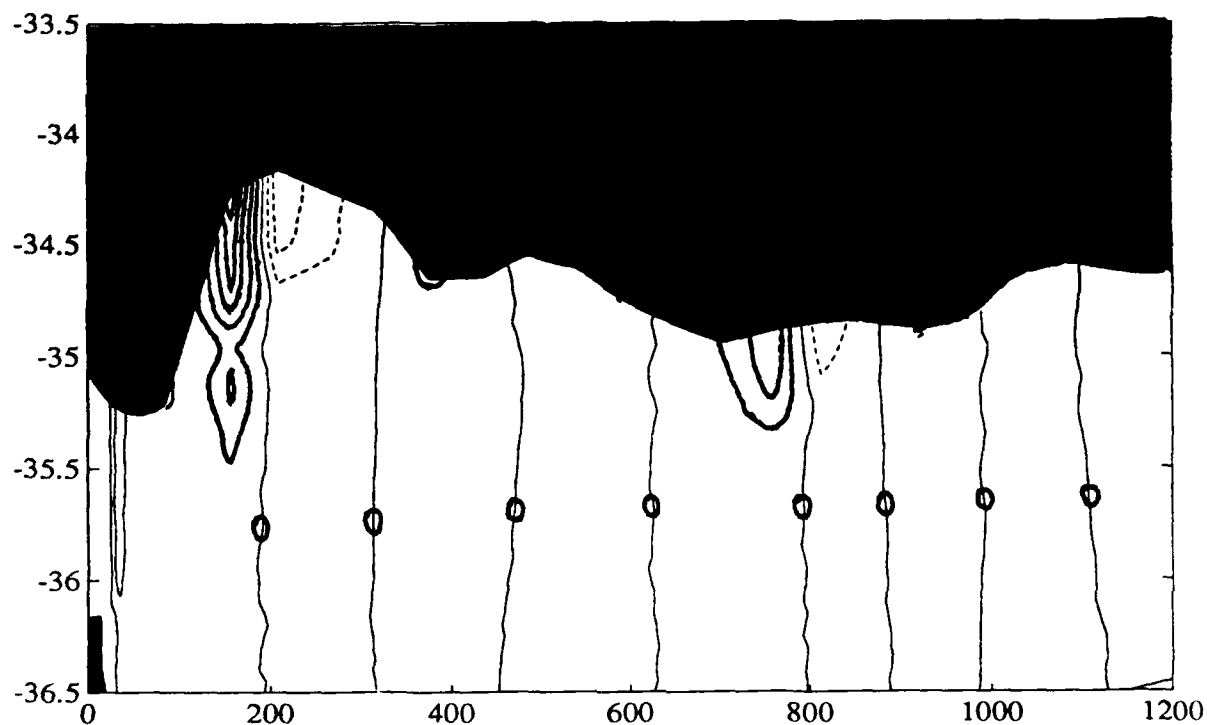


Figure 5.5: Contoured map of relative potential vorticity at  $36^\circ$  S on a grid of distance (km) and density ( $\sigma_2$ ). The surface and bottom are indicated by the blackened areas. Positive vorticity is indicated with solid lines; negative with dashed. The contour interval is  $200 \text{ E-}9 \text{ m}^{-1} \text{ s}^{-1}$ .

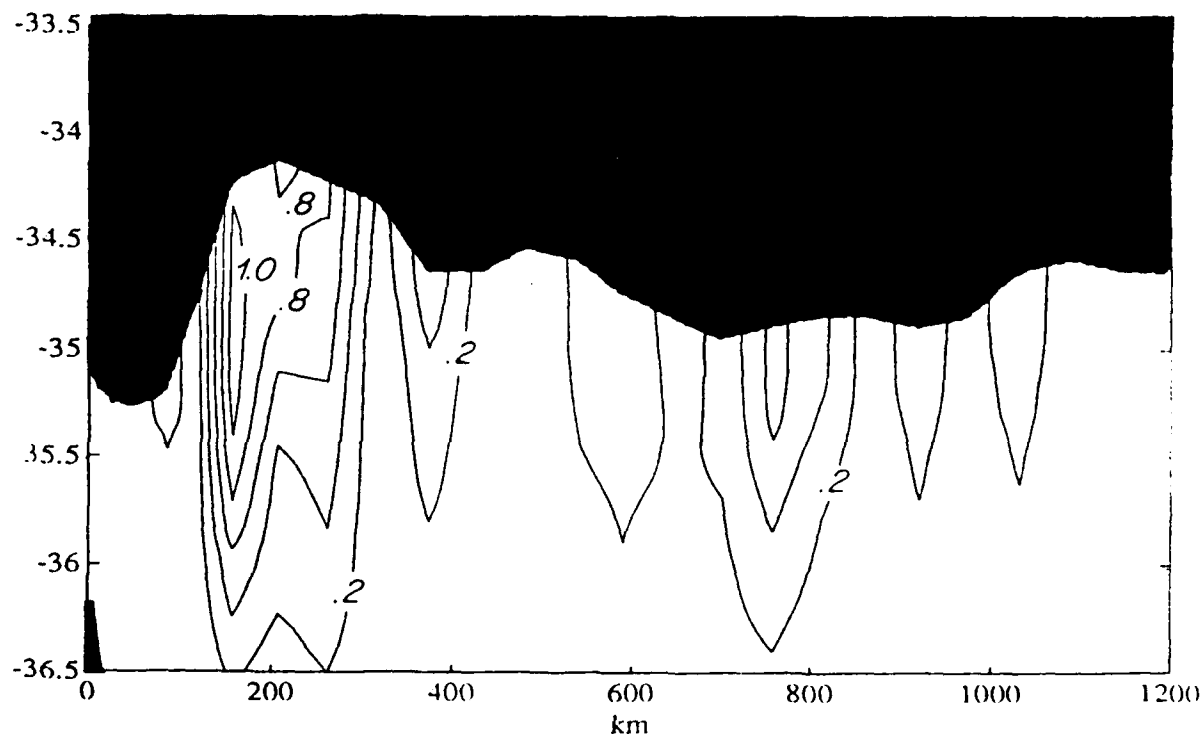


Figure 5.6: Contoured map of the ratio of relative to planetary potential vorticity at  $36^\circ$  S on a grid of distance (km) and density ( $\sigma_2$ ). The surface and bottom are indicated by the blackened areas. The contour interval is .2

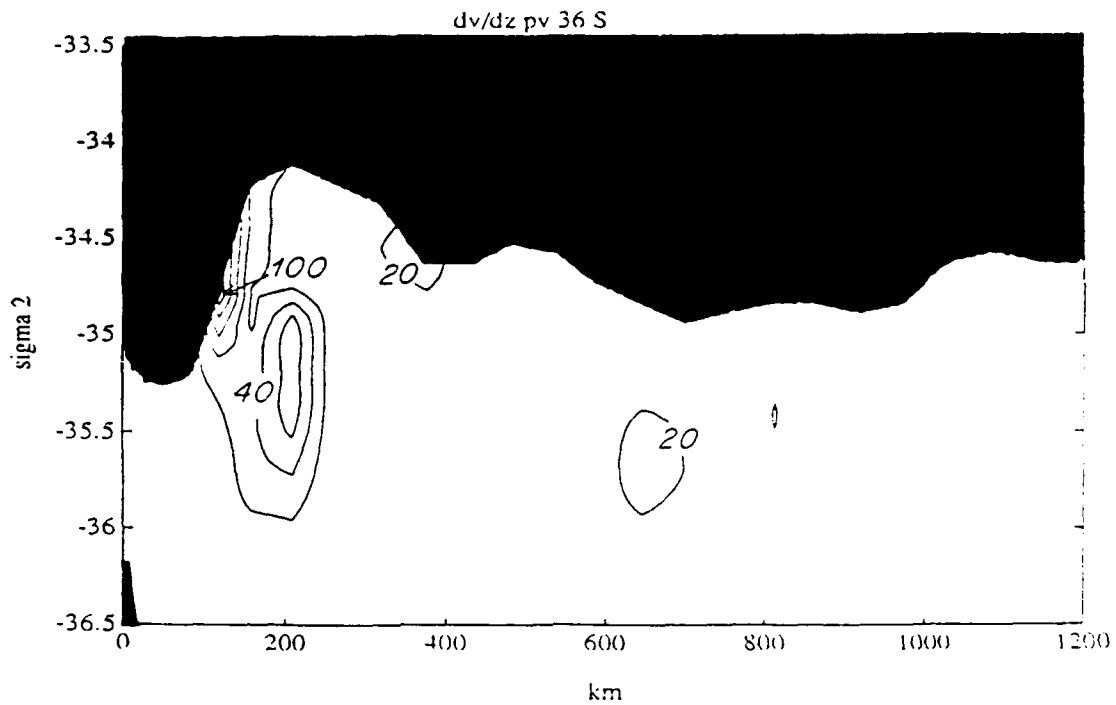


Figure 5.7: Contoured map of the contribution from the vertical shear of velocity,  $\frac{dv}{dz}$  at  $36^\circ$  S on a grid of distance (km) and density ( $\sigma_2$ ). The surface and bottom are indicated by the blackened areas. The contour interval is  $20 \text{ E-}9 \text{ m}^{-1} \text{ s}^{-1}$ .

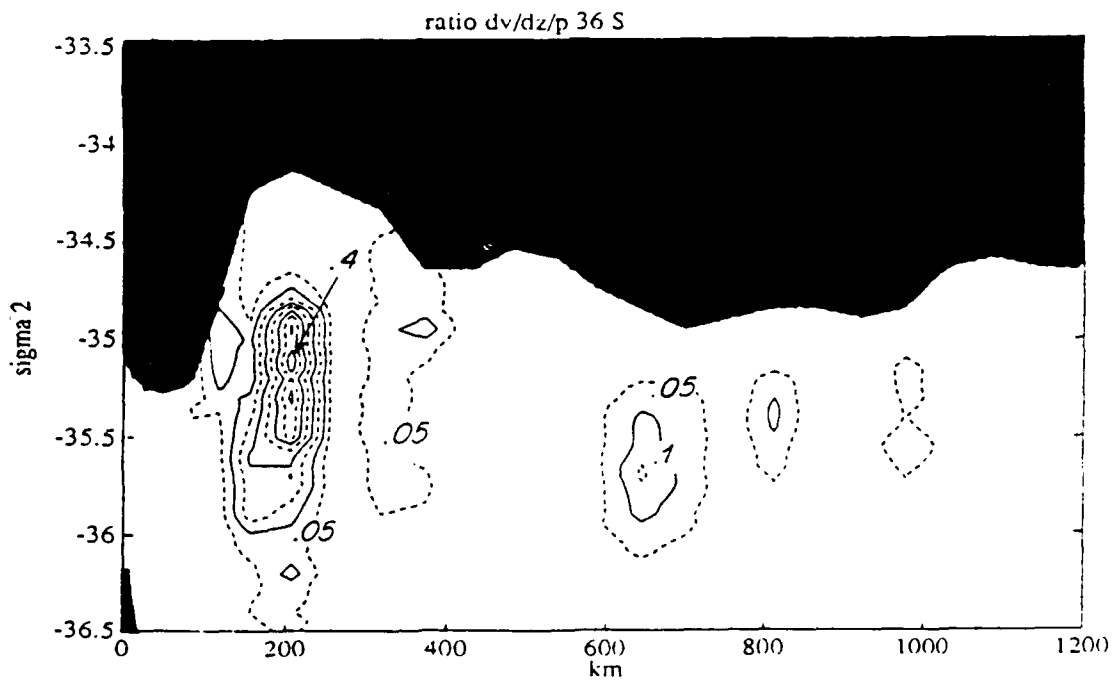


Figure 5.8: Contoured map of the ratio of the vertical velocity shear component to planetary potential vorticity at  $36^\circ$  S on a grid of distance (km) and density ( $\sigma_2$ ). The surface and bottom are indicated by the blackened areas. The dashed contour interval is .05.

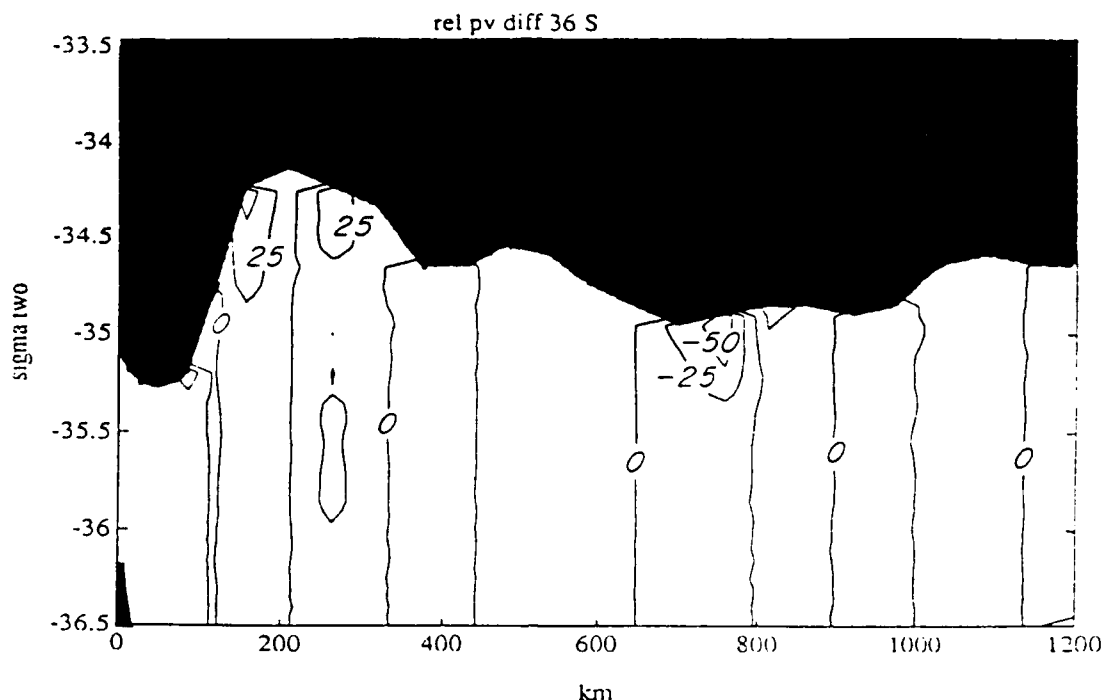


Figure 5.9: Contoured map of the change in relative potential vorticity resulting from a ZVS choice of 1800 m. Data from 36° S on a grid of distance (km) and density ( $\sigma_2$ ). The surface and bottom are indicated by the blackened areas. The contour interval is  $25 \text{ E-}9 \text{ m}^{-1} \text{ s}^{-1}$

data. Problems may occur if the stations are widely spaced or if the current is not crossed perpendicular to the flow. Although problems might be anticipated with the ZVS, it actually contributes minimally to the measurement. The ability to estimate  $Q$  from hydrographic data should be useful in strong current regimes.

## 5.2 Potential Vorticity as a Tracer

The description given in chapter 2 from the sections of oxygen, salt, temperature and silica provided a fairly coherent picture of the flow patterns. If  $Q$  is to be useful as a tracer, it should confirm some of the patterns determined by the other tracers, as well as adding new information. However, the above sections of  $P$  and  $Q$  show little variation below  $36.0 \sigma_2$ . By plotting only  $P$  in the deeper waters more horizontal detail can be resolved, since  $P$  is a single station calculation. Fig 5.10

- 5.13 are plots of  $\mathcal{P}$  as a function of pressure, from 600 db to the bottom. This depth range includes all the water masses except CW; separate plots of  $\mathcal{Q}$  will be used to explore the shallower water. Two main features are found in these sections. The first is a high in  $\mathcal{P}$  of  $15.0 \text{ E-}9\text{m}^{-1}\text{s}^{-1}$  at about 3600 m depth. In the two southern sections the highs are large, basinwide features, which line up fairly well with the LCPW information (the break in the contour at station 123 in the  $36^\circ \text{ S}$  section occurs where the flow direction reverses). In the northern two sections the highs are near the bottom. The other strong feature is the low between the  $15 \text{ E-}9\text{m}^{-1}\text{s}^{-1}$  contours at about 2700 m, near the core of NADW. It is strongest in the northern section, where the  $7.5 \text{ E-}9\text{m}^{-1}\text{s}^{-1}$  contour spans most of the deep portion of the section. At  $31^\circ \text{ S}$ , there are cores of  $7.5 \text{ E-}9\text{m}^{-1}\text{s}^{-1}$ , but the  $10 \text{ E-}9\text{m}^{-1}\text{s}^{-1}$  contour is basinwide. At the two southern sections the  $10 \text{ E-}9\text{m}^{-1}\text{s}^{-1}$  contour is reduced to small cores; at  $34^\circ \text{ S}$  they align well with the strongest cores of NADW, but at  $36^\circ \text{ S}$  the  $10 \text{ E-}9\text{m}^{-1}\text{s}^{-1}$  core under the recirculation (sta. 117) is displaced from the strongest salinity core (sta. 114). One wonders how the high and low cores effect each other.

Finding cores which are consistent with the other tracers is important, but having new information is more useful. By plotting  $\mathcal{Q}$  with density ( $\sigma_2$ ) as a vertical coordinate the surface layers are spread out so that variations within them can be seen (fig 5.14 - 5.17). Two features stand out. The first is the maximum of  $\mathcal{Q}$  found at the  $35.5 \sigma_2$  ( $26.8 \sigma_0$ ) level. At  $27^\circ \text{ S}$  the strongest core is found in the recirculation stations, with a much smaller one within the Brazil Current. In the next section to the south the core in the recirculation is slightly larger than that at  $27^\circ \text{ S}$ , that in the Brazil Current is much larger. At  $34^\circ \text{ S}$  the high is broken into pockets in the current and is continuous from the righthand side of the recirculation to the offshore edge of the section (Note that the  $\mathcal{P}$  plot is not broken. This is the section with the odd Brazil Current velocity structure, which is manifested in  $\mathcal{Q}$ ). The last section has a strong maximum in the recirculation, but in the current the high  $\mathcal{Q}$  of the surface layers is extending deeper so there is no core. The pattern

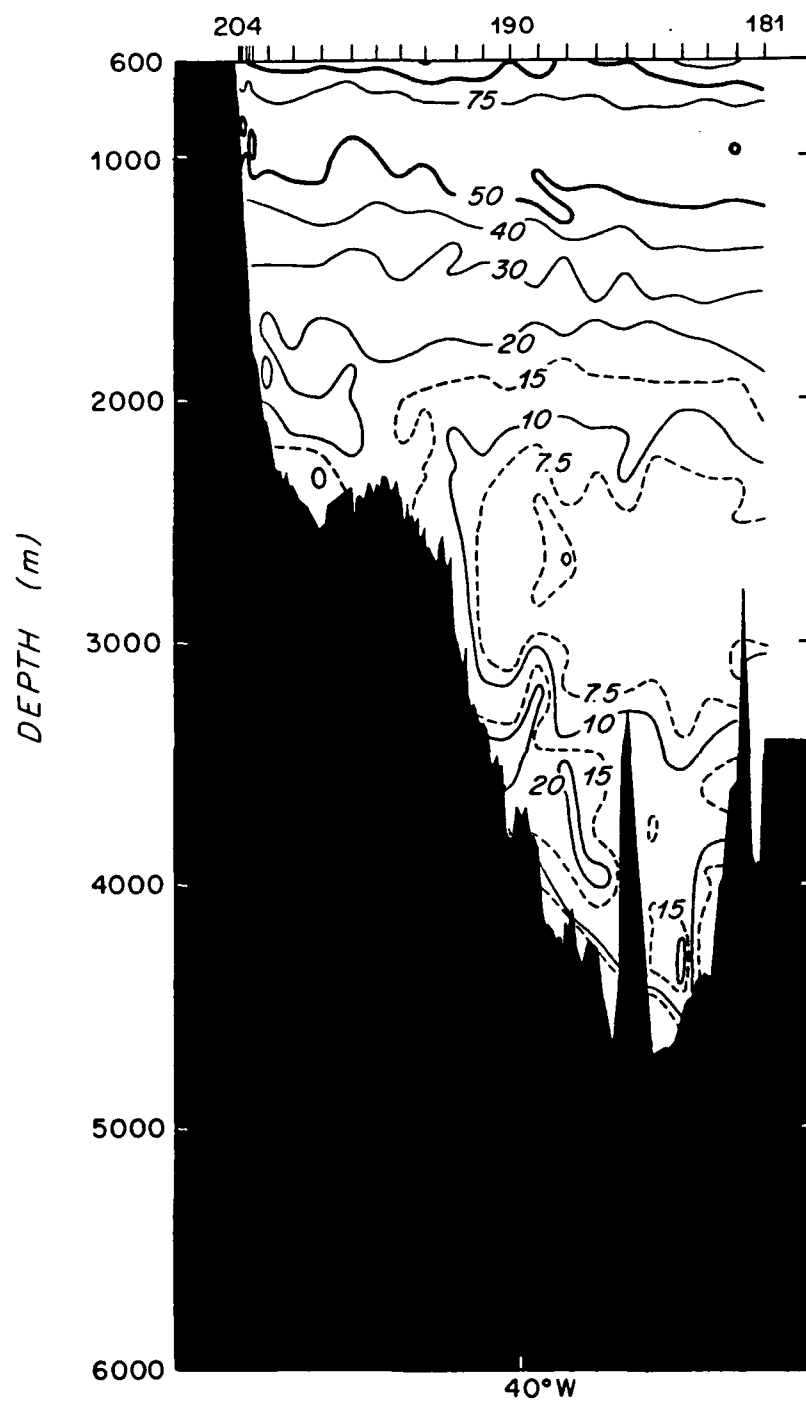


Figure 5.10: Contoured map of total potential vorticity at 27° S on a grid of distance (km) and depth. Contours are as indicated,  $E-9m^{-1}s^{-1}$ .

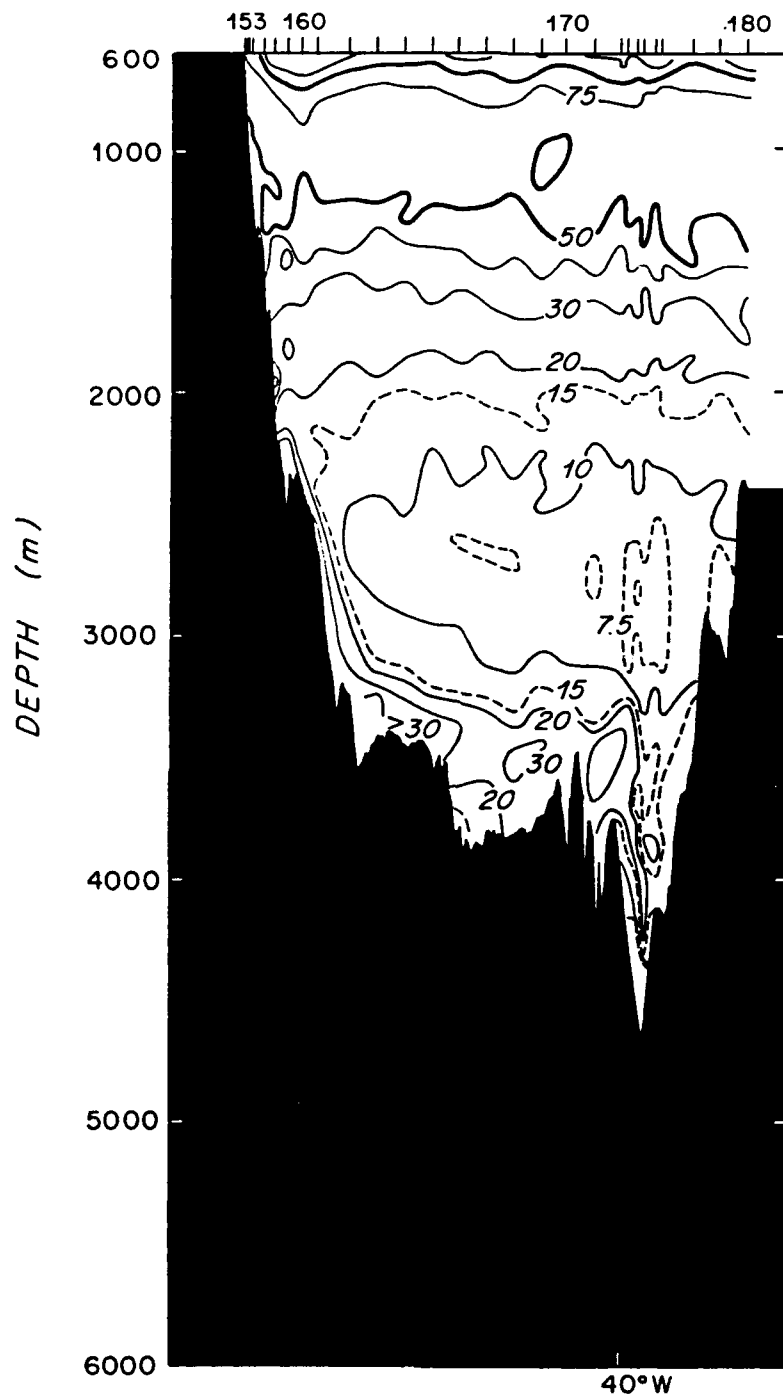


Figure 5.11: Contoured map of total potential vorticity at 31° S on a grid of distance (km) and depth. Contours are as indicated,  $E-9m^{-1}s^{-1}$ .

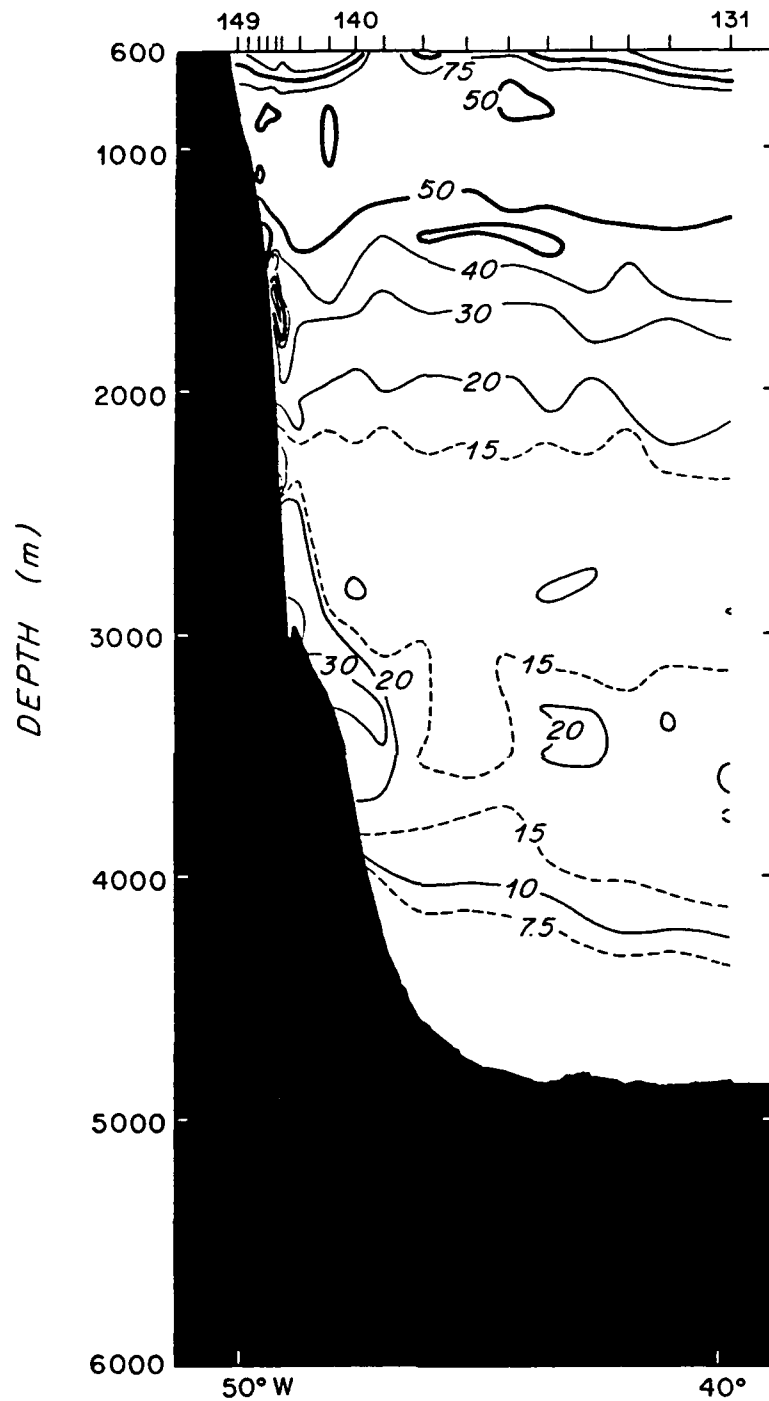


Figure 5.12: Contoured map of total potential vorticity at 34° S on a grid of distance (km) and depth. Contours are as indicated,  $E-9m^{-1}s^{-1}$ .



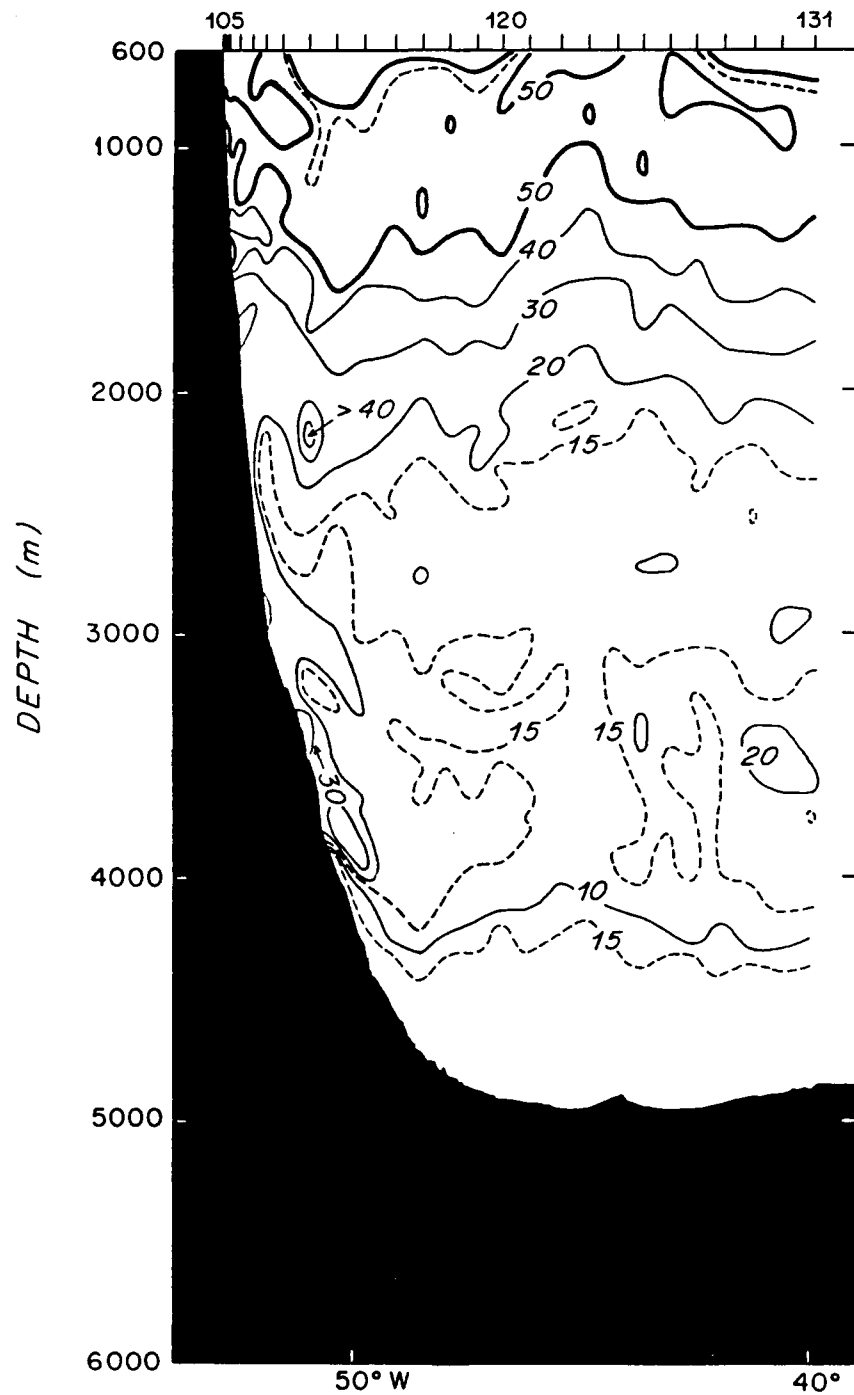


Figure 5.13: Contoured map of total potential vorticity at  $36^{\circ}$  S on a grid of distance (km) and depth. Contours are as indicated,  $E-9m^{-1}s^{-1}$ .

recirculation strengthening the maximum in the Brazil Current. Thus the small maximum core in the Brazil Current at  $27^{\circ}$  S grows downstream. Although other tracers suggested a recirculation in the cores of AAIW, the signal in  $Q$  is clearer.

The other strong feature in these sections is the wall of  $Q$  found in the surface waters of the Brazil Current, similar to that found in the Gulf Stream by Leaman, Johns and Rossby (1989) and in the Agulhas by Bennett (1988). This is not solely a result of including  $\mathcal{R}$ . Although the strength of the wall is enhanced by the inclusion of  $\mathcal{R}$ , the wall is present in  $\mathcal{P}$  sections as well. The presence of a wall with high  $Q$  on one side and lower  $Q$  can be seen in the density sections (fig 2.8). The density layers are thickest at the bottom of the bowl, with a large decrease in the current and a slight decrease in the recirculation. This results in a wall of  $\mathcal{P}$  against the coast. The inclusion of a canonical jet Brazil Current and recirculation sharpens the wall (fig 5.18). Discussion of the wall will continue in the next section.

The sections of  $Q$  support the conclusions drawn from the other tracer sections, particularly in the deeper layers. More importantly, changes in the cores in the Brazil Current and offshore counterflow suggest that the counterflow is feeding back into the Brazil Current to form a recirculation. The circulation diagrams of chapter 3 suggest that this is the case, but this is the clearest evidence of such a link in the tracer fields.

### 5.3 Potential Vorticity as a Dynamical Tool

There are many ways one could look at the  $Q$  data, depending on what one wants to accomplish. The approach taken here is quite simple. Layer averaged  $Q$ s are calculated for five layers: the four layers discussed previously, with the surface layer divided in two. Since isopycnals outcrop to the south, those isopycnals which outcrop at the southern section are in the upper surface layer (defined by  $26.5 \sigma_0$ ). The lower surface layer is thus continuous through all four sections. No discussion

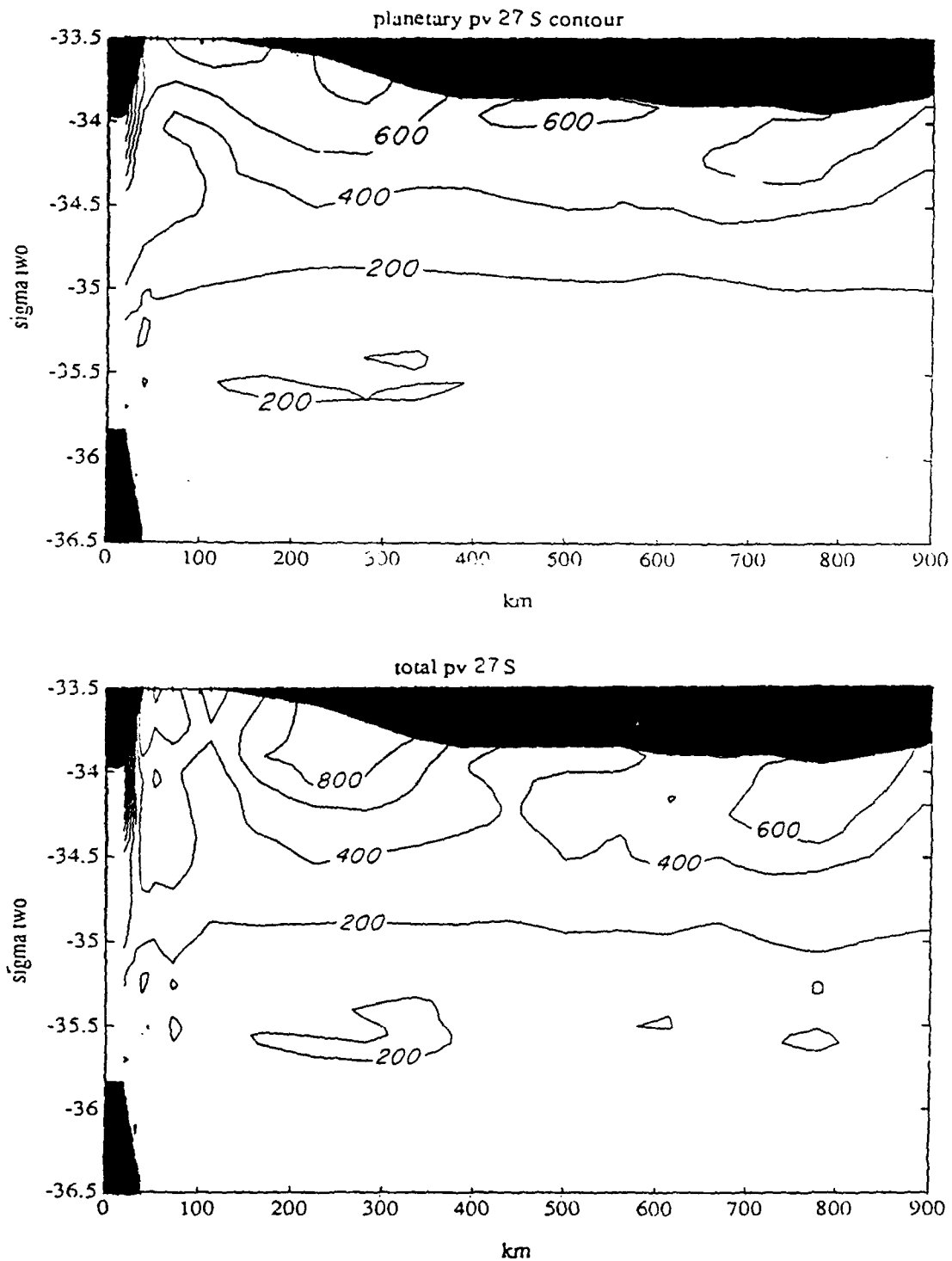


Figure 5.14: Contoured maps of (a) planetary potential vorticity and (b) total potential vorticity, at 27° S on a grid of distance (km) and density ( $\sigma_2$ ). The surface and bottom are indicated by the blackened areas. The contour interval is  $200 \text{ E-}9 \text{ m}^{-1} \text{ s}^{-1}$ .

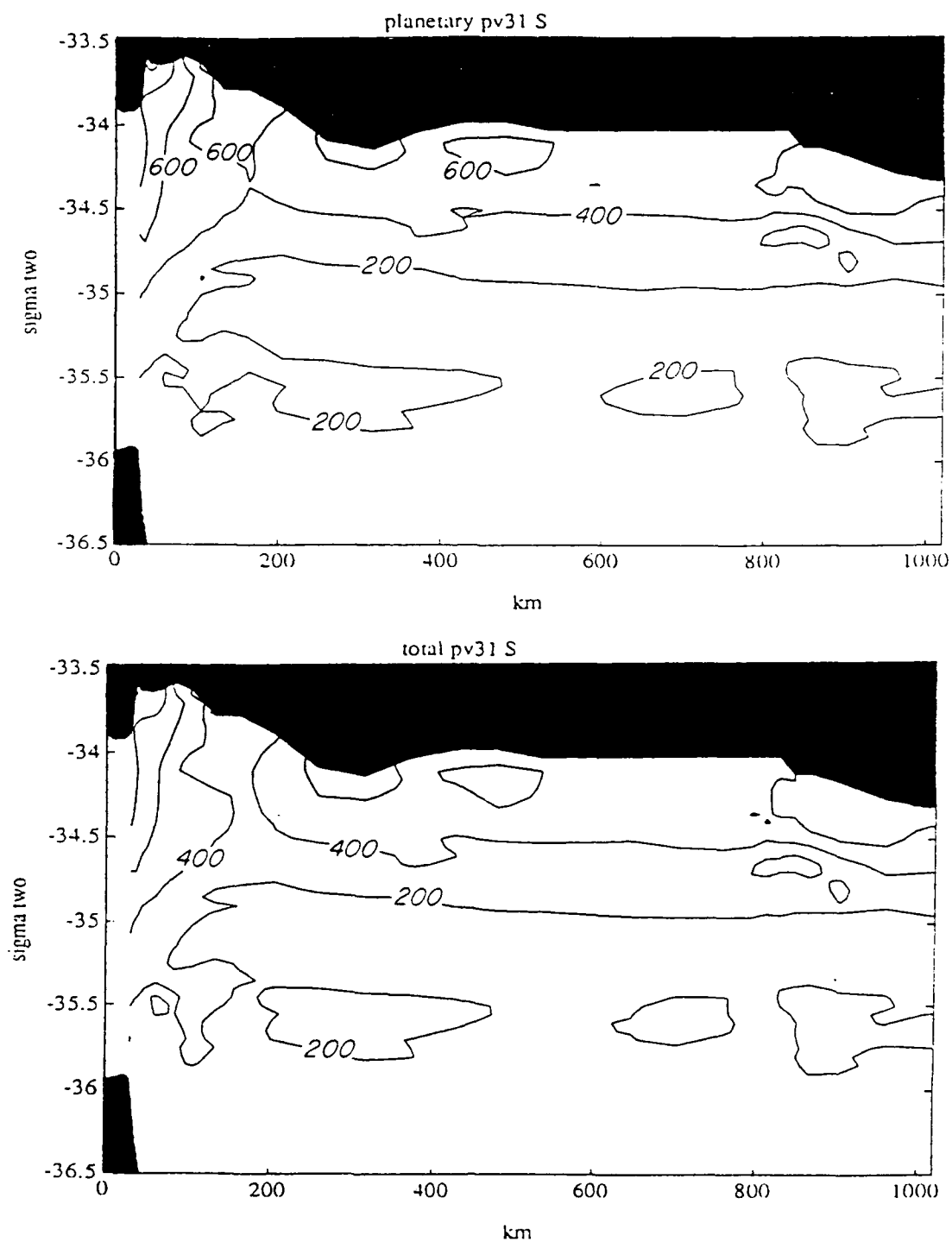


Figure 5.15: Contoured maps of (a) planetary potential vorticity and (b) total potential vorticity, at 31° S on a grid of distance (km) and density ( $\sigma_2$ ). The surface and bottom are indicated by the blackened areas. The contour interval is 200  $\text{E-9m}^{-1}\text{s}^{-1}$ .

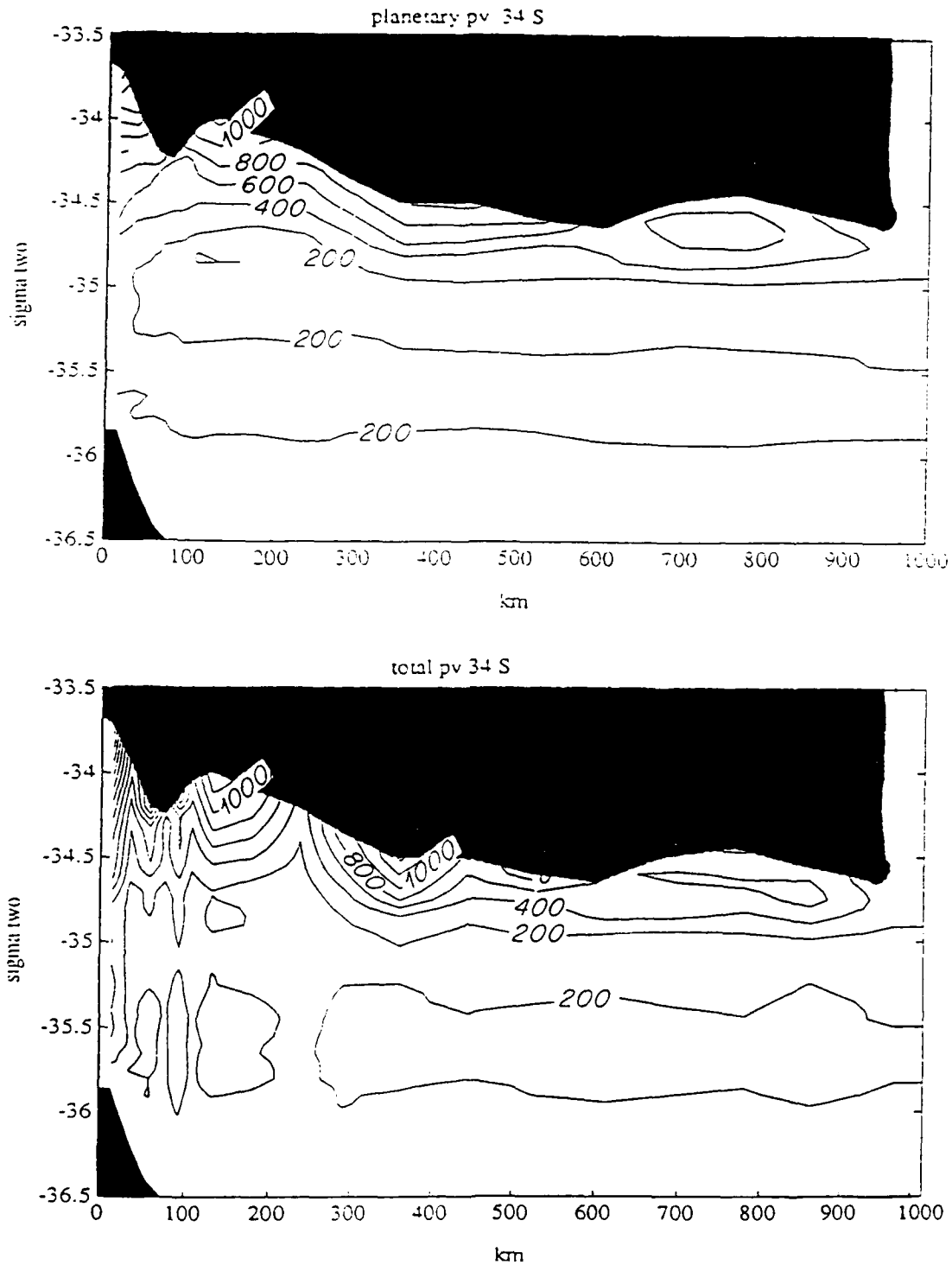


Figure 5.16: Contoured maps of (a) planetary potential vorticity and (b) total potential vorticity, at 34° S on a grid of distance (km) and density ( $\sigma_2$ ). The surface and bottom are indicated by the blackened areas. The contour interval is  $200 \text{ E-}9 \text{ m}^{-1} \text{ s}^{-1}$

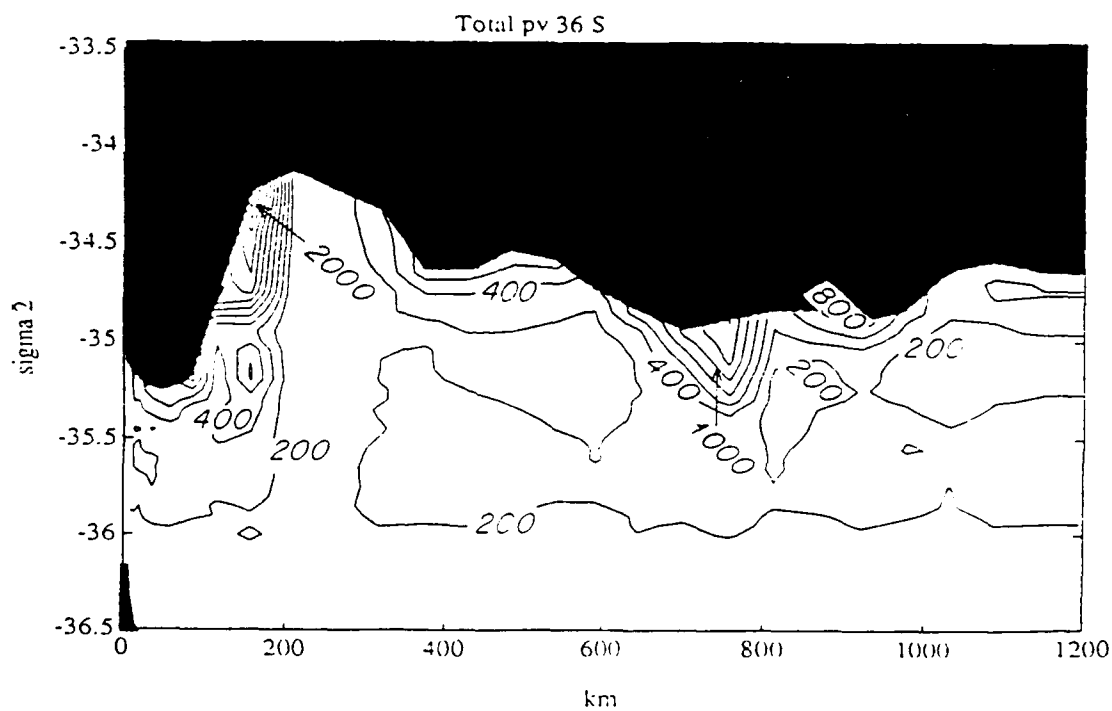
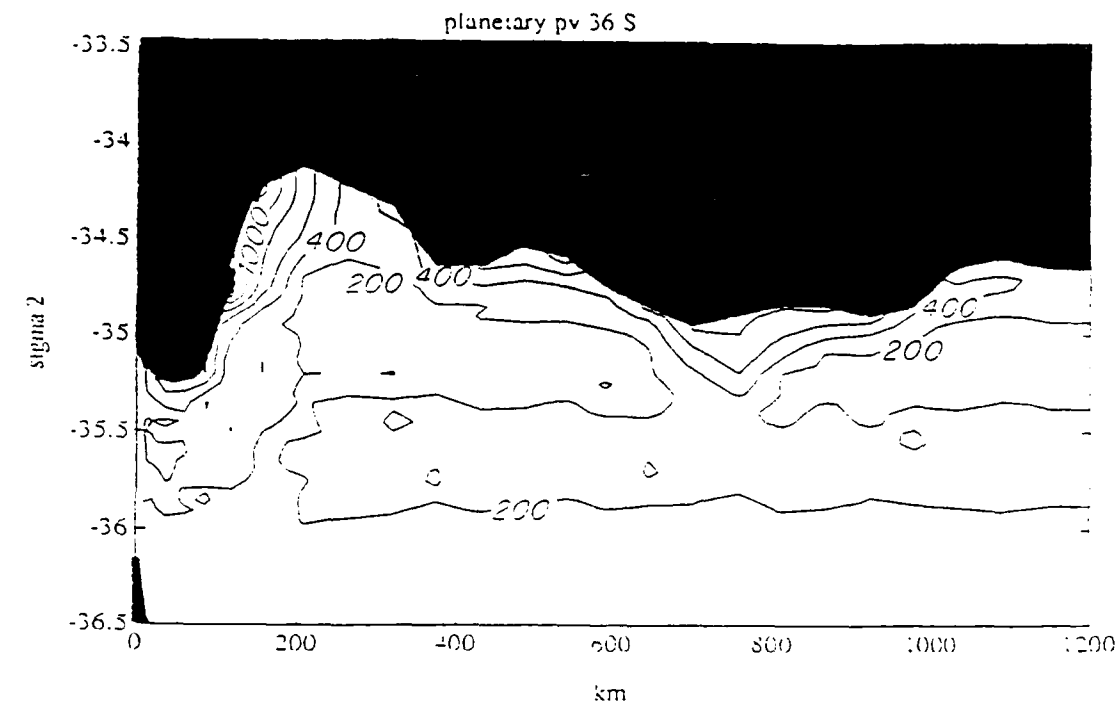


Figure 5.17: Contoured maps of (a) planetary potential vorticity and (b) total potential vorticity, at 36° S on a grid of distance (km) and density ( $\sigma_2$ ). The surface and bottom are indicated by the blackened areas. The contour interval is 200  $\text{E-9m}^{-1}\text{s}^{-1}$ .

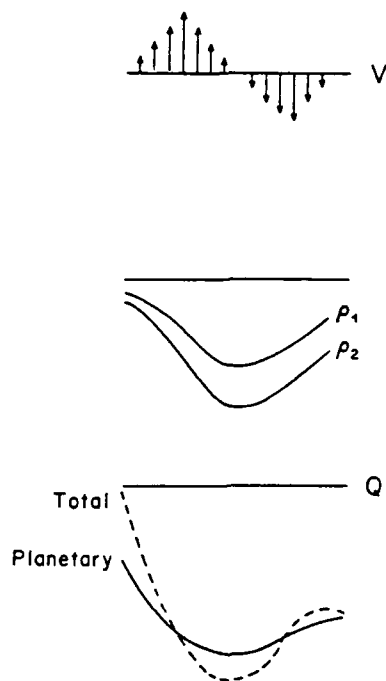


Figure 5.18: Cartoon showing how the change in thickness of the density layers, combined with a canonical jet and counter current, conspire to form a wall of potential vorticity.

The lower surface layer is thus continuous through all four sections. No discussion will be made of either the exposed surface layer or the deepest layer, which is dominated by bottom effects. With the layer averages we will look for a  $Q$ - $\Psi$  relationship and whether it is conserved, or whether there is evidence of a frictional boundary regime. The construction of such a  $Q$ - $\Psi$  relation would be of great value in western boundary current models, and the approach taken here towards such a relation seems fairly straightforward. One finds, however, that the Brazil Current is not a smooth, jet-like current, and the resulting derivatives are even less smooth.

The details of the layer average computation are in Appendix H. In addition we need to calculate  $\Psi$ , from the layer averaged, meridional velocity ( $\bar{V}$ ) field

$$\Psi = \Psi_0 + \int_0^x \bar{V} h dx \quad (5.6)$$

The stream function calculation begins at the first onshore station; thus there is a wide shallow region of the shelf over which there are no data;  $\Psi_0$  is not required to

be zero. No estimate of  $\Psi_0$  is provided here (although farther to the north estimates of shelf transport from ship drift data are as high as 7 Sv). If a relationship between  $Q$  and  $\Psi$  is established which is consistent from section to section, one might be able to go back and estimate  $\Psi_0$  by assuming  $Q$  should be conserved on lines of constant  $\Psi$ . If  $\Psi_0$  is initially taken to be zero, departures of  $Q$  from conservation could be used to infer changes in  $\Psi_0$  downstream. These changes would then provide an estimate of transport which is inshore of the measurements. For now  $\Psi_0$  is taken to be zero.

Based on the sections of  $Q$  we saw earlier, one might expect to see high  $Q$  at low  $\Psi$ , a minimum partway across the current, with  $Q$  leveling off to a low value as  $\Psi$  increases. Figures 5.19 and 5.20 show  $Q$  and  $\mathcal{P}$  for layer two.  $\mathcal{P}$  does look as described, but the inclusion of  $\mathcal{R}$  reduces the onshore peak of  $Q$  and introduces more variation offshore. The overall effect is a more uniform  $Q$ . The southernmost section is different from the others on the inshore edge because of the presence of low  $Q$  Falkland Current water. Figure 5.21 shows  $Q$  plotted as a function of  $\Psi$  for just the Brazil Current. The large downstream increase in transport, combined with the jittery signal, make any quantitative conclusions about a  $Q$ - $\Psi$  relationship impossible; the most one might say is that the curves overlies each other, and the peaks and valleys appear to average out to a fairly uniform  $Q$  value. The effect of  $\mathcal{R}$  in the previous figures is interesting. It is suggestive of Lozier and Riser's inertial region in the upper layer, where  $\mathcal{R}$  is important. The  $\mathcal{P}$  plots show the peak value increasing downstream, but the increase is offset by  $\mathcal{R}$ , keeping  $Q$  fairly constant (fig 5.2). The absence of a dissipative regime is consistent with the topography of the region, since a dissipative boundary could be inshore of the sections.

The inshore peak also occurs in the next layer down (fig 5.22). The picture is complicated, though, because this is the AAIW layer, and the alternately northward and southward flow causes the two northern sections to appear as a cloud about  $\Psi$  equal to zero.



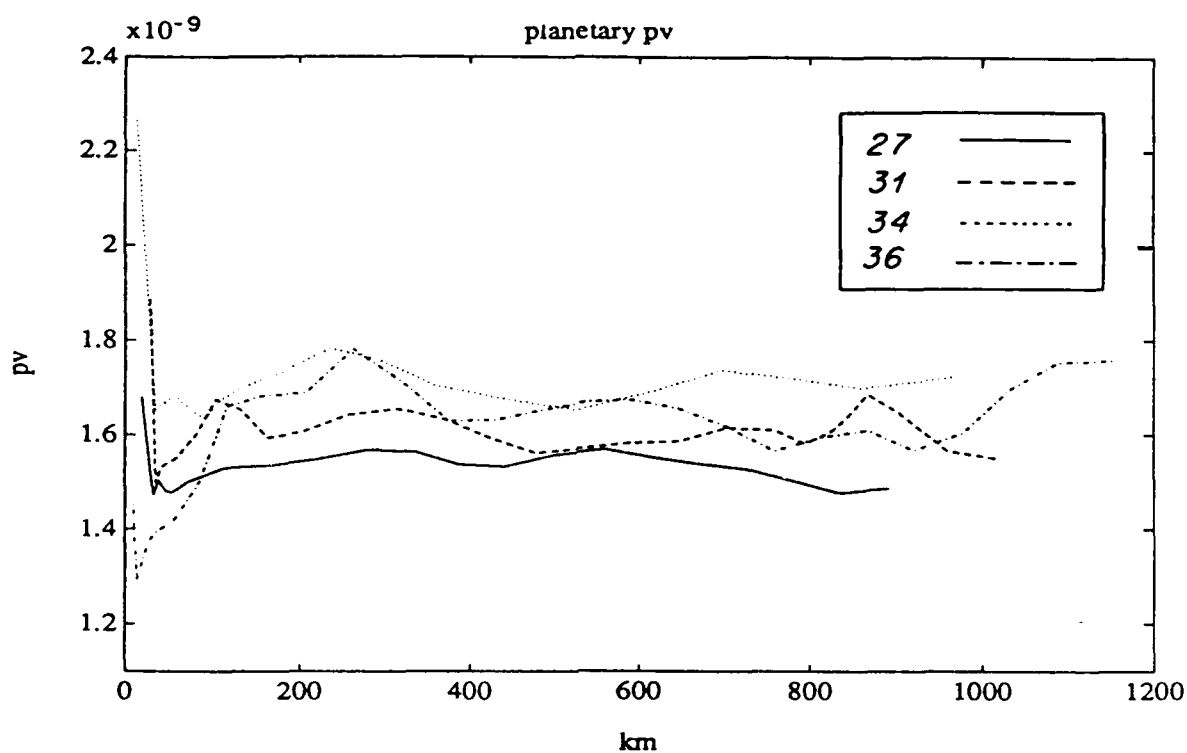


Figure 5.19: Plots of the planetary potential vorticity in the unexposed surface layer.

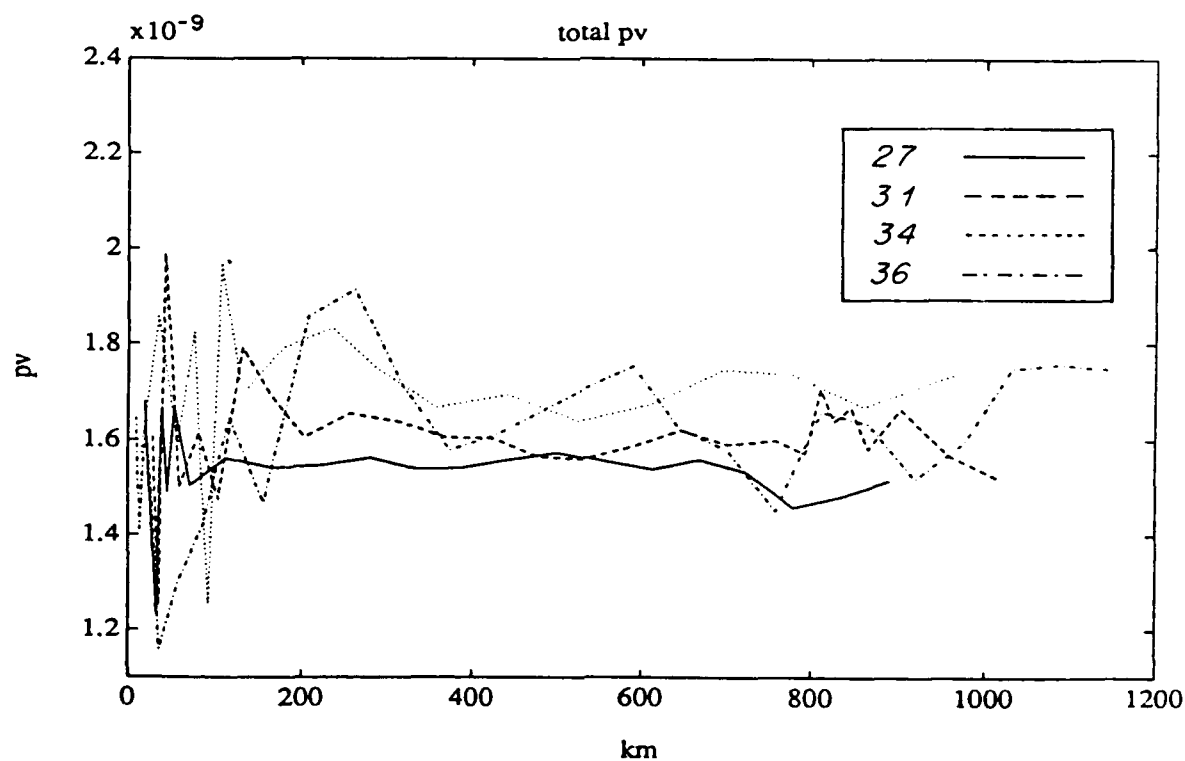


Figure 5.20: Plots of the total potential vorticity in the unexposed surface layer.

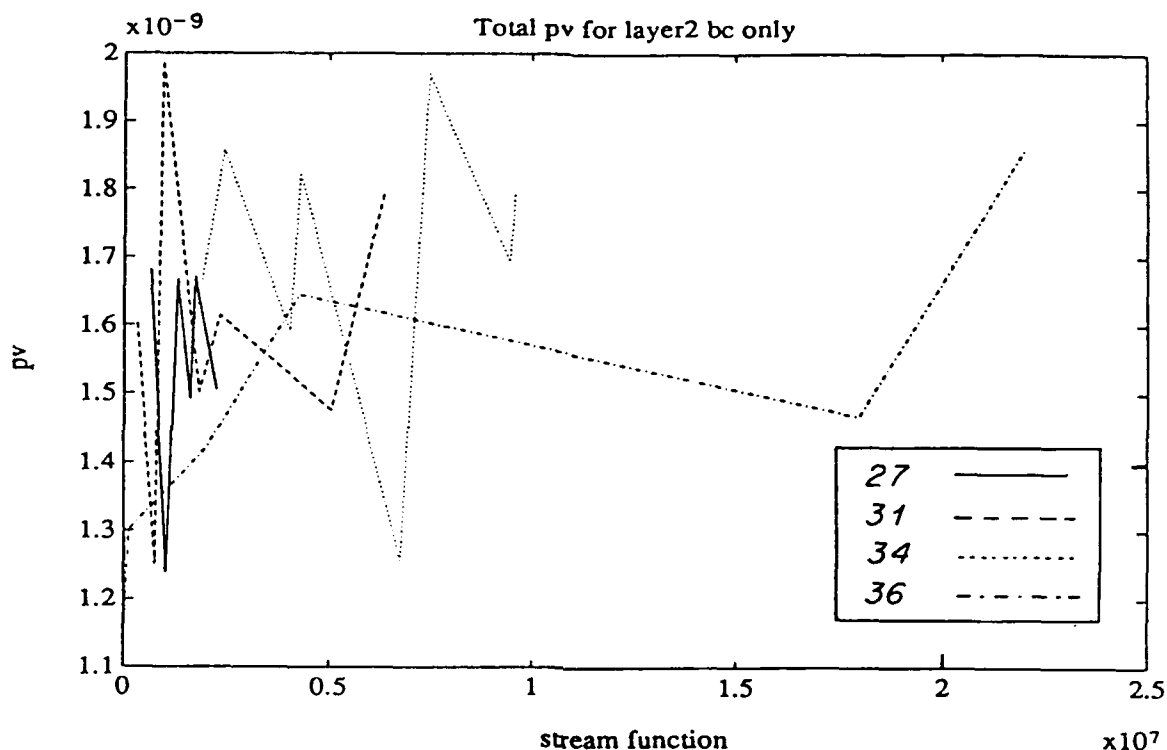


Figure 5.21: Plots of the total potential vorticity in the Brazil Current, for the unexposed surface layer. Horizontal axis is the stream function,  $\Psi$ .

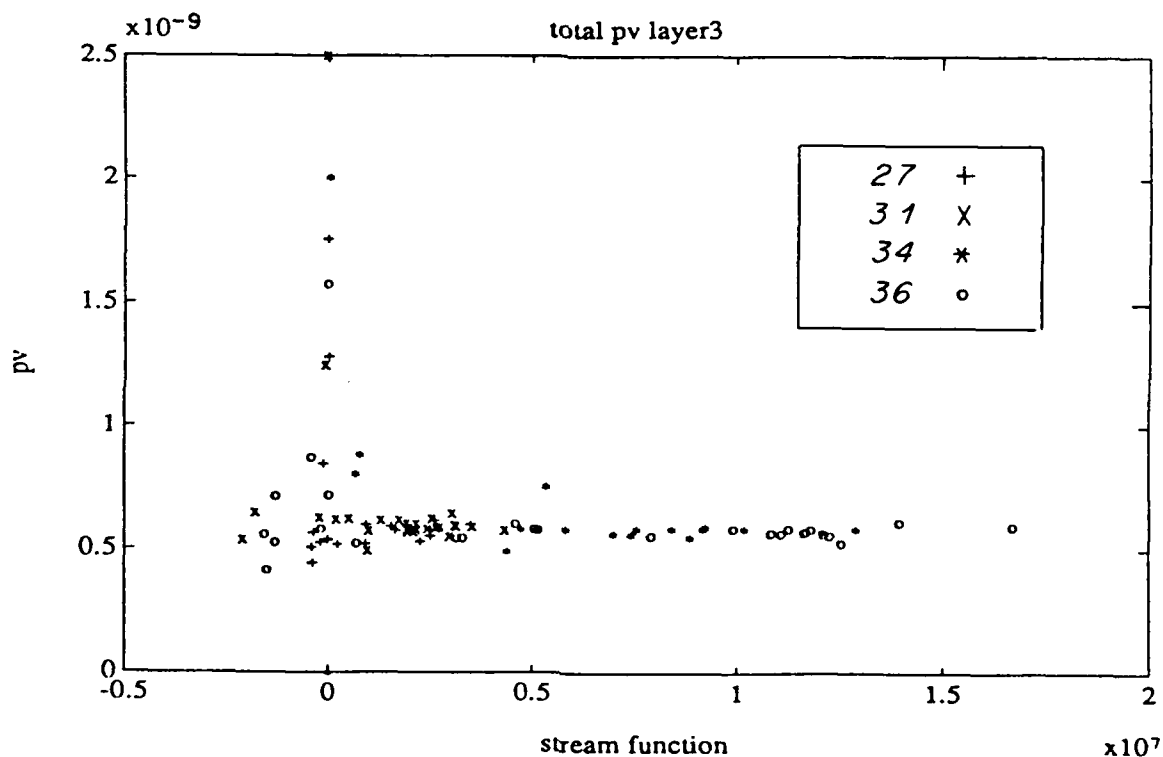


Figure 5.22: Plots of the total potential vorticity in the AAIW layer, with  $\Psi$  as the x coordinate.

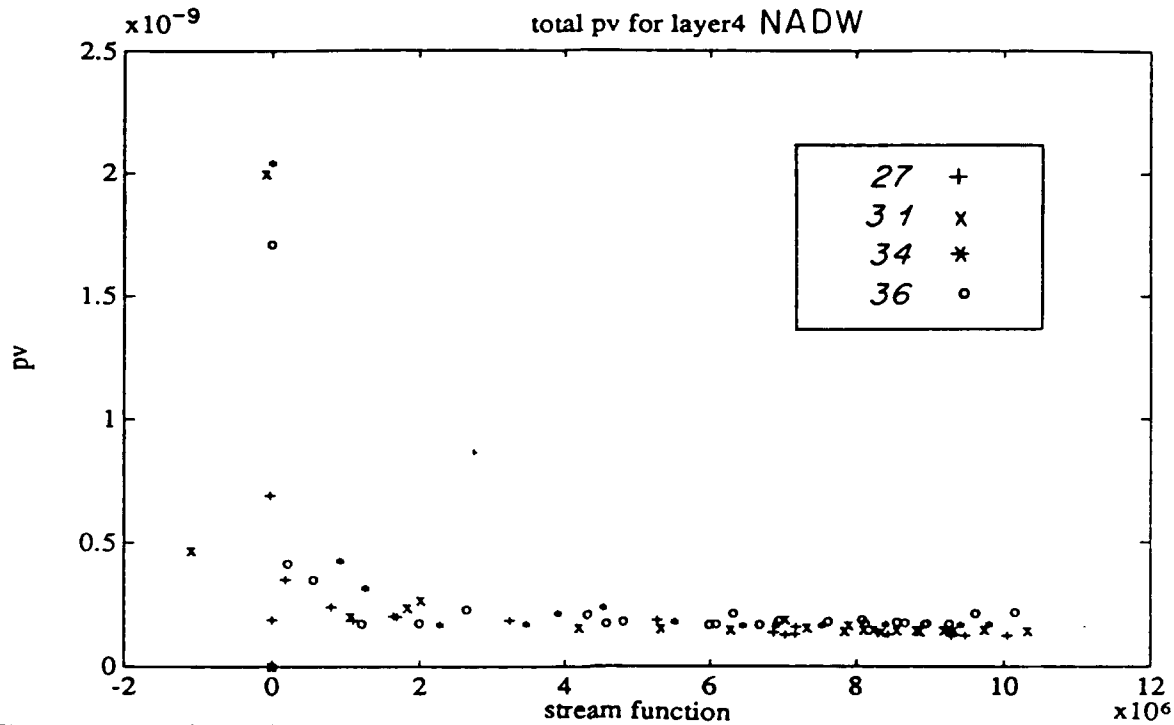


Figure 5.23: Plots of the total potential vorticity in the NADW layer, with  $\Psi$  as the x coordinate.

The NADW layer is perhaps the most straightforward. Because of its depth, its inshore edge intersects the topography, and so is completely sampled. The flow on the inshore edge is predominantly southward, so the problems with treating  $Q$  as a function of  $\Psi$  found in the AAIW layer do not occur. All four sections show an inshore maximum, decaying offshore to a constant value (fig 5.23 and 5.24). The difference between the northern and southern sections in the offshore value reflects the presence in the southern sections of LCPW; the circulation map for this layer did not connect the flow of the eastern edges of the 31 and 34° S sections. The inshore maximum at each section, caused by the thinning of the layer at the western edge, increases in value downstream for the first three sections. The downstream increase is consistent with being in a dissipative boundary, where  $Q$  increases with the change in coriolis force. In the region offshore of the maximum (about 1 to 6  $E6$   $m^3s^{-1}$  or 200 to 500 km) the  $Q$  value is fairly constant between sections;  $\mathcal{R}$  is not important in this layer, so the balance must be between stretching and the Coriolis force (as in Lozier and Riser's second layer).

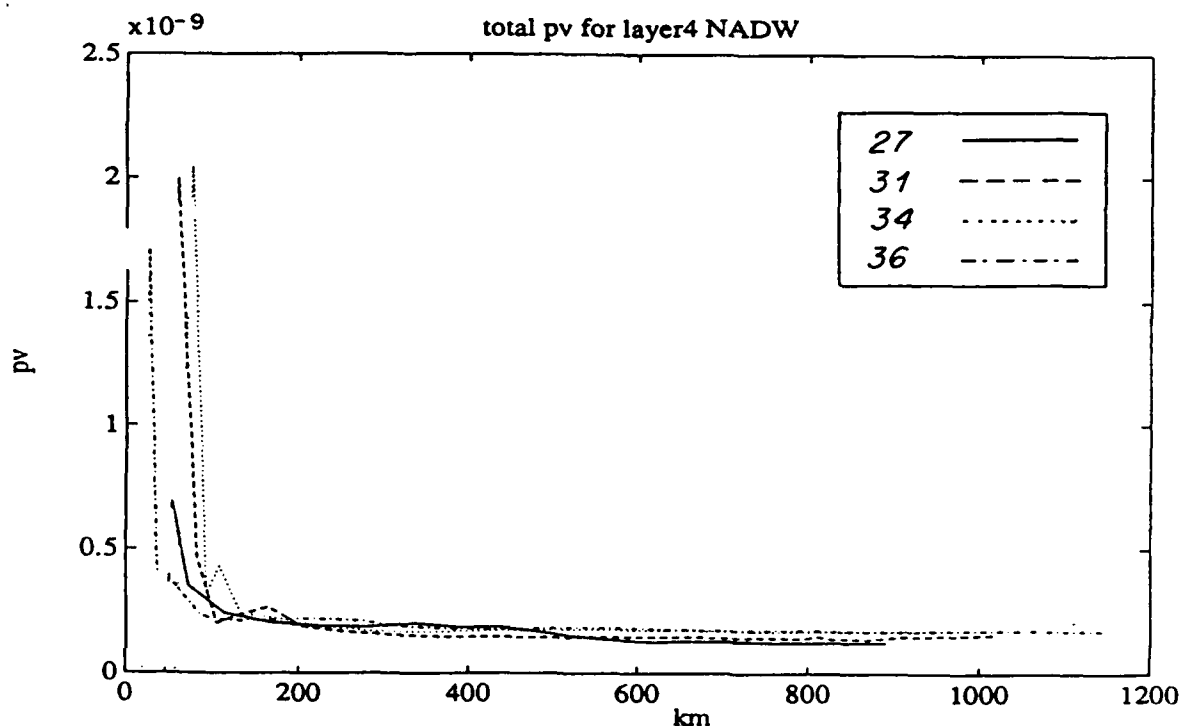


Figure 5.24: Plots of the total potential vorticity in the NADW layer, with along track distance (km) as the x coordinate.

## 5.4 Conclusions

Despite the anticipated problems, it appears that good estimates of  $Q$  can be made from closely spaced hydrographic data.  $\mathcal{R}$  proved to be fairly insensitive to the ZVS choice.  $Q$  is useful as a tracer, giving clear evidence of the recirculation in the surface layers. Although the presence of the recirculation is deduced in the previous chapters,  $Q$  produces the first clear picture in the surface layer of a tracer's signature in the Brazil Current being altered by the addition of water from the recirculation. The sections also shows the existence of a  $Q$  "wall" in the Brazil Current, similar to that found in the Gulf Stream and Agulhas. The presence of the wall in the  $\sigma_2$  sections indicates that water conserving both its density and its potential vorticity cannot cross from one side of the front to the other. The wall is present in the sections of  $\mathcal{P}$ , but the inclusion of  $\mathcal{R}$  greatly enhances the strength of the front.

The cross stream structure of potential vorticity is altered significantly by the inclusion of  $\mathcal{R}$ . In the upper layer the onshore maximum of  $\mathcal{P}$  increases at each

downstream section, but the inclusion of  $\mathcal{R}$  results in no net increase in  $\mathcal{Q}$ . The importance of  $\mathcal{R}$  in this layer is similar to that found in the surface layer of Lozier and Riser's multi-layer, quasi-geostrophic, eddy-resolving model. The balance of terms suggests that this is an inertial regime; a frictional regime may well occur farther inshore. In the deeper NADW layer, the downstream increase in the onshore  $\mathcal{P}$  maximum is not reduced by the inclusion of  $\mathcal{R}$ , suggesting a near-shore frictional regime. Farther offshore the change in Coriolis force is balanced by stretching, and no change in  $\mathcal{Q}$  occurs downstream. The balance of stretching against changes in Coriolis force is similar to that found in the second layer of Lozier and Riser's model.

Although the ability to detect these different flow regimes is useful, being able to compute an actual  $\mathcal{Q}$ - $\Psi$  would be more significant. Unfortunately, the process of taking two horizontal derivatives of the density field results in a jittery  $\mathcal{R}$  and  $\mathcal{Q}$ . This raises difficulties since the high Rossby numbers (as high as 1) computed from the potential vorticity data indicate  $\mathcal{R}$  cannot be ignored. More work will have to be done to determine whether the variability can be removed through either time averaging (using either current meters or repeat sections) or some other creative manipulation of the data.

## Chapter 6

### Conclusions

The collection of hydrographic sections through the Brazil Current is greatly enhanced by the addition of the Thomas Washington Marathon Cruise Leg 9 data set. The four sections detail the change of the current from a relatively small, surface feature to a large, deep current. While it does not appear to develop transports as large as the Gulf Stream (150 Sv), the Brazil Current surely exceeds the 20 Sv attributed to it at 38° S (Gordon and Greengrove, 1986). The Brazil Current in the north is fairly shallow, extending down to about 700 m at 27°S; it transports approximately 12 Sv south, which is consistent with estimates farther north. Downstream, surface layer transport increases, the current deepens, and the transport reaches a maximum of 80 Sv at 36°S. In addition to the deepening shear, part of the growth comes from the tight recirculation found just offshore the Brazil Current. Gordon and Greengrove (1986) suggest a recirculation is needed to close the transport gap between 24° and 38° S, and Stramma (1989) finds evidence of a 7.5 Sv recirculation at 30° S. This data set really provides the first picture of the changes in the recirculation, increasing in strength and depth to the south.

With more sections between 33° and 38° S, one could address a number of different issues. It would be interesting to see how the Brazil Current and NADW align and what adjustments take place between the two as a result. I have written of the Brazil Current overriding the NADW as if it were a fairly straightforward process,

but I imagine the actual junction of the two southward flowing currents has an impact on each. A cleaner section at  $34^{\circ}$  S would aid this analysis. In addition, one would like to know what effect variability has on the transport calculations. In particular, Olsen et al. (1988) found that the movement of the Brazil Current off the continental shelf and into deeper water may occur anywhere from  $33^{\circ}$  to  $38^{\circ}$  S. The separation of the Brazil Current from the continental shelf is almost surely tied to the strong growth found in the south; an analysis of such a link would be intriguing. It would also point out the problems involved in comparing transport values between different experiments; a large degree of variability might occur as a consequence of different separation points for the Brazil Current.

Analysis of the interaction of the Brazil Current with the rest of the subtropical gyre is possible with a basin-wide, four layer model. The model is able to extend the view of the current beyond that of an isolated ocean feature. By setting constraints on the exchanges between various water mass layers, limits are imposed on the size of the Brazil Current and its recirculation. The constraints for the model are on the sense, or direction, of the various layer-to-layer conversions occurring south of the section (one could also reinterpret them as measures of the net flow of a given layer across the section). Initially, a two layer model is employed. Governed by the conservation of mass in each layer, the two layer model has only one constraint on the resulting solutions: a conversion of cold-to-warm water in the south (or the surface layer flowing north and the deep layer flowing south). Such a meridional flow pattern is consistent with the equatorward heat flux in the South Atlantic. The single constraint, however, is not strong enough to limit the solution region in any significant way. A subsequent three layer model, in which all three layers conserve mass, has the additional constraint of AABW flowing northward across the section. The combination of northward flowing AABW and a conversion of NADW to AAIW (cold-to-warm) places some limits on the acceptable range of solutions. Finally, the four layer model adds another constraint such that the net transports of the surface layer and the bottom water are northward and AAIW is formed from

NADW. The resulting solution set has a fairly small range of transports for the Brazil Current. Given the complex interleavings of the South Atlantic water masses, the four layer model performs remarkably well.

One would like to extend the use of the model to other latitudes to see if it performs equally well elsewhere. Such a simple model, however, does not deal well with regions with high variability. When, in the early stages of development, sensitivity checks were performed for the various input, the eastern boundary conditions were found to be the most sensitive parameter. This will be a problem if the model is applied farther south, where the Capetown Eddy and the Agulhas retroflection affect the eastern boundary. Applying the model north of  $31^{\circ}$  S may be more fruitful. Farther north, Reid (1989) shows a large cyclonic gyre across most of the basin (a cyclonic gyre in the low latitudes is not unusual, but this one extends to higher latitudes on the eastern edge). The cyclonic gyre is centered in the middle of the basin, whereas the anticyclonic subtropical gyre (where the present data is situated) is western intensified. The broader scale of the northern gyre may require the model to be altered, with the interior split into two parts; one would expect the two interior regions to have opposite signs of barotropic transport. Looking at the IGY section at  $24^{\circ}$  S (Fuglister, 1960), one finds a similar geometry in the surface and NADW layers, but the second layer, the AAIW, is deeper in the east than in the west. The baroclinic imbalance in that layer will be the opposite of that found at  $31^{\circ}$  S. If AAIW is still to have a net northward transport at that latitude, then either a lot of NADW will have to be converted to AAIW, or an adjustment will take place barotropically. It is possible that both the Brazil Current and the recirculation might have northward barotropic transports in such a situation. Certainly that would be consistent with the smaller Brazil Current estimates at that latitude.

The estimation of total potential vorticity proved to be the most vexing problem faced in this dissertation. Contrary to what one might expect, the reference level choice is not a significant problem: where currents are large, most of the signal in relative potential vorticity comes from the measured shear, and where currents are



small, the relative potential vorticity is not significant compared to the planetary vorticity. Unfortunately, the process of taking two horizontal derivatives of the density field results in a jittery relative potential vorticity signal. As a result, a potential vorticity profile could not be constructed for the current. This variability may be real —the ocean is frequently much noisier than one imagines. It may also be possible, though, to smooth the data sufficiently so that a cleaner picture emerged.

Despite the problems involved in obtaining a quantitative profile of the potential vorticity, qualitative changes are useful in detecting different flow regimes. By comparing the downstream changes in total and planetary potential vorticity, one can deduce frictional and inertial regimes in the different layers. The presence of a frictional regime at the inshore edge suggests that care should be taken in assuming that potential vorticity is conserved in western boundary currents.

It would be fascinating to use the calculated potential vorticity to explore the interaction of the Brazil Current with the changes in topography it experiences as it moves on and off the continental shelf and across the continental slope into deep waters. Such a study may involve some more creative manipulation of the data, or it may require a different type of data, such as a series of moored arrays.

At the beginning of this dissertation I made the point that it is difficult to do interpretive work on an oceanographic feature whose very definition is subject to interpretation. Is the Brazil Current a classic western boundary current, developing deep shear and large transports, or is it merely a shallow surface current that feeds into the more interesting Brazil-Falklands confluence? In an effort to separate the observations from the interpretation, I have presented the data so one might interpret it in either way. However, I strongly believe that the term "Brazil Current" should refer to all water flowing southward contiguous with the surface expression of the current. Such a definition is particularly appropriate when comparing the Brazil Current to other western boundary currents; certainly it should lead to the Brazil

Current being regarded as one of the *four* big western boundary currents. +

## References

- Bennett, S.L. (1988). **Where three oceans meet: The Agulhas retroflection region.** Doctoral dissertation, Joint program in oceanography and oceanographic engineering between the Woods Hole Oceanographic Institution and the Massachusetts Institute of Technology, 367 pp.
- Bower, A.S., Rossby, H.T., and Lillibridge, J.L. (1985). The Gulf Stream — Barrier or blender? J. Phys. Ocean. **15**:24-32.
- Bryan, K. (1962). Measurements of meridional heat transport by ocean currents. J. Geophys. Res. **67**:3403-3414.
- Buscaglia, J.L. (1971). On the circulation of the Intermediate Water in the southwestern Atlantic Ocean. J. Mar. Res. **29**:245-255.
- Ertel, H. (1942). Ein neuer hydodynamischer Wirbelsatz. Meteor. Z. **59**:271-281.
- Evans, D.L., Signorini, S.R., and Miranda, L.B. (1983). A note on the transport of the Brazil Current. J. Phys. Oceanog. **13**:1732-1738.
- Evans, D.L., and Signorini, S.R. (1985). Vertical structure of the Brazil Current. Nature **315**:48-50.
- Findlay (1853). Oceanic currents and their connection with the proposed Central America canals. J. R. Geogr. Soc. **23**:217-240.
- Fofonoff, N.P. (1954). Steady flow in a frictionless homogenous ocean. J. Mar. Res. **13**:254-262.
- Fuglister, F.C. (1960). **Atlantic Ocean atlas of temperature and salinity profiles and data from the International Geophysical Year of 1957-1958, Atlas Series, Volume 1.** Woods Hole, MA: Woods Hole Oceanographic Institution, 209 pp.

- Garfield, N. (1988). Surface characteristics of the Brazil Current. Eos 69(44):1237.
- Garzoli, S.L., and Garraffo, Z. (1989). Transport, frontal motions and eddies at the Brazil-Malvinas Confluence as revealed by inverted echo sounders. J. Geophys. Res. 92:1914- 1922.
- Gill, A.E. (1982). Atmosphere-Ocean Dynamics. New York: Academic Press, 662 pp.
- Godfrey, J.S. (1989). A Sverdrup model of the depth-integrated flow for the world ocean allowing for island recirculations. Geophys. Astrophys. Fluid Dynamics 45:89-112.
- Gordon, A.L., and Greengrove, C.L. (1986). Geostrophic circulation of the Brazil-Falkland confluence. Deep-Sea Research 33:573-585.
- Hellerman, S., and Rosenstein, M. (1983). Normal monthly wind stress over the World Ocean with error estimates. J. Phys. Oceanog. 13:1093-1104.
- Hogg, N.G., Biscaye, P., Gardner, W., and Schmitz, W.J. (1982). On the transport and modification of Antarctic Bottom Water in the Vema Channel. J. Mar. Res. 40(Suppl.):231-263.
- Holland, W.R., and Lin, L.B. (1975). On the generation of mesoscale eddies and their contribution to the oceanic general circulation. J. Geophys. Res. 5:642-657.
- Johns, E., Watts, D.R., and Rossby, H.T. (1989). A test of geostrophy in the Gulf Stream. J. Geophys. Res. 94:3211-3222.
- Knauss, J.A. (1969). A note on the transport of the Gulf Stream. Deep-Sea Research 16 (Suppl.)117-123.
- Leaman, K.D., Johns, E., and Rossby, T. (1989). The average distribution of volume transport and potential vorticity with temperature at three sections across the Gulf Stream. J. Phys. Oceanog. 19:36-51.

- Lozier, M.S., and Riser, S.C. (1989). Potential vorticity dynamics of boundary currents in a quasi-geostrophic ocean. J. Phys. Oceanog. **19**(9):1373-1396.
- Miranda, L.B., and Castro Filho, B.M. (1982). Geostrophic flow conditions of the Brazil Current at 19degS. Ciencia Interamericana **22**:44-48.
- Munk, W.H. (1950). On the wind-driven ocean circulation. J. Meteorology **7**:79-93.
- Olson, D.B., Podesta, G.P., Evans, R.H., and Brown, O.B. (1988). Temporal variations in the separation of Brazil and Malvinas currents. Deep-Sea Research **12**:1971-1990.
- Pedlosky, J. (1979). **Geophysical Fluid Dynamics**. New York: Springer-Verlag, 624 pp.
- Peterson, R.G. (1990). On the volume transport in the southwestern Southern Atlantic Ocean. Abstract in Eos **71**(17):542.
- Peterson, R.G., and Stramma, L. (1991). Upper-level circulation in the South Atlantic Ocean. Prog. Oceanog. **26**:1-73.
- Reid, J.L. (1989). On the total geostrophic circulation of the South Atlantic Ocean: Flow patterns, tracers and transports. Prog. Oceanog. **23**:149-244.
- Reid, J.L., Nowlin, W.D., and Patzert, W.C. (1977). On the characteristics and circulation of the southwestern Atlantic Ocean. J. Phys. Oceanog. **7**:62-91.
- Rennell, J. (1832). **An investigation of the currents of the Atlantic Ocean, and those of which prevail between the Indian Ocean and the Atlantic**. London: J.G.&F. Rivington, 299 pp.
- Rintoul, S.R. (1988). **Mass, heat and nutrient fluxes in the Atlantic Ocean determined by inverse methods**. Doctoral dissertation, Joint program in oceanography and oceanographic engineering between the Woods Hole Oceanographic Institution and the Massachusetts Institute of Technology. 287 pp.

- Roden, G.I. (1986). Thermohaline fronts and baroclinic flow in the Argentine Basin during the austral spring of 1984. J. Geophys. Res. **91**:5075-5093.
- Rossby, C.G. (1936). Dynamics of steady ocean currents in the light of experimental fluid mechanics. Pap. Phys. Oceanog. Meteor. **5**:1-43.
- Signorini, S.R. (1978). On the circulation and the volume transport of the Brazil Current between the cape of São Tomé and Guanabara Bay. Deep-Sea Research **25**:481-490.
- Stommel, H. (1948). The westward intensification of wind-driven ocean currents. Trans. Amer. Geophys. Union **29**:202-206.
- Stommel, H. (1957). A survey of ocean current theory. Deep-Sea Research **4**:149-184.
- Stommel, H. (1965). **The Gulf Stream**. Berkeley, CA: University of California Press, 248 pp.
- Stommel, H., Niiler, P., and Anati, D. (1978). Dynamic topography and recirculation of the North Atlantic. J. Mar. Res. **36**(3):449-468.
- Stramma, L. (1989). The Brazil Current south of 23degS. Deep-Sea Research **36**:639-646.
- Talley, L.D., and McCartney, M.S. (1982). Distribution and circulation of Labrador Sea Water. J. Phys. Oceanog. **12**(11):1189-1205.
- Talley, L.D., and Raymer, M.E. (1982). Eighteen degree water variability. J. Mar. Res. **40**(Suppl.):757-775.
- Warren, B.A. (1963). Topographic influences on the path of the Gulf Stream. Tellus **15**:167-183.
- Wüst, G. (1935). Schichtung und Zirkulation des Atlantischen Ozeans. Die Stratosphäre. Wissenschaftliche Ergebnisse der Deutschen Atlantischen Expedition auf dem

Forschungs-und Vermmessungsschiff *Meteor* 1925-1927, 6:Teil 1, Lieferung 2, 1-288.

## APPENDIX A

Hand contoured section profiles of temperature, phosphate and nitrate for the four transects from the *Thomas Washington* Marathon cruise, Leg 3 (see Figure 1.3 for station locations).



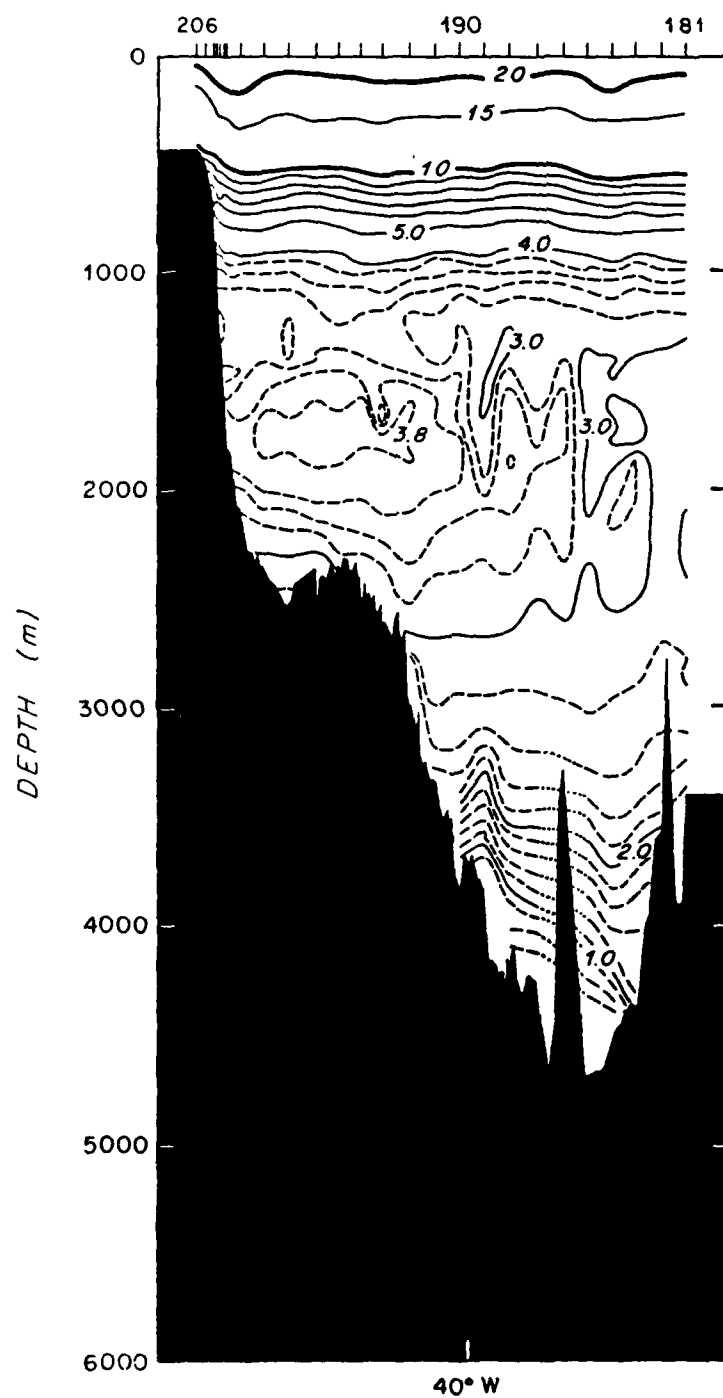


Figure A.25: Section profile of in situ temperature ( $^{\circ}$  C) at  $27^{\circ}$  S, from the Thomas Washington Marathon cruise, Leg 9

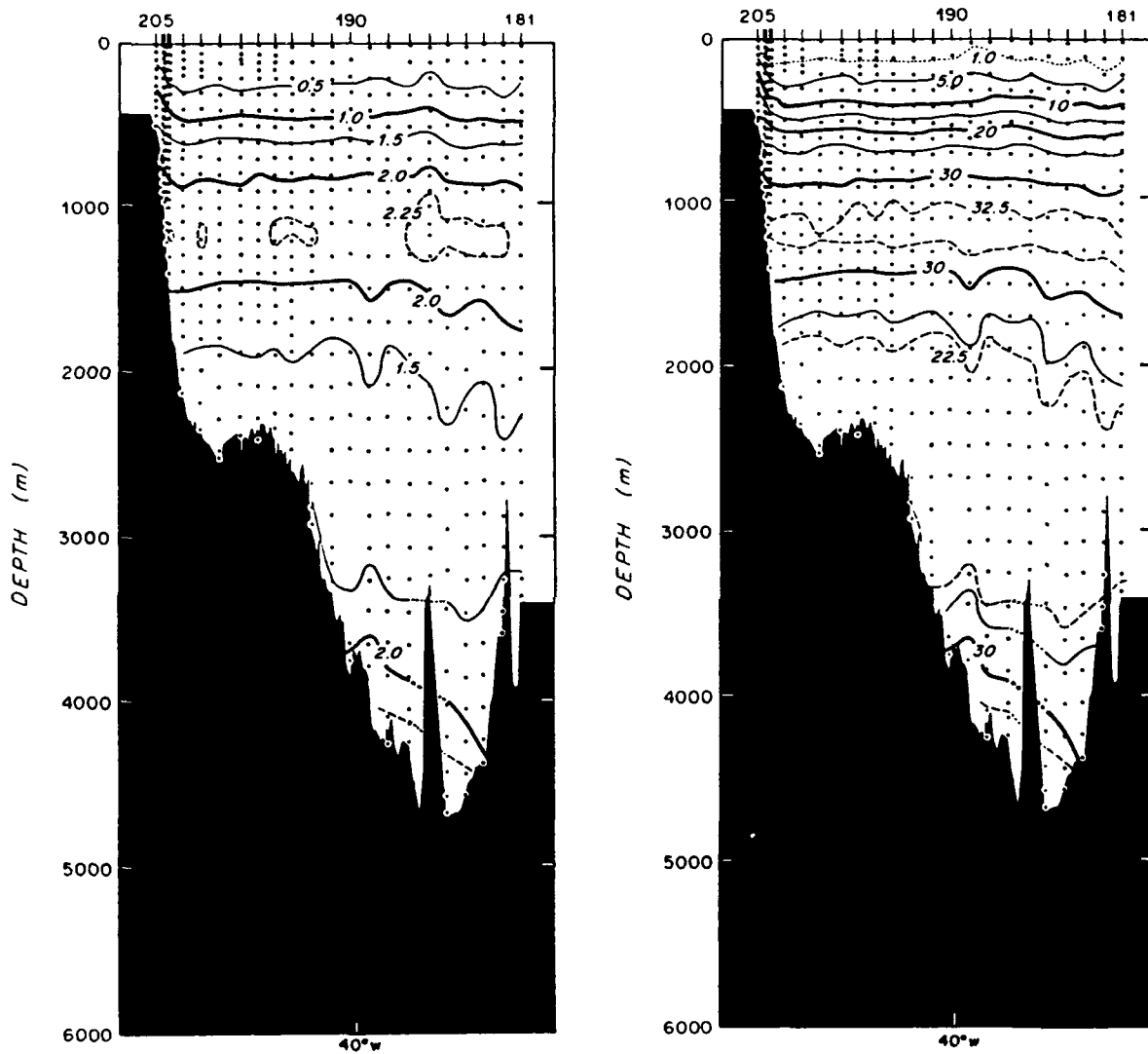


Figure A.26: Section profiles of phosphate and nitrate at 27° S, from the Thomas Washington Marathon cruise, Leg 9

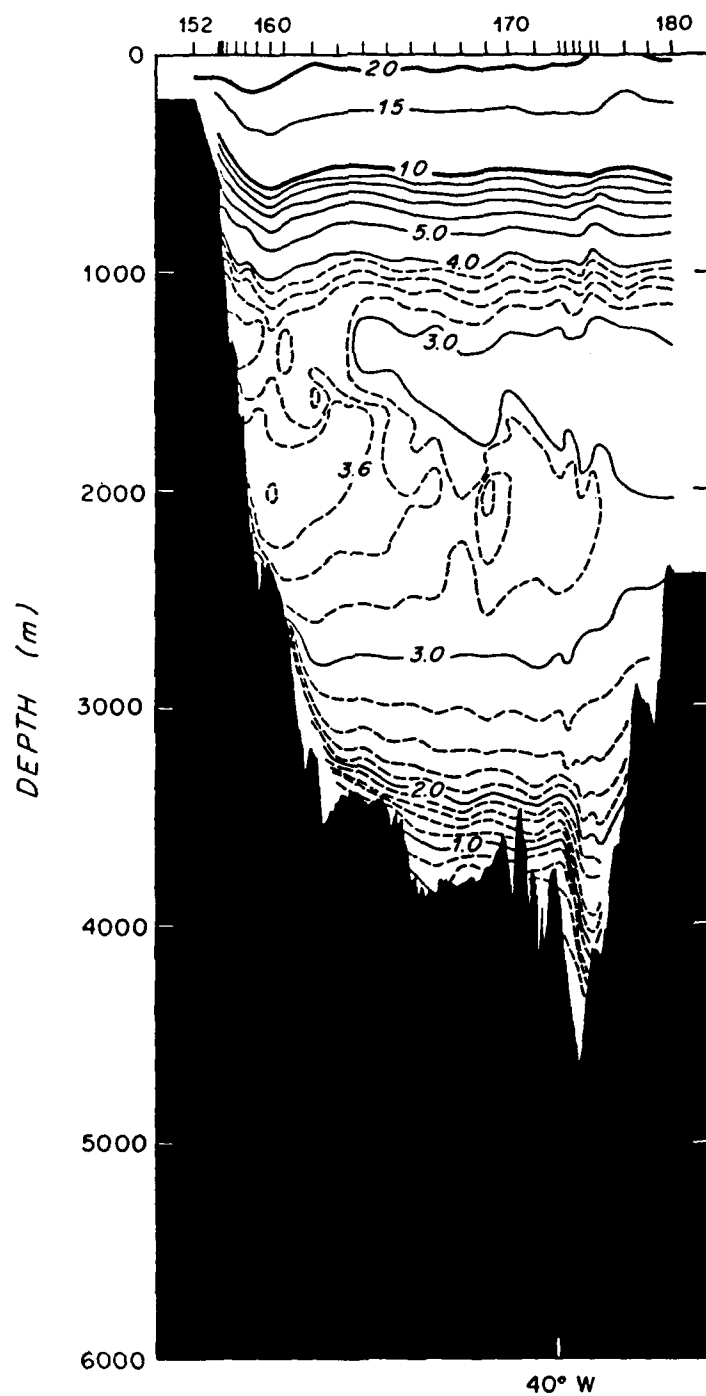


Figure A.27: Section profile of in situ temperature ( $^{\circ}$  C) at  $31^{\circ}$  S, from the Thomas Washington Marathon cruise, Leg 9



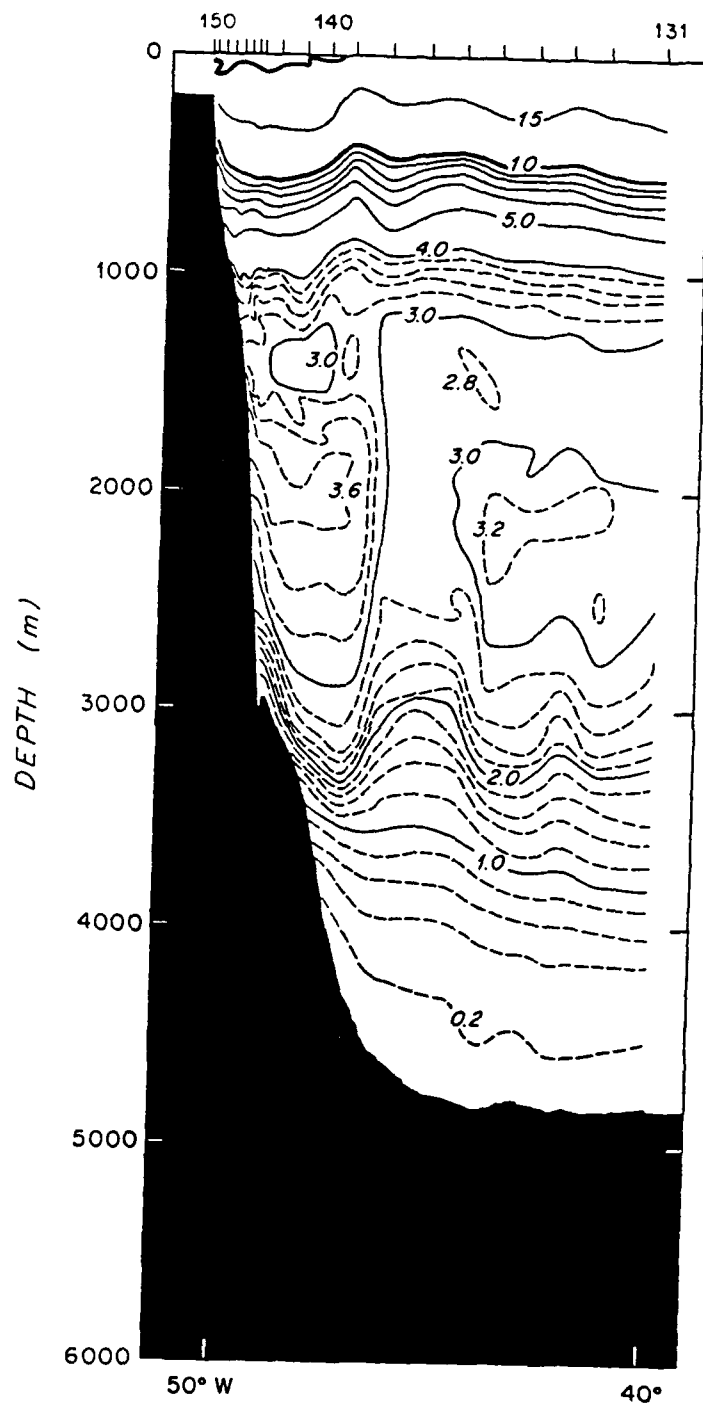


Figure A.29: Section profile of in situ temperature ( $^{\circ}$  C) at  $34^{\circ}$  S, from the Thomas Washington Marathon cruise, Leg 9

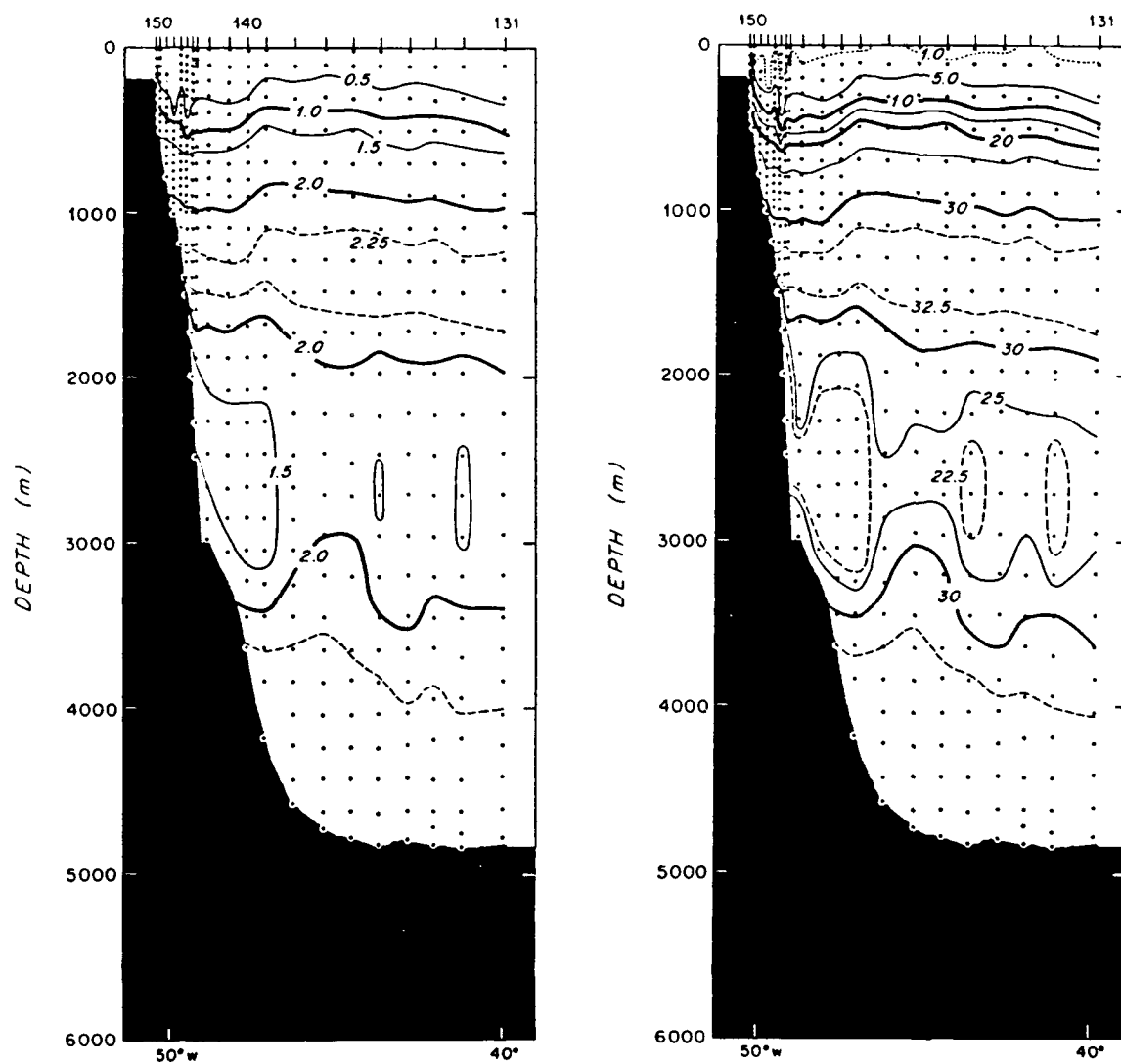


Figure A.30: Section profiles of phosphate and nitrate at 34° S, from the Thomas Washington Marathon cruise, Leg 9

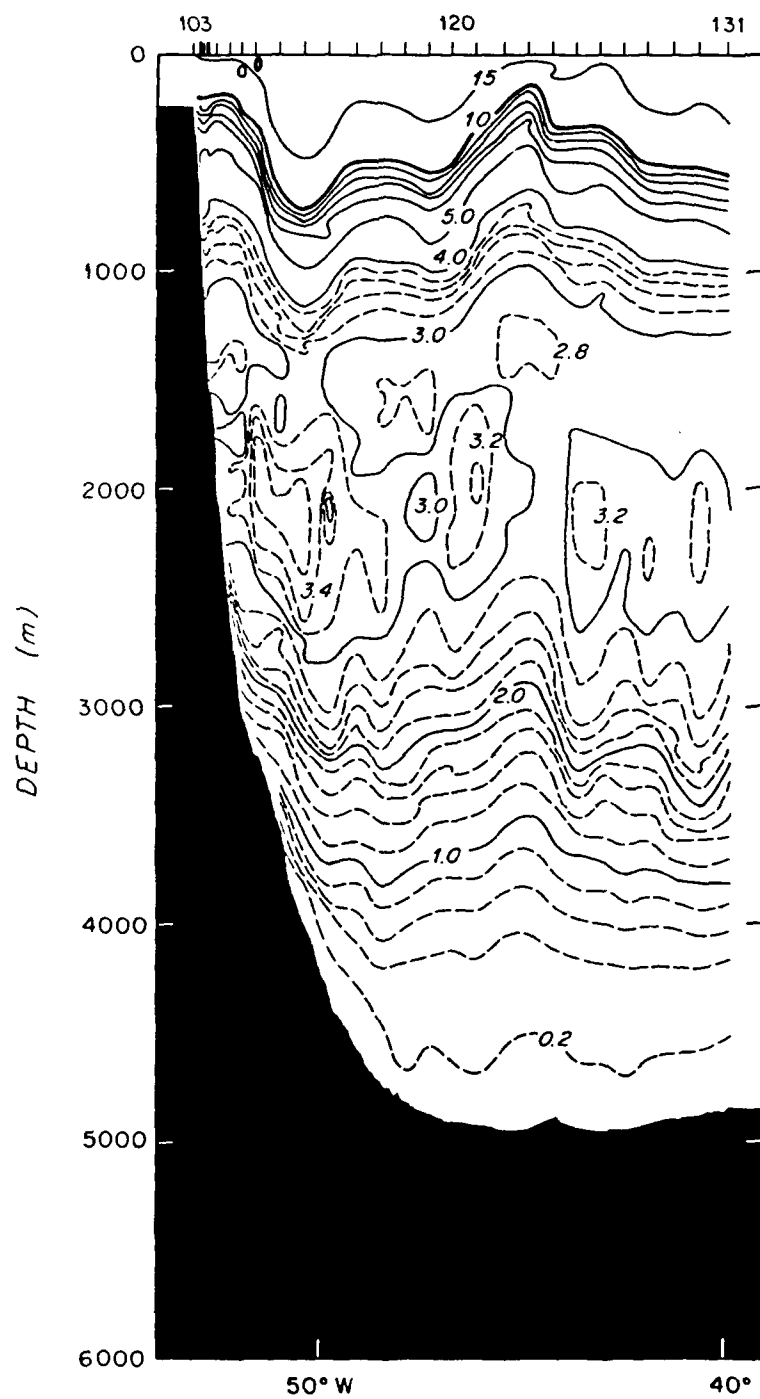


Figure A.31: Section profile of in situ temperature ( $^{\circ}$  C) at  $36^{\circ}$  S, from the Thomas Washington Marathon cruise, Leg 9

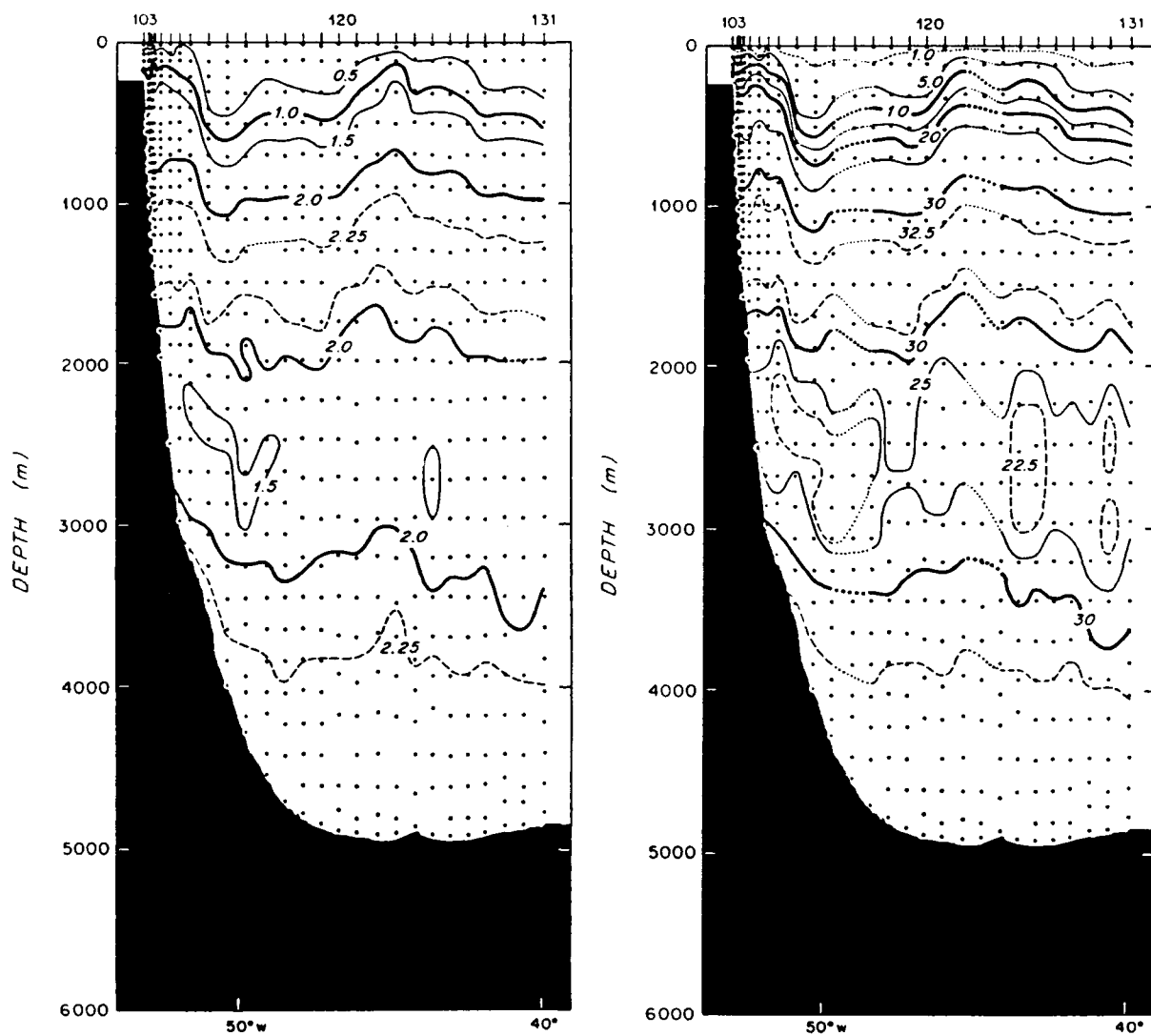


Figure A.32: Section profiles of phosphate and nitrate at 36° S, from the Thomas Washington Marathon cruise, Leg 9



## APPENDIX B

Programs which compute velocity from hydrographic data abound, and most are quite similar to each other. Like the program used here, they calculate velocity shear using the thermal wind equation. Given data from two stations, a and b, the equation for the vertical velocity shear is

$$v_{shear}(p) = \frac{1}{Lf} \left[ \int_0^p \delta_b dp - \int_0^p \delta_a dp \right] \quad (A.1)$$

$L$  is the separation between the two stations.  $\delta$ , the specific volume anomaly, is defined by

$$\frac{1}{\rho} = \alpha = \delta + \alpha(35.0, p) \quad (A.2)$$

where  $\alpha(35.0, p)$  is a reference specific volume. Once  $v_{shear}$  is calculated relative to the surface, a reference for the shear profile is chosen. This is added to  $v_{shear}$  to compute  $v$

$$v(p) = v_r + v_{shear}(p) \quad (A.3)$$

The problem comes when the bottom is reached. If the bottom is fairly flat, and the stations are taken to approximately the same depth, then the equations above will give velocity estimates for the most of the water column. However, if one station is deeper than the other, the question of how to compute velocity in the "bottom triangle" (the region where only one set of data exists) arises. This is particularly important with this data set, which has the Brazil Current running along a strongly sloping bottom. Most programs deal with this in one of three ways: setting the velocity to zero, setting the velocity to that of the deepest common level or setting the velocity shear to that of the deepest common level (DCL). The first treatment surely underestimates the velocity. The second treatment probably underestimates the velocity, in addition, if the ZVS is in the bottom triangle the entire triangle is set to zero. The third treatment probably overestimates the velocity. An alternative is to scale the DCL shear by the measured vertical density gradient. Mathematically

this can be written

$$\frac{\partial \rho}{\partial x} = \frac{\partial \rho}{\partial z} \frac{\partial z}{\partial x} \Big|_{\rho} \quad (\text{A.4})$$

$$\frac{\partial \rho}{\partial x}(p) \cong \frac{\partial \rho}{\partial z}(p) \frac{\partial z}{\partial x}(DCL) = \frac{\frac{\partial \rho}{\partial z}(p) \frac{\partial \rho}{\partial x}(DCL)}{\frac{\partial \rho}{\partial z}(DCL)} \quad (\text{A.5})$$

In general, this results in a velocity shear profile that lies between the constant velocity and constant shear profiles (fig A.9). Setting the velocity to a constant results in noticeably lower velocities where the deeper station shows strong vertical density shear. Setting the velocity shear to a constant results in somewhat higher velocities which do not reflect the modulation in vertical density shear which occurs as the bottom was approached. By using all the density information available, an intermediate profile is obtained. This is particularly important in the Brazil Current, where strong shears are found right against the continental slope.

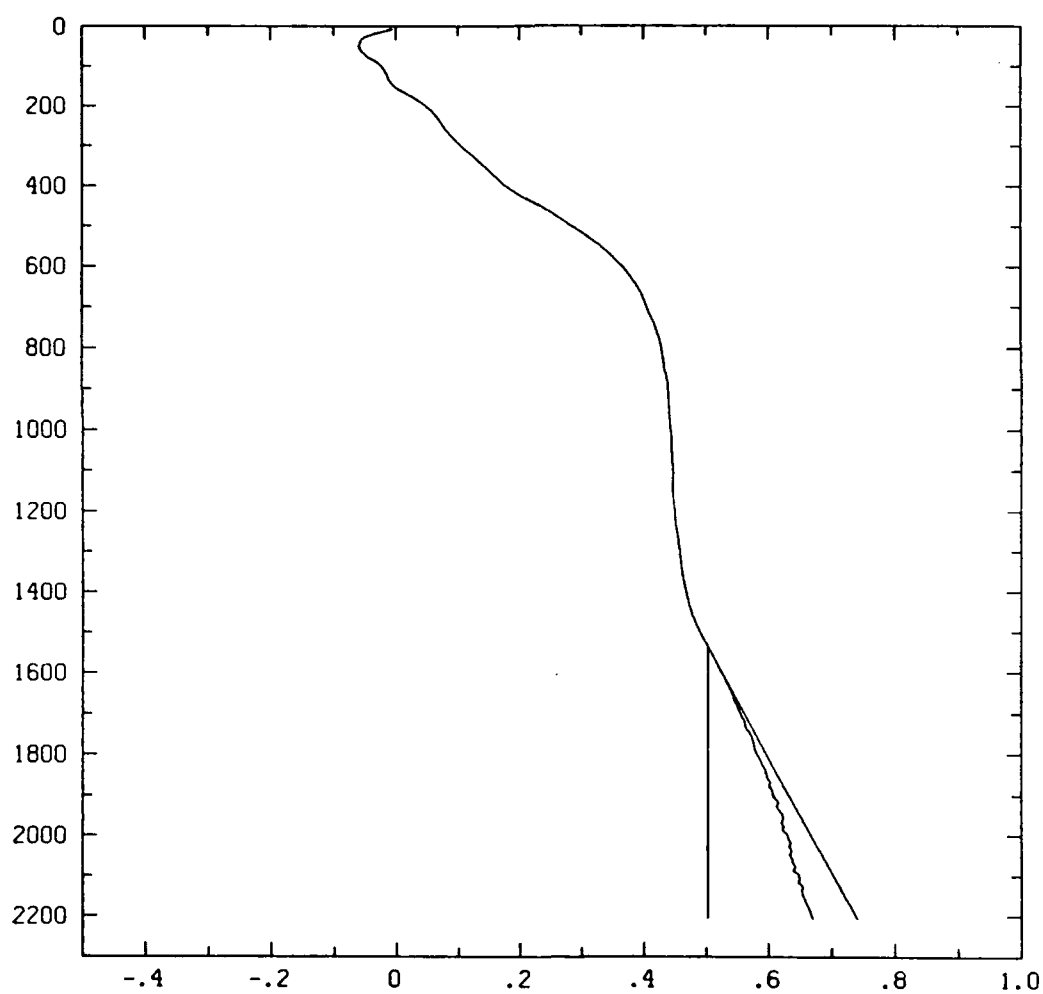


Figure A.33 Comparison of three velocity shear profiles, different only below the deepest common level. The three methods of computation are constant velocity, constant shear, and shear scaled by the vertical density gradient.

## APPENDIX C

Contoured section profiles of relative potential vorticity and  $\frac{dv}{dz}$  components for the transects at 27, 31 and 34° S from the *Thomas Washington* Marathon cruise, Leg 9 (see Figure 1.3 for station locations).

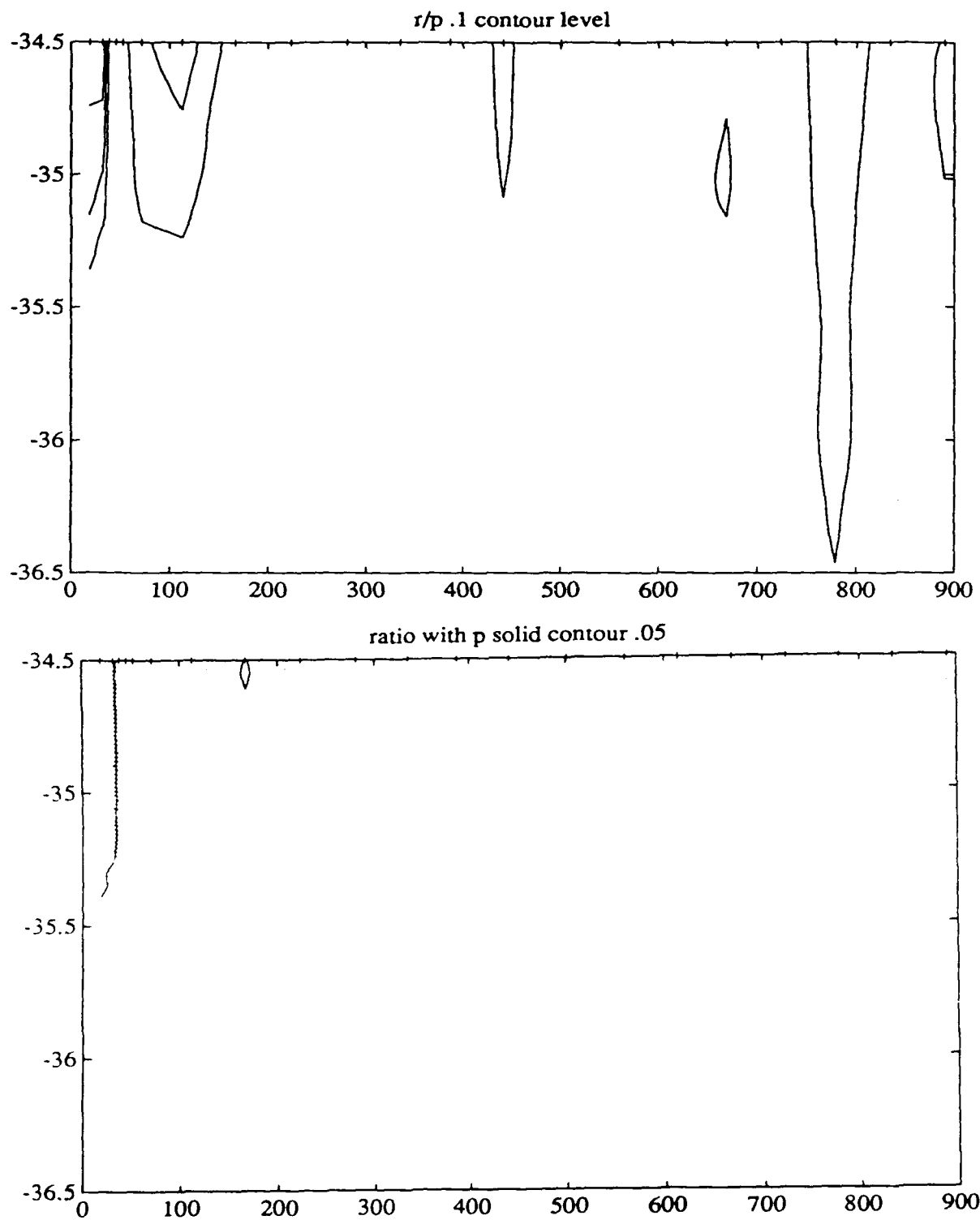


Figure A.34: Contribution of (a) relative potential vorticity and (b)  $\frac{dv}{dz}$  to the total potential vorticity at 27° S.

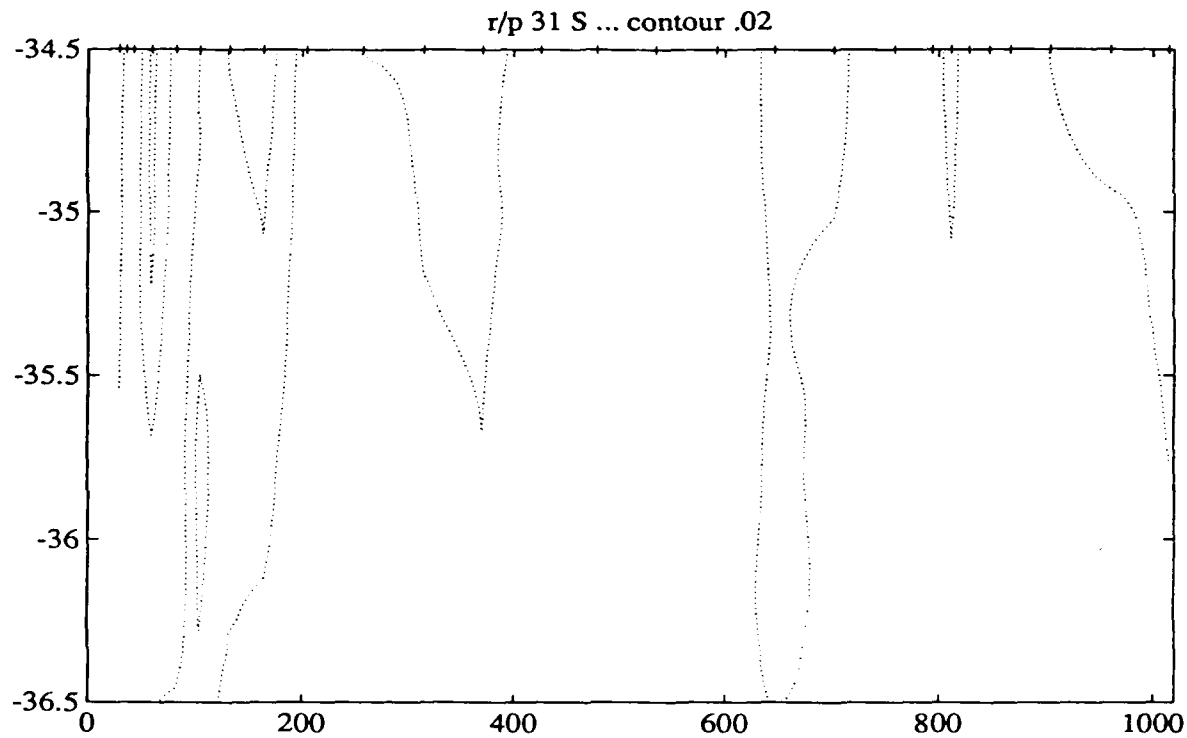


Figure A.35: Contribution of (a) relative potential vorticity and (b)  $\frac{dv}{dz}$  to the total potential vorticity at 31° S.

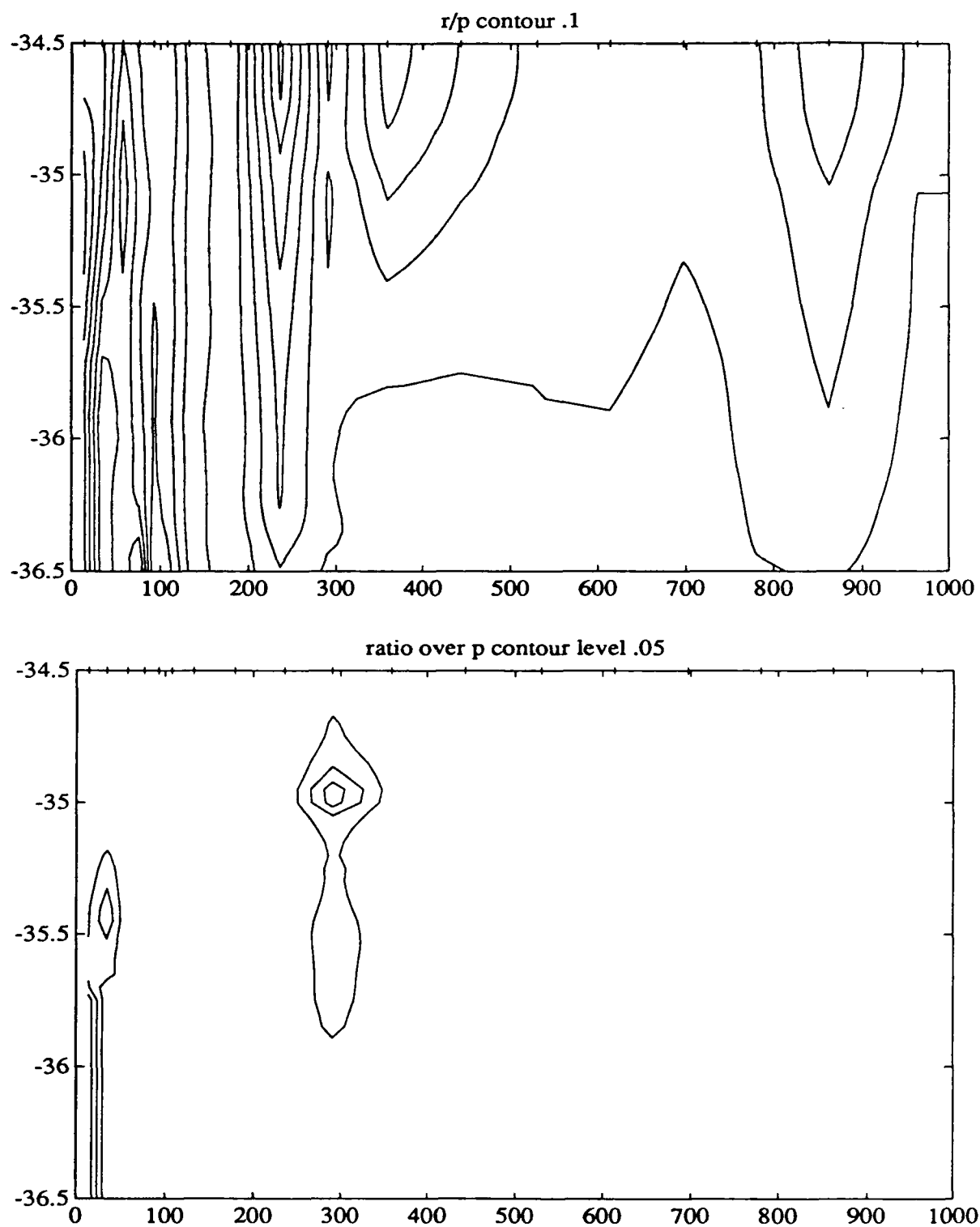


Figure A.36: Contribution of (a) relative potential vorticity and (b)  $\frac{dv}{dz}$  to the total potential vorticity at 34° S.

## APPENDIX D

To compute layer averaged total potential vorticity, we begin with a potential vorticity equation in which the cross stream velocity has been assumed negligible, and  $\sigma_2$  is the conserved scalar.

$$Q = \left( f - \frac{\partial V}{\partial x} \right) \frac{\partial \sigma_2}{\partial z} \quad (0.1)$$

This is averaged over a  $\sigma_2$  layer, where  $H$  is the height of the layer averaged between stations.

$$\overline{Q} = \frac{1}{H} \int_{z_1}^{z_2} \left( f - \frac{\partial V}{\partial x} \right) \frac{\partial \sigma_2}{\partial z} dz \quad (0.2)$$

Changing the variable of integration yields

$$\overline{Q} = \frac{1}{H} \int_{\sigma_{21}}^{\sigma_{22}} \left( f - \frac{\partial V}{\partial x} \right) d\sigma_2 = f \frac{\sigma_{22} - \sigma_{21}}{H} - \frac{1}{H} \frac{\partial}{\partial x} \int_{\sigma_{21}}^{\sigma_{22}} V d\sigma_2 \quad (0.3)$$

The last term is just the average velocity, but it must be the average with respect to density, not pressure or depth. The  $\sigma_2$  profiles are an average over two stations, consistent with the velocity which is computed as an average between two stations.

Potential vorticity tends to decrease in magnitude with depth. Thus, when a layer intersects the bottom topography only lower values of potential vorticity are removed from the average. One worries that this will result in artificially large potential vorticities at the edge. To check for this effect, potential vorticity is calculated for a thin layer, 36.95 - 36.97  $\sigma_2$  (fig A.37); this layer does not have the topographic bias described above. For each section, the shallowest station which has 36.95  $\sigma_2$  water also has 36.97  $\sigma_2$  water. If this plot is compared to the layer average for all NADW (fig A.38), one finds that the relative change across each section is similar. The specific values should not be compared directly, only the shape of the curves. The bias does not appear to distort the shape of the potential vorticity curves for each section.



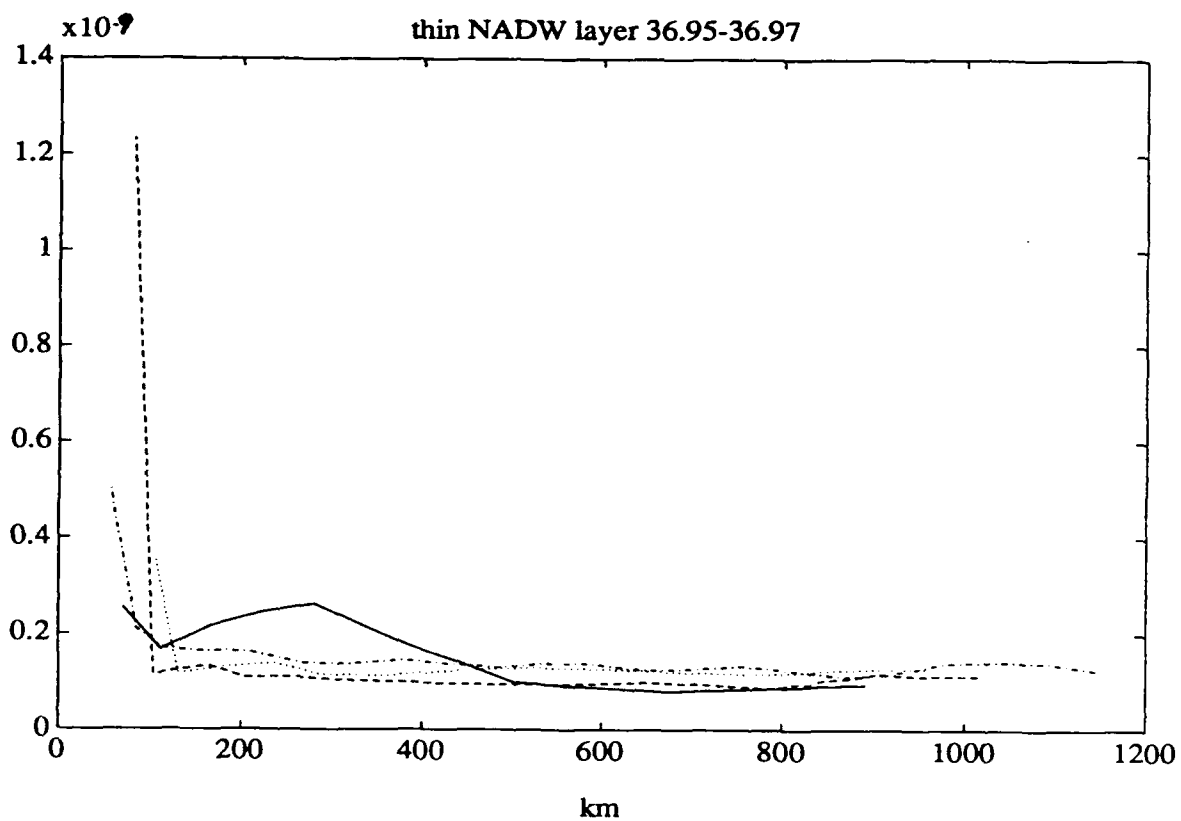


Figure A.37: Total potential vorticity averaged over the layer defined by 36.95 - 36.97  $\sigma_2$ .

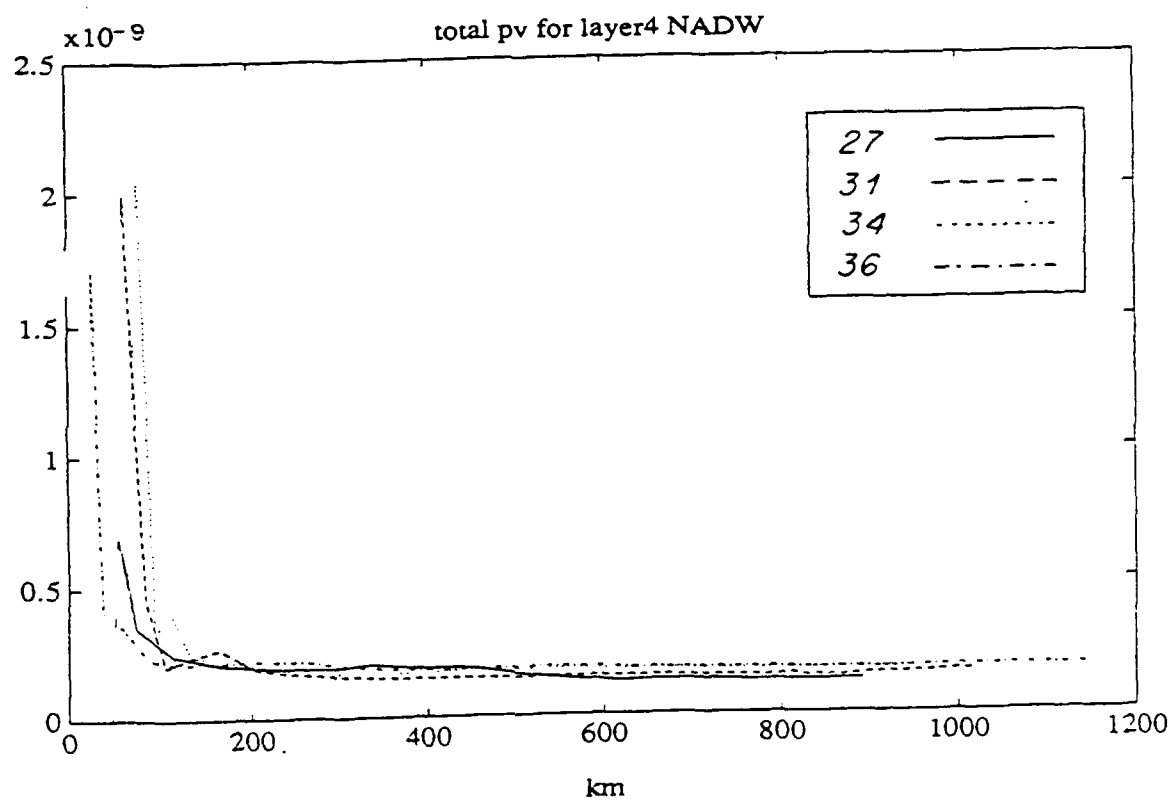


Figure A.38: Total potential vorticity averaged over the entire NADW layer.

## DOCUMENT LIBRARY

March 11, 1991

### *Distribution List for Technical Report Exchange*

Attn: Stella Sanchez-Wade  
Documents Section  
Scripps Institution of Oceanography  
Library, Mail Code C-075C  
La Jolla, CA 92093

Hancock Library of Biology &  
Oceanography  
Alan Hancock Laboratory  
University of Southern California  
University Park  
Los Angeles, CA 90089-0371

Gifts & Exchanges  
Library  
Bedford Institute of Oceanography  
P.O. Box 1006  
Dartmouth, NS, B2Y 4A2, CANADA

Office of the International  
Ice Patrol  
c/o Coast Guard R & D Center  
Avery Point  
Groton, CT 06340

NOAA/EDIS Miami Library Center  
4301 Rickenbacker Causeway  
Miami, FL 33149

Library  
Skidaway Institute of Oceanography  
P.O. Box 13687  
Savannah, GA 31416

Institute of Geophysics  
University of Hawaii  
Library Room 252  
2525 Correa Road  
Honolulu, HI 96822

Marine Resources Information Center  
Building E38-320  
MIT  
Cambridge, MA 02139

Library  
Lamont-Doherty Geological  
Observatory  
Columbia University  
Palisades, NY 10964

Library  
Serials Department  
Oregon State University  
Corvallis, OR 97331

Pell Marine Science Library  
University of Rhode Island  
Narragansett Bay Campus  
Narragansett, RI 02882

Working Collection  
Texas A&M University  
Dept. of Oceanography  
College Station, TX 77843

Library  
Virginia Institute of Marine Science  
Gloucester Point, VA 23062

Fisheries-Oceanography Library  
151 Oceanography Teaching Bldg.  
University of Washington  
Seattle, WA 98195

Library  
R.S.M.A.S.  
University of Miami  
4600 Rickenbacker Causeway  
Miami, FL 33149

Maury Oceanographic Library  
Naval Oceanographic Office  
Stennis Space Center  
NSTL, MS 39522-5001

Marine Sciences Collection  
Mayaguez Campus Library  
University of Puerto Rico  
Mayaguez, Puerto Rico 00708

Library  
Institute of Oceanographic Sciences  
Deacon Laboratory  
Wormley, Godalming  
Surrey GU8 5UB  
UNITED KINGDOM

The Librarian  
CSIRO Marine Laboratories  
G.P.O. Box 1538  
Hobart, Tasmania  
AUSTRALIA 7001

Library  
Proudman Oceanographic Laboratory  
Bidston Observatory  
Birkenhead  
Merseyside L43 7 RA  
UNITED KINGDOM

REPORT DOCUMENTATION PAGE	1. REPORT NO. WHOI-91-37	2.	3. Recipient's Accession No.
4. Title and Subtitle The Structure and Transport of the Brazil Current between 27° and 36° South			5. Report Date June 1991
7. Author(s) Jan Campbell Zemba			8. Performing Organization Rept. No. WHOI-91-37
9. Performing Organization Name and Address The Woods Hole Oceanographic Institution Woods Hole, Massachusetts 02543, and The Massachusetts Institute of Technology Cambridge, Massachusetts 02139			10. Project/Task/Work Unit No.
			11. Contract(C) or Grant(G) No. (C) N00014-82-C-0019 (G) OCE86-14486
12. Sponsoring Organization Name and Address Office of Naval Research and the National Science Foundation			13. Type of Report & Period Covered Ph.D. Thesis
			14.
15. Supplementary Notes This thesis should be cited as: Jan Campbell Zemba, 1991. The Structure and Transport of the Brazil Current between 27° and 36° South. Ph.D. Thesis, MIT/WHOI, WHOI-91-37.			
16. Abstract (Limit: 200 words)  An analysis of four hydrographic sections from the Thomas Washington marathon cruises – 27, 31, 34 and 36° S – identifies downstream changes in the Brazil Current. They detail the current's change from a relatively small (12 Sv), near surface feature to a large (80 Sv), deep current. Growth comes from a recirculation cell, deepening shear and a deeper zero velocity surface (required if NADW is to flow south). A four layer, basinwide model at 31° S ties the size of the Brazil Current and recirculation to various limits on layer-to-layer exchanges south of the section. The resulting flow pattern is consistent with equatorward meridional heat flux in the South Atlantic. Qualitative downstream changes in the total potential vorticity illuminate the presence of both frictional and inertial flow regimes. The presence of a frictional regime at the inshore edge suggests that care should be taken in assuming that potential vorticity is conserved in western boundary currents. The final picture which emerges is not of a small, surface-trapped Brazil Current; rather, it is that of a classic western boundary current, increasing in strength and depth before turning east into the interior ocean.			
17. Document Analysis    a. Descriptors 1. Brazil current 2. South Atlantic 3. Western boundary current  b. Identifiers/Open-Ended Terms  c. COSATI Field/Group			
18. Availability Statement Approved for publication; distribution unlimited.		19. Security Class (This Report) UNCLASSIFIED	21. No. of Pages 164
		20. Security Class (This Page)	22. Price